Faculty of Science and Technology
Department of Physics and Technology

UiT
THE ARCTIC
UNIVERSITY
OF NORWAY

Temperature and thermal emission of cosmic dust around the Sun, Vega and Fomalhaut

—

Margaretha Myrvang

Fys-3900 Master's thesis in physics
May 2018

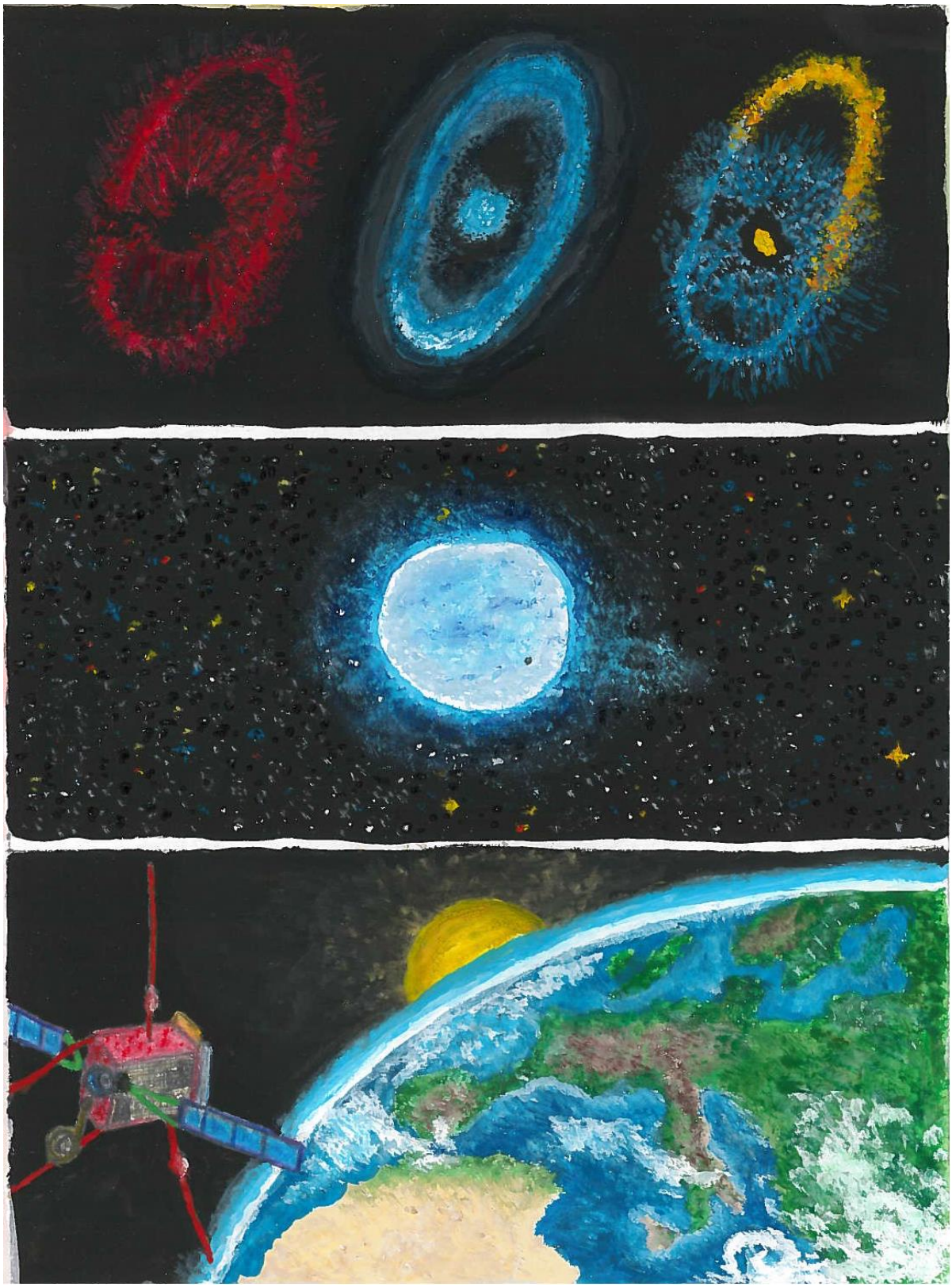

Image on cover

Image by Margaretha Myrvang, 2018

The panel at the top:

The panel to the left shows a sketch of the Fomalhaut system with its dust disk, where the sketch is inspired by a visible-light image taken by the Hubble telescope. This image is taken at a shorter wavelength compared to the one in the middle panel and the panel to the right.
Credit: NASA/Hubble.
Sources:
Wikipedia. *File: Fomalhaut b entire-Hubble telescope.jpg.* Read: 12.05.2018.
https://en.wikipedia.org/wiki/File:Fomalhaut_B_entire-Hubble_Telescope.jpg
NASA. *Hubble Space Telescope.* Read: 12-05.2018.
https://www.nasa.gov/mission_pages/hubble/science/fomalhaut.html

The panel in the middle is a sketch of the Fomalhaut system, inspired by in image taken with ALMA (wavelengths of 320-3600 μm), but the colour has been changed from yellow to blue.
Credit: European Sothern Observatory.
Sources:
Wikipedia. *File: ALMA Explores Fomalhaut's Debris Disc.jpg.* Read: 12.05.2018.
https://en.wikipedia.org/wiki/File:ALMA_Explores_Fomalhaut%E2%80%99s_Debris_Disc.jpg
ESO. *ALMA: In search of our cosmic origins.* Read: 12.05.2018.
http://www.eso.org/public/teles-instr/alma/

The panel to the right shows a sketch which is inspired by an image taken by the NASA/ESA Hubble Space Telescope (wavelengths of 320-3600 μm).
Credit: ALMA (ESO/NAOJ/NRAO). Visible light image: The NASA/ESA Hubble Space Telescope.
Source:
Wikipedia. *File: ALMA observed a ring around the bright star Fomalhaut.jpg.* Read: 12.05.2018.
https://en.wikipedia.org/wiki/File:ALMA_observes_a_ring_around_the_bright_star_Fomalhaut.jpg.

The panel in the middle:
The sketch is inspired by an image taken by the NASA's Spitzer Space Telescope.
Credit: NASA. Jet Propulsion Laboratory.
Sources:
Wikipedia. *File: Vega Spizter.jpg.* Read: 12.05.2018.
https://commons.wikimedia.org/wiki/File:Vega_Spitzer.jpg

The panel at the bottom:
Artistic impression of the ESA mission Solar Orbiter. A sketch of the Earth is shown in the background.

Abstract

Many stars are known to have dust disks, which are created through collisions between planetesimals, comparable to comets and asteroids in our solar system. Cosmic dust around a star absorbs electromagnetic radiation and re-radiates at a longer wavelength, determined by its temperature. The thermal emission of the dust can be observed. In certain systems, including the solar system, some of the dust, referred to as “hot dust”, is also observed in the close vicinity of the star. Understanding the hot dust component is important for investigating the evolution of the dust disk.

In this work, model calculations of the temperature and thermal emission of cosmic dust around Sun, Vega and Fomalhaut are presented. By calculating absorption and scattering efficiencies based on Mie theory, dust temperatures and radiation pressure cross-sections were derived. It was assumed that the dust is in thermal equilibrium. The temperature and thermal emission brightness were calculated for dust with assumed composition of amorphous carbon, astronomical silicate, ice or a mixed iron/magnesium oxide (MgO/FeO). This has been done for dust in a size distribution from 5 nm to 20 nm and for dust with a size of 100 nm and 1 µm. Initially, it was assumed that the dust resides in a narrow ring at 0.18-0.2 AU around the star, a constraint set in a previous work (Su et al. 2013). A ring around 1 AU was tested for comparison. The spectral energy distribution (SED) of the thermal emission depends on the temperature, the size and the total emission surface of the dust. They were calculated for different sets of parameters and compared to observations around Vega and Fomalhaut.

Model calculations showed that the dust temperatures differ from black body for all the compositions and sizes that were considered. Modelling of SEDs showed that dust located at 0.18-0.2 AU, which is composed of a mixture of MgO/FeO or amorphous carbon, explain the observed brightness around Vega. The observations around Fomalhaut can best be described with emission from dust consisting of MgO/FeO or amorphous carbon, located at 0.18-0.2 AU. Observations around Vega and Fomalhaut are best explained by thermal emission from dust with sizes smaller or equal to 100 nm. Larger dust particles, dust composed of ice or astronomical silicate or a dust ring located at ~1 AU from the star, could not explain the observations. The calculations also describe the total dust mass since this determined the absolute brightness of the SED.

The total dust mass required to explain the observations was found to be equivalent to the mass of ~60 Halley comets. For a young planetary system that contains a large number of planetesimals, this is a reasonably small amount, provided that the dust stays close to the star after formation. However, the dust can be removed by destruction or because it is ejected from the stellar system. Computed dust temperatures of this thesis were used in a work (C. Baumann and J. F. Aasmundtveit) to estimate sublimation lifetimes. Calculations on sublimation lifetimes around Vega and Fomalhaut showed that dust with a size of 100 nm or smaller is influenced by sublimation inward of ~0.9 AU if the dust is composed of MgO/FeO and inward of ~0.4-0.6 AU if the dust is composed of amorphous carbon. In addition, the radiation pressure values that were computed showed that dust with sizes smaller or equal to 1 µm is likely to be ejected from Vega and Fomalhaut. Thus, dust in the close vicinity of Vega and Fomalhaut has to be replenished rapidly to be able to give rise to a thermal emission that explains the observational data. It is also possible that the hot dust component is a transient phenomenon or that the observed excess brightness is caused by another process. In this work, dust near the Sun was considered for a comparison. New observations with spacecrafts in the inner solar system, the ESA mission Solar Orbiter and the NASA mission Parker Solar probe, is expected to provide data to better understand the dust destruction processes and the importance of dust ejection.

Acknowledgements

I would like to thank my supervisor Professor Ingrid Mann for her guidance and support, and for assisting me in the search for new achievements and the discovery of interesting results. Thanks to Ingrid Mann for giving me the opportunity to participate at the EGU conference in Wien with a poster presentation. In addition, thank to Carsten Baumann and Jan Fredrik Aasmundtveit for helping me with the sublimation lifetimes and also for giving me useful feedback. My fellow master student Johann Stamm has helped me with a lot, among others providing me with information related to dust dynamics around the Sun, Vega and Fomalhaut and I would like to thank him for that. I would also like to thank my friend and fellow office-sharing master student Åse Mari. Thanks to the proof-readers Kristian and Johann. You are not forgotten. Lastly, I would like to thank my sister for showing me that even though writing a master thesis can be tiring, it will work out in the end.

Table of contents

1 Introduction

Many stars are known to have dust disks, which are created through collisions between planetesimals, comparable to comets and asteroids in our solar system. An overview of these systems is given by Wyatt (2009). The colliding planetesimals are fragmented into dust and the dust is distributed throughout these disks. Dust around a star absorbs electromagnetic radiation and emits radiation at a longer wavelength, determined by its temperature. The stellar brightness is made up predominantly by emission from the stellar photosphere and therefore the temperature of the photosphere determines the amount and the shape (spectral slope) of the stellar brightness, i.e. the spectral energy distribution SED[1]. Thermal emission from dust contributes to the observed stellar brightness, that is to say it generates an additional brightness. This so-called excess emission typically has its maximum in the infrared because it is generated by relatively cooler dust, where the dust is located at a given distance from the star. Even if there are no spatial resolved observations, the dust might be discovered by looking at the SEDs from thermal emission by dust. Today many stars are known to have such an infrared excess and they are believed to be planetary systems in an early stage of evolution where the collisions of planetesimals generates large amounts of dust (Wyatt 2009).

Around certain stars an excess emission is observed in the mid to near infrared (Su et al. 2013) and this is possibly generated by dust in close vicinity of the star, similar to dust close to the Sun. This dust is generally hotter compared to dust located further away from the star and therefore its infrared brightness has a maximum at shorter wavelengths in the near infrared (~2 μm). Such excess brightness is observed around different main-sequence, including A-type stars. Vega and Fomalhaut are well studied cases where excess emission from hot dust is discussed (Su et al. 2013). A-type stars have a higher photospheric temperature and a larger brightness in comparison to the Sun and this has two consequences for dust around these stars: the dust is hotter and the radiation pressure force that is exerted on the dust is larger.

The objective of this thesis was to explore if SEDs from dust emission can explain observations around Vega and Fomalhaut and if the dust has to be located close to the star in order to explain the observations. Exploring which dust sizes that explained the observations was also a part of the thesis. This is done be detailed calculations of light scattering and absorption by dust. Dust temperatures were need to compute the SEDs and they were derived as a function of material, size and distance from the star. These temperatures were used in another project (J.F. Aasmundtveit, bachelor project in preparation) to compute dust sublimation lifetimes, which are important since they give an indication on how close to the star the dust can survive without sublimating. The light scattering calculations are also used to estimate the radiation pressure force and dust ejection. It should be noted that charged dust particles can possibly also be trapped by the magnetic field, which is considered in another project (J. Stamm, master thesis in preparation). For this work, dust near the Sun was considered as a comparison. The ESA mission Solar Orbiter and the NASA mission Parker Solar probe will possibly detect dust impacts near the Sun and optical instruments will detect scattered light from dust. This can provide a better understanding of dust fluxes and how close dust can be to the Sun without sublimation, i.e. locate dust free-zones.

[1] This term was adapted since it is commonly used in the literature.

This thesis is organized as follows. Chapter 2 provides background knowledge on the Sun, Vega and Fomalhaut. In addition, observations of dust around these stars are introduced, which includes a discussion on how dust is detected and the composition of dust. Chapter 3 describes the theoretical background. This chapter introduces Mie theory, used to calculate single particle light scattering, single particle dust temperature and thermal emission by dust distributed in a ring. The thermal emission from dust particles in a size distribution is derived for a ring which is optically thin, therefore optical thickness is discussed. The radiation pressure force is also derived by using Mie theory and the ratio between the radiation pressure force and gravity for a dust particle around a star can then be computed. This ratio is often called “beta-value”. There is also an introduction on sublimation lifetime in chapter 3. In chapter 4, the method is described. Here, optical constants used in Mie calculations and testing of Matlab Mie code are presented, followed by an elaboration on how the dust temperature and thermal emission brightness of dust was computed. Chapter 5 presents the result, in chapter 6 the results are discussed and there is a conclusion in chapter 7. The references can be found in chapter 8, while the appendix is presented in chapter 9.

2 Background

This chapter explains some of the features associated with the Sun, Vega and Fomalhaut. In addition, it discusses different aspects of cosmic dust, including a discussion on how dust is detected and the composition of dust. In addition, small bodies around the Sun, Vega and Fomalhaut will be discussed.

2.1 The Sun, Vega and Fomalhaut

In this section, the effective temperature of the Sun, Vega and Fomalhaut is discussed. The effective temperature is a quantity that is commonly used to describe the surface temperature of a star. Furthermore, the radius of the Sun, Vega and Fomalhaut will be considered, as well as the classification of these stars, thereunder the Harvard classification and the Hertzsprung-Russel diagram.

The Sun is the star that is closest to Earth and the mean distance between the Sun and Earth is one astronomical unit (AU), corresponding to 1.5×10^{11} meters. For the Sun, many astronomical phenomena like starspots and stellar rotation can be observed directly. Therefore, the knowledge concerning the Sun is in general more extensive compared to other stars since they may only be studied indirectly. The effective temperature for the Sun is 5772 K and the photospheric radius of the Sun is $R_{sun} = 6.957 \times 10^8$ meters (Mamajek et al. 2015).

Vega is a star that has been studied extensively by astronomers and it has been used as a primary absolute standard when measuring the flux of stars. Its distance from Earth is 7.76 parsec (Köhler and Mann 2002). Due to its fast rotation ($v \sim 275\ km\ s^{-1}$ at the equator), the star has a temperature gradient throughout its disk with an effective temperature of ~8152 K at the equator and ~10059 K at the pole. The radius of Vega is $R_{eq} = 2.818 \times R_{sun}$ meters at the equator and $R_p = 2.362 \times R_{sun}$ meters at the pole (Yoon et al. 2010).

Fomalhaut is a star with a distance of 7.69 parsec from Earth (Köhler and Mann 2002). It has a resolved debris disk and it is a possible candidate for an extrasolar planet. Fomalhaut has an effective temperature of 8750 K (Su et al. 2013) and a radius given by $R = 1.842 \times R_{sun}$ meters (Mamajek 2012). The important parameters for the Sun, Vega and Fomalhaut are summarized in Table 1.

Stars can be classified according to the Hertzsprung-Russel diagram, as described by Karttunen et al. (2006). The Hertzsprung-Russel diagram displays the relation between the absolute magnitude and the spectral type of the star. The absolute magnitude is the flux density at a distance of 10 parsec from the star and the spectral type classifies stars according to their surface temperature with the letters O, B, A, F, G, K and M, where O is hottest and M is coolest. This spectral classification is known as the Harvard classification. In this classification there is also a subclass represented by the numbers 0-9, 0 being the hottest and 9 the coldest. The Sun is classified as G2V (Karttunen et al. 2006), meaning that it is a yellow star with a surface temperature around 5500 K. It also means that the Sun is a star in the main sequence, its fusion of hydrogen into helium giving rise to a thermal pressure which is in balance with the gravitation force, preventing it from imploding. Vega is a spectral type A0V star (Yoon et al. 2010), that is to say a main sequence blueish star. Like Vega, Fomalhaut is also a main sequence blueish-white star, but slightly cooler, classified as an A3V star (Mamajek 2012).

Table 1: Radius, effective temperature, distance to Earth and spectral class for the Sun, Vega and Fomalhaut.

Star	Radius	Temperature [K]	Distance	Spectral class
The Sun	6.957×10^8 m	5772	1 AU	G2V
Vega	$2.818 \times R_{Sun}$	9500	7.76 pc	A0V
Fomalhaut	$1.842 \times R_{Sun}$	8750	7.69 pc	A3V

2.2 Cosmic dust around the Sun, Vega and Fomalhaut

This section discusses the distinction between dust around stars, known as circumstellar dust and dust in the space between stars, referred to as interstellar dust. A common term for circumstellar and interstellar dust is cosmic dust, which is dust located in outer space. Cosmic dust can be found, among others, in the upper parts of the atmosphere of Earth, in the Solar system, in the interstellar medium between stars and between galaxies, called intergalactic dust. Various methods for detecting dust around stars will also be mentioned, mainly detection by looking for stars with an infrared excess and there will also be a discussion on how dust is detected in the solar system. Dust composition will also be discussed. Then, small bodies in the solar system and around Vega and Fomalhaut are presented, followed by a discussion of dust which is located in the close vicinity of a star, thereunder how close the dust is believed to be located to the star and the size range of this dust.

This section follows the reasoning of Evans (1993) and Li (2009). Dust that is associated with a single star is referred to as circumstellar dust and it has certain properties that differ from interstellar dust. Since circumstellar dust is close to a star, the motion is mainly determined by the radiation pressure and the gravity force from the star and in first approximations the dust has circular, elliptic or hyperbolic orbits. This applies to uncharged dust particles. The temperature is governed by the absorption of stellar radiation, where the absorbed energy is then re-emitted in the infrared, corresponding to a wavelength of a few micrometres. Compared to the temperature of interstellar dust, the circumstellar dust will in general be hotter since the photon flux is considerably higher in a stellar system than in the interstellar medium. Interstellar dust will only be heated by stars in the background and the temperature will therefore. As an example, in the interstellar medium the temperature of carbon dust particles with a size of 10-500 nm is approximately 15-20 K (Evans 1993). For circumstellar dust, the temperature varies as a function of distance from the star and it is dependent on the luminosity of the star. Another difference is the number density which is generally higher for circumstellar dust, as well as varying with distance.

2.2.1 Detection of dust

In this section, the analysis given by Evans (1993), Wyatt (2009), Mann et al. (2006) and Mann et al. (2003) was followed. Dust around stars can be detected by looking for an infrared excess in observations done on nearby stellar systems, since the dust emits in the infrared. To validate if there is an infrared excess around a star, the star's photospheric spectrum has to be compared to measurements of the spectral energy distribution from the stellar system. There exist different methods for predicting the photospheric spectrum of a star in the infrared. It is for instance possible to extrapolate to these wavelengths if the spectrum has been measured for shorter wavelengths. A model can also be used to predict the spectrum at wavelengths in the infrared, for example simply assuming a black body

spectrum or use the empirical Kurucz atmospheric model (Su et al. 2013) for predicting the stellar photosphere. Detecting an infrared emission that is higher than the predicted spectrum of the star may indicate that there is dust in the stellar system. The dust can also be detected by direct imaging, although this will require special techniques and it can for the most part only be done for the nearest and brightest debris disk. In the solar system, observations on dust includes studying scattered light and thermal emitted radiation from interplanetary dust and direct measurements from spacecraft.

Observations on interplanetary dust has predominantly been done for distances of 0.3-1.7 AU from the Sun. For dust inward of 0.3 AU, there are not many studies, but the Parker Solar Probe (NASA 2018a) and the Solar Orbiter (NASA 2018b), will possibly do in-situ measurements near the Sun and these spacecraft will hopefully provide information about dust optical properties, number density etc. An artistic impression of the Parker Solar probe is shown in Figure 1. In addition, samples collected on Earth provide information on dust properties, thereunder dust composition.

Figure 1: Artistic illustration of the NASA mission Parker Solar probe to be launched in 2018 © NASA. Credit: Johns Hopkins University Applied Physics Laboratory.

2.2.2 Composition of dust

Cosmic dust can be produced from collisions between planetesimals, a collective term for asteroids and comets. The colliding planetesimals will be fragmented into smaller pieces with a wide variety of sizes and it has been shown, both empirically and with collision models, that the size distribution of the fragments can be described by a power law. (Wyatt 2009). Production of cosmic dust can also come from sublimation of comets passing close to the Sun. For asteroids, the composition ranges from carbon to silicates like olivine, as well as metals like iron and nickel (Karttunen et al. 2006) and (Nakamura and Michel 2009). Silicates from asteroids can yield metal oxides like MgO and FeO (Su et al. 2013) when they are broken down for instance by eroding processes like sputtering and sublimation (Wurz 2012). Comets consist mainly of ice, dust and frozen gases such as carbon monoxide, carbon dioxide, methane, ammonia and organic components (Karttunen et al. 2006). The composition of dust can therefore vary a great deal and it will depend on whether it was produced from asteroids or comets. Unfortunately, there is not much information about the mineral composition of dust in interplanetary space. (Mann et al. 2003). Figure 2 shows a meteorite collected on Earth.

Figure 2: Iron-nickel meteorite collected on Earth. © NASA. Credit: Courtesy NASA/JPL- Caltech.

2.2.3 Small bodies in the solar system

This section is based on Karttunen et al. (2006), Nakamura and Michel (2009) and Mann et al. (2006). In the solar system, there are planets, dwarf planets and Small Solar System Bodies (Karttunen et al. 2006), as defined by the International Astronomical Union. Small Solar System Bodies includes asteroids, comets, meteoroids and interplanetary dust. Most of the asteroids are confined to a main belt between the orbits of Mars and Jupiter, orbiting around the Sun at a distance that is centered approximately at 2.8 AU. Their size ranges from some hundreds of meters to hundreds of kilometres. The motion of asteroids are under the influence of the gravitational perturbation of nearby planets, in particular Jupiter, leading to a variation of the distribution of asteroids inside the main belt. There are asteroids outside the main belt and some of these asteroids orbit between the Earth and Mars. If an asteroid is less than a given size it is often called a meteoroid, but the size limit is not definite. Meteoroids that survive the entry in Earth's atmosphere are known as meteorites. Comets are usually 10 kilometres or less in size. Their orbits are generally highly elliptical with a large eccentricity and the orbit period differs from comet to comet, ranging from short-period comets with a period less than 200 years to long-period comets. Sun-grazing comets, which are comets passing much closer than 1 AU to the Sun, form a coma or tail due to the sublimation of ice and dust and it may be visible from Earth. The Kuiper belt, located from the orbit of Neptune and to the outer edge of the solar system, forms a disk-like cloud and is believed to contain comets which may be the origin of short-period comets in the solar system. From Earth, it is possible to observe the zodiacal light and gegenschein, which are the results of interplanetary dust scattering light from the Sun and emission from absorbed radiation. The zodiacal light can be observed above the rising or setting Sun, while the gegenschein can be observed exactly opposite the Sun. These dust particles have a size that ranges from 10-100 µm and they are mostly concentrated on the plane of the ecliptic. In Figure 3, there is a depiction of the plane of the ecliptic with the Sun and Earth.

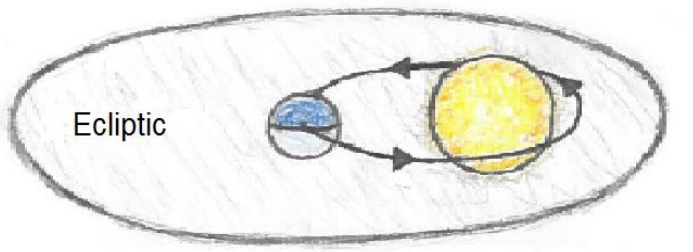

Figure 3: Schematic of the Earth and the Sun with an illustration of the plane of the ecliptic. The schematic is not to scale.

2.2.4 Small bodies around Vega and Fomalhaut

Vega and Fomalhaut are thought to have two planetesimal belts, a cold belt and a warm belt. Both stars have a cold belt that is analogous to the Kuiper belt in our solar system and which is believed to contain most of the planetesimals that were leftover after the possible formation of planets. These cold belts have a large surface area and can therefore be detected through infrared observations. The cold belts have been resolved, that is to say the exact location is known and it is suggested that they have a temperature of ~50 K. For Vega this corresponds to a distance of 110 AU and for Fomalhaut, 140 AU from the star. In addition, both Fomalhaut and Vega have an unresolved warm excess, believed to come from thermal emission by dust (Su et al. 2013). Even though this excess is not resolved, the distance of the dust from the star can be inferred by looking at the spectral energy distribution, which gives an indication of the temperature of the dust under the condition that the dust is in thermal equilibrium, i.e. the temperature is constant (Wyatt 2009). The warm emission detected around Vega is suggested to be a planetesimal belt near the water-frost line, the distance where water freezes. It is suggested to be analogous to the asteroid belt in our solar system, but with a larger mass. The shape of

the spectrum for the warm excess around Vega can apparently be represented by a blackbody at 170 K, which corresponds to a distance of ~14 AU from Vega (Su et al. 2013). Like Vega, it is suggested that the warm excess around Fomalhaut is from a planetesimal belt, similar to the asteroid belt in our solar system and that the spectrum can be represented by a blackbody at 170 K, corresponding to ~11 AU from Fomalhaut (Su et al. 2013). The dust temperature will depend on the optical properties of the material and the size and thus the location of the dust is tentative. It is proposed that the warm excess seen around Vega and Fomalhaut is separated from the cold belt and that the separation may be maintained by multiple planets. The presence of planets can lead to a perturbation of dust trajectories, ejecting dust particles from the gap between the cold and the warm belt (Su et al. 2013).

There have been observations of an excess emission at ~2 μm around Vega and Fomalhaut, revealed through ground-based observations. This excess emission points to the existence of a hot dust component. For Vega an excess of 1.29 ± 0.19 % in the K-band (Absil et al. 2006) and 1.23 ± 0.45 % in the H-band (Defrère et al. 2011) was discovered. It was described that Fomalhaut had an excess of 0.88 ± 0.12 % in the K-band (Absil et al. 2009) and an excess with a mean value of 0.35 ± 0.10 % in the N-band from 8-11 μm (Mennesson et al. 2013). The infrared K-band ranges from 1.94-2.34 μm (Absil et al. 2006), while the infrared H-band ranges from 1.50-1.80 (Defrère et al. 2011) and the full N-band ranges from 8-13 μm (Mennesson et al. 2013). Supposedly, the excess emission is caused by the presence of hot dust in the close vicinity of the star, since it has been excluded that this excess is caused by stellar winds or low-mass companions. For both stars there are indications that the excess emission is not spatially connected to the warm excess. At the moment, it is unknown where the hot dust comes from. It might be produced from comets or asteroids sublimating close to the star. The dust can then be lost through several mechanisms like sublimation, sputtering, Poynting-Robertson drag or due to stellar radiation pressure. (Su et al. 2013). If the dust is rapidly lost through one of these mechanisms, it has to be replenished, otherwise the dust will be short-lived. With this scenario, it should perhaps only be possible to observe the dust over a short amount of time. Therefore, whether the dust is in a steady-state, where the production of dust balances the loss, or if it is in a dynamical state and the amount of dust varies with time, is not entirely clear, but if there is a large variation of dust brightness this might indicate that the dust is in a dynamical state.

Concerning the issue about dust replenishment, there is a proposal that the hot dust is charged by the photoelectric effect or the stellar wind and that it is then trapped by the magnetic field of the star. Given that this proposal is proven correct, this means that the replenishing rate does not have to be so high since the dust particles will be prevented from escaping. The dust may still be lost through sublimation, so in order for the dust to survive close to the star, the sublimation temperature has to be high compared to the temperature of the dust (Su et al. 2013).

By combining all interferometric measurements of the excess emission at ~2 μm observed around Vega, Mennesson et al. (2011) concluded that the hot dust have to reside from within 0.2 AU of Vega under the assumption that thermal emission by dust is responsible for the emission. Furthermore, they concluded that the observed excess would have to come from a very narrow ring between 0.1-0.15 AU with an outer limit of 0.2 AU. They found that thermal emission by dust located further out than 2 AU could be ruled out. This constraint on the distances have apparently been found by looking at detailed Mie calculations. Scattering of starlight by dust located inward of 0.2 AU or outward of 2 AU was not ruled out. Defrère et al. (2011) came to the conclusion that the dust is located between 0.1-0.3 AU from Vega and modelling of spectral energy distributions showed that carbonaceous grains had to be

present in order to fit the data, and a mass equivalent to $2 \times 10^{-2} M_{earth}$ was needed. When it comes to the size range of the dust, Mennesson et al. (2011) concluded that the dust consists of particles that are much smaller than those in the zodiacal cloud, that is to say the dust is micron-sized or smaller, while Defrère et al. (2011) concluded that the dust has a minimum particle size of 10 nm to 200 nm.

Modelling of SEDs by Lebreton et al. (2013) showed that the excess emission observed around Fomalhaut could be explained by two distinct dust populations. They found that one dust population could be located at ~0.1-0.3 AU distributed in a narrow ring and with dust consisting of a carbonaceous materials where the size of the dust particles ranges from 10 nm to 500 nm. The other dust population could be located at ~2 AU and have a size of >1 μm and a higher mass compared to the ring at ~0.1-0.3 AU.

3 Theory

The first part of this chapter reviews light scattering, thereunder Mie theory. Then, a parameter called the beta-value is discussed. Furthermore, computations on dust temperature will be examined and there will be a discussion on sublimation and sublimation lifetime. The last part of this chapter is a discussion on thermal emission by dust.

3.1 Single particle light scattering

This overview of Mie theory follows the description by Bohren and Huffman (1983). When a given particle is influenced by an electromagnetic wave, i.e. illuminated by light, electric charges in the material will start to oscillate because of the incident electric field. Electric charges which are accelerated emit electromagnetic radiation in all directions and this radiation is known as scattered radiation. This process determines the refractive index of a solid. Some of the energy from the electromagnetic wave can also be absorbed, which means that the energy is transformed into other forms. The absorbed energy can for example be transformed into internal energy, which for an ideal gas is the statistical mean of the kinetic energy of the gas particle. It can also lead to excitation of electrons or for molecules, vibrational states or rotational states. How light is scattered and absorbed by a particle is determined by the size, shape and composition of the particle described by its refractive index (Li 2009). There are different approaches to solve phenomena linked to scattering and absorption by small particles, for instance by applying Mie theory, but if the particles are much smaller than the incident wavelengths, Rayleigh theory, an approximation, can be applied.

3.1.1 Mie theory

Mie theory is a description of the absorption and scattering by small, spherical particles of arbitrary radius and refractive indices. It is an exact solution consisting of an infinite series expansion, as shall be shown. The physics behind the interaction between an electromagnetic wave and a spherical particle is extremely complicated and the mathematical derivation is quite long and tedious. Consider a dust particle which is exposed to an incident electromagnetic wave and the objective is to find an expression for the electromagnetic field at all points inside the particle and in the medium surrounding the particle. The electromagnetic field must satisfy Maxwell's equations wherever the permittivity ε and permeability μ are continuous and the electric and magnetic fields in a linear, isotropic and homogeneous medium must also satisfy the vector wave equation. The permittivity is a measure of resistance encountered when forming an electric field in a medium and the permeability is the degree of magnetization of a material in response to an applied magnetic field. Due to a discontinuity at the boundary between the particle and medium where ε and μ may be changing, certain boundary conditions are imposed upon the electromagnetic fields in order to find a solution to the problem. In Mie theory the scalar wave equation is solved instead of the vector wave equations since this is much easier. Since the goal is to find a solution for spheres, the scalar wave equation is therefore expressed in spherical polar coordinates. It can then be split into three differential equations, all which can be solved separately. Expressions for the vector spherical harmonics $\boldsymbol{M}_{emn}$, $\boldsymbol{M}_{omn}$, $\boldsymbol{N}_{emn}$ and $\boldsymbol{N}_{omn}$ can be generated from these solutions. These are needed to find a solution for the electromagnetic fields. After the incident electromagnetic plane have been expanded into an infinite series of vector spherical harmonics, solutions for the internal field $\mathbf{E}_1$ and $\mathbf{H}_1$ inside the sphere and the scattered field $\mathbf{E}_s$ and $\mathbf{H}_s$ can be found:

$$\boldsymbol{E}_1 = \sum_{n=1}^{\infty} E_n \left(E_n \boldsymbol{M}_{o1n}^{(1)} - i d_n \boldsymbol{N}_{e1n}^{(1)} \right) \tag{1}$$

$$\boldsymbol{H}_1 = \frac{-\kappa_1}{\omega \mu_1} \sum_{n=1}^{\infty} E_n \left(d_n \boldsymbol{M}_{e1n}^{(1)} + i c_n \boldsymbol{N}_{o1n}^{(1)} \right) \tag{2}$$

$$\boldsymbol{E}_s = \sum_{n=1}^{\infty} E_n \left(i a_n \boldsymbol{N}_{e1n}^{(3)} - a_n \boldsymbol{M}_{o1n}^{(3)} \right) \tag{3}$$

$$\boldsymbol{H}_s = \frac{\kappa}{\omega \mu} \sum_{n=1}^{\infty} E_n \left(i b_n \boldsymbol{N}_{o1n}^{(3)} + a_n \boldsymbol{M}_{e1n}^{(3)} \right) \tag{4}$$

by using the boundary conditions and the vector spherical harmonics. $\mathbf{E}_1$, $\mathbf{H}_1$, $\mathbf{E}_s$ and $\mathbf{H}_s$ are expressed as an infinite series where $E_n = i^n E_0 (2n+1)/n(n+1)$ and E_0 is the amplitude of the incident electric field, μ_1 is the permeability of the sphere, μ is the permeability of the surrounding medium , $\kappa = 2\pi/\lambda$ is the wave number in vacuum, κ_1 is the wavenumber in the sphere and λ is the wavelength. In order to compute the internal and scattered fields, the following assumption are made: the scattered field is at a large distances from the sphere, i.e. in the far-field and the sphere is homogeneous and isotropic with a radius a. In order to see how different physical parameters varies with the size and the optical properties of the sphere, expression for the scattering coefficients a_n and b_n have to be obtained. This can be done by using the equations for the internal and scattered field and boundary conditions and the scattering coefficients can then be expressed as:

$$a_n = \frac{\mu m^2 j_n(mx)[x j_n(x)]' - \mu_1 j_n(x)[mx j_n(mx)]'}{\mu m^2 j_n(mx)\left[x h_n^{(1)}(x)\right]' - \mu_1 h_n^{(1)}(x)[mx j_n(mx)]'} \tag{5}$$

$$b_n = \frac{\mu_1 j_n(mx)[x j_n(x)]' - \mu j_n(x)[mx j_n(mx)]'}{\mu_1 j_n(mx)\left[x h_n^{(1)}(x)\right]' - \mu h_n^{(1)}(x)[mx j_n(mx)]'} \tag{6}$$

where $x = \kappa a = 2\pi a/\lambda$ is the size parameter, $m = N_1/N_2$ is the sphere's relative refractive index with N_1 representing the refractive index of the sphere and N_2 representing the refractive index of the surrounding medium. For vacuum $N_2 = 1$. In perfect vacuum μ will be equal to μ_0. j_n and h_n are spherical Bessel functions of order n where $n = 1,2,\ldots,n_{max}$ (Bohren and Huffman 1983).

The refractive index of a material, also known as optical constant, describes how an electromagnetic wave propagates through the material and is given by:

$$N = n + ik$$

where n determines the phase velocity, describing refraction and k describes how the wave is attenuated. The wavenumber and the imaginary part of the refractive index are two physical quantities which are related, but they are not the same. The scattering coefficients given in equation *(5)* and *(6)*

are important because they can be used to find Mie efficiencies and cross-sections. Cross-sections for absorption and scattering can be found by considering the rate at which energy of an incident electromagnetic field I_i is absorbed and scattered by a sphere. Using expressions for the scattered electromagnetic field $\mathbf{E}_s$ and $\mathbf{H}_s$, the scattering and absorption cross-section will then be:

$$C_{sca} = \frac{W_{sca}}{I_i}$$

$$C_{abs} = \frac{W_{abs}}{I_i}$$

with dimension of area and where W_{abs} is the rate at which energy is absorbed and W_{sca} is the rate at which energy is scattered. The Mie efficiencies can be defined as:

$$Q_{sca} = \frac{C_{sca}}{G} = \frac{2}{x^2}\sum_{n=1}^{\infty}(2n+1)(|a_n|^2 + |b_n|^2) \tag{7}$$

$$Q_{ext} = \frac{C_{ext}}{G} = \frac{2}{x^2}\sum_{n=1}^{\infty}(2n+1)Re\{a_n + b_b\} \tag{8}$$

where Q_{ext} is the extinction cross-section and G is a particle's cross-sectional area projected onto a plane perpendicular to the incident electromagnetic field. For a sphere the geometric cross-section is $G = \pi a^2$. Extinction is the sum of scattering and absorption and due to conservation of energy the absorption efficiency can be found by:

$$Q_{abs} = Q_{ext} - Q_{sca} \tag{9}$$

However, it should be noted that particles with a size that is smaller or equivalent to the wavelength can have absorption and scattering efficiencies that are significantly larger than 1. It may seem as though the particles scatter and absorb more light than which is geometrically incident upon them, but the concept of light geometrically incident upon an object comes from geometric optics and it is only valid for objects that are much larger than the incident wavelength. In general, calculations on absorption and scattering should be done with optical constants that are dependent on wavelength.

3.1.2 Beta-values

In the following section, beta-values as described by Mann et al. (2006), Wyatt (2009), Köhler and Mann (2002) and Wilck and Mann (1995) will be discussed. For dust near a star, the most important acting forces are the radiation pressure and the gravitational force. The interaction between stellar electromagnetic radiation and dust is known as radiation force. Stellar radiation will exert a force on the dust due to the fact that scattering and absorption by dust removes energy from the radiation, and due to conservation of momentum. For dust particles moving in an orbit around the star, the radiation force has two components, one that acts in a radial outward direction, called radiation pressure and one that acts tangential. The latter is called Poynting-Robertson force. It causes a drag because it has a direction that is opposite to the dust particle's motion around the star, causing a loss of orbital energy and a drift towards the star. On astronomical time scales the Poynting-Robertson drag limits the lifetime of the dust that orbits a star, since it would finally fall into the star. Generally, the radiation pressure plays a more important role than the Poynting-Robertson drag when it comes to determining how the orbit of the dust evolves. The radiation pressure F_{rad} can be given as:

$$F_{rad} = \int_0^{\infty} \frac{L(\lambda)}{4\pi r^2} \frac{G}{c} Q_{pr}(\lambda, N(\lambda), a) d\lambda \tag{10}$$

and where $L(\lambda)$ is the stellar luminosity in units of watt, c is the speed of light in vacuum, G is the effective geometric cross-section and R_{star} is the radius of the star, N_1 is the refractive index and r is the distance from the star. The radiation pressure will be stronger for A-type stars like Vega and Fomalhaut compared to the Sun, a G-type, since they have a higher effective temperature. Q_{pr} is the radiation pressure efficiency and it can be defined by looking at the momentum transfer between the light and a dust particle due to absorption and scattering. The momentum transfer caused by absorption and scattering will depend on the intensity of the light, as well as C_{abs} and C_{sca}, which can be viewed as an effective area. For the momentum transfer in scattering, the efficiency will also depend on the angular distribution of the scattered light. Therefore, the radiation pressure efficiency can be given as:

$$Q_{pr} = Q_{ext} - Q_{sca}\langle cos\,\theta \rangle \tag{11}$$

with $g = \langle \cos\theta \rangle$ defined as the asymmetry parameter which indicates whether the light is scattered isotropically or more towards a forward or backward direction. The asymmetry parameter usually depends on the polarization of the incident light, but for a spherical dust particle, the asymmetry parameter is independent on the polarization. By assuming a black body spectrum for the star, the stellar luminosity will be:

$$L(\lambda) = 4\pi {R_{star}}^2 \pi B_{\lambda}(T_{star}) \tag{12}$$

where $B_{\lambda}(T_{star})$ is the Planck function and T_{star} is the effective temperature of the star. The factor π comes from integrating over all possible solid angles:

$$\int_{\varphi=0}^{2\pi} \int_{\theta=0}^{\pi/2} sin\,\theta\, cos\,\theta\, d\theta d\varphi = \pi$$

The Planck function is defined as:

$$B_{\lambda}(T) = \frac{2hc^2}{\lambda^5} \frac{1}{e^{hc/\lambda \boldsymbol{k_b} T} - 1} \tag{13}$$

in which h is Planck's constant, k_b is Boltzmann constant and T is the temperature. Dust in a stellar system will be under the influence of a gravitational force caused by the main star, but it can also be affected by nearby planets which can lead to orbital perturbations. The gravitational force F_{grav} acts radially inward and can be expressed as:

$$F_{grav} = \frac{\gamma M_{star} m_{dust}}{r^2} \tag{14}$$

where γ is the gravitational constant, M_{star} is the mass of the star, m_{dust} is the mass of the dust particle and again, r is the distance from the star. Both the radiation pressure and the gravitational force depends on the distance from the star as $1/r^2$ and the ratio between these two forces is given by a parameter called the beta-value and which it is defined as:

$$\beta = \frac{F_{rad}}{F_{grav}}$$

$$\beta = \frac{{R_{star}}^2 G}{\gamma M_{star} m_{dust} c} \int_0^\infty \pi B_\lambda(T)\, Q_{pr}(\lambda, N(\lambda), a) d\lambda \tag{15}$$

which shows that the beta-values are independent of the distance from the star.

In the large particle limit, the beta-values can be approximated as:

$$\beta_{abs} = \frac{C_{pr} {R_{star}}^2 \sigma T^4}{\gamma M_{star} m_{dust} c} \tag{16}$$

if all the incident radiation is completely absorbed by the dust particle:

$$\beta_{ref} = \frac{2 C_{pr} {R_{star}}^2 \sigma T^4}{\gamma M_{star} m_{dust} c} \tag{17}$$

and if all the incident radiation is completely reflected by the dust particle. The term σT^4 is given by Stefan-Boltzmann law:

$$\int_0^\infty \pi B_\lambda(T)\, d\lambda = \sigma T^4$$

and σ is Stefan-Boltzmann constant. The radiation pressure cross-section can be approximated as:

$$C_{pr} = G Q_{pr} = \pi a^2$$

where it is assumed that the dust particle is spherical and that the radiation pressure efficiency is equal to 1 for all wavelengths.

The beta-values can indicate whether or not the dust particles are in a bound or unbound orbit around the star. If the dust particles are in an unbound orbit, they can be ejected from the stellar system, but they can also be destroyed by collisions, drift inward due to P-R-drag and sublimate close to the star or be destroyed by sputtering in the solar/stellar wind. Sputtering is a process that results in erosion of dust particle due to impact of ions (Evans 1993). Dust particles in a bound orbit can also be destroyed be these mechanisms, but they will not be ejected from the stellar system.

3.2 Single particle temperature

This sections describes the calculation of temperature of dust around a star. These calculations are based on the assumption that the dust is in thermal equilibrium. The section follows the derivations as described by Wurz (2012), Asmus et al. (2014) and Bohren and Huffman (1983).

The temperature of cosmic dust in a stellar system can be estimated by considering different heating and cooling mechanisms. For circumstellar dust the most important source of heat is absorption of stellar radiation, but impact by atoms and ions and exothermic chemical heating may also contribute. Heating of the dust particle will cause it to attain a certain temperature, leading to energy emittance in the form of radiation at a wavelength determined by its temperature. How efficiently the energy is absorbed and emitted by the dust particle is determined by the absorption and emission efficiency, respectively, which both depend on size and composition and which also vary with wavelength. If the dust particle is in thermal equilibrium, the rate of absorbed energy will be equal to rate of the emitted energy and the temperature remains constant. For dust in the interstellar medium, thermal equilibrium may not be a valid assumption since the dust can be significantly heated by single events like absorption by a single photon or impact by a single ion or molecule. Depending on how often these

single events occur and how long it takes for the dust to cool down, the temperature can therefore vary in a statistical way. On the other hand, dust in stellar system is more likely to attain an equilibrium temperature because the flux of radiation is a stronger (Evans 1993) (Li and Mann 2012) Regardless, by assuming a black body spectrum for the star, the absorbed power at a distance r can be defined as:

$$P_{abs} = \pi a^2 \left(\frac{R_{star}}{r}\right)^2 \int_0^\infty \pi B_\lambda(T_{star}) Q_{abs}(\lambda, N(\lambda), a) d\lambda \tag{18}$$

The dust is assumed to be concentrated at the plane of the ecliptic and the equatorial radius of Vega will therefore be used when computing the absorbed power. The emitted power can be expressed as:

$$P_{rad} = 4\pi a^2 \int_0^\infty \pi B_\lambda(T_p) Q_{abs}(\lambda, N(\lambda), a) d\lambda \tag{19}$$

where T_p is the surface temperature of a dust particle. It is assumed that the radiation is emitted isotropically. In equation *(*19*)*, the absorption efficiency is assumed to be equal to the emissivity, which is the ratio of the power emitted by the particle divided by the power emitted by a black body according to the Planck function in equation *(*13*)*. For this to be a valid assumption, there has to be strict thermodynamic equilibrium between the particle and the surrounding field of radiation. This assumption can be interpreted as Kirchhoff's law for emission and absorption. Then finally, with the assumption of thermal equilibrium, the temperature T_p of a dust particle can be calculated from the following equation by setting P_{abs} equal to P_{rad}:

$$\pi a^2 \left(\frac{R_{star}}{r}\right)^2 \int_0^\infty \frac{2hc^2}{\lambda^5} \frac{1}{e^{hc/\lambda k T_{star}} - 1} Q_{abs}(\lambda, N(\lambda), a) d\lambda = 4\pi a^2 \int_0^\infty \frac{2hc^2}{\lambda^5} \frac{1}{e^{hc/\lambda k T_p} - 1} Q_{abs}(\lambda, N(\lambda), a) d\lambda \tag{20}$$

Calculating T_p analytically from equation *(*20*)* can be challenging. The equation is easier to solve numerically. This provides the temperature of cosmic dust with different sizes and compositions and the temperature as a function of distance from the star, which are the most important parameters determining the temperature.

3.3 Integrated thermal emission by dust

This section explains thermal emission by dust and how the brightness was computed. The computed spectrum of the thermal emission by dust is the spectral energy distribution which shows the flux in units of W/m^2 per frequency or wavelength.

3.3.1 Thermal emission brightness

In this section, the derivation of Wyatt (2009), Rieke et al. (2016) and Lebreton et al. (2013) is followed. A population of dust particles at a distance r from the star, distributed in a ring of width dr, emit thermal radiation which is strongly dependent on the temperature of the dust grains and the absorption efficiency. As mentioned in section 3.2, the temperature can be calculated numerically and it is a function of size, material and distance from the star. Assuming that the dust particles are spherical, the absorption efficiency can be estimated by using Mie theory. There will be a minimum size a_{min} and a maximum size a_{max} with a given size distribution. The ring has a minimum radius of r_{min} and a maximum radius of r_{max}. Within the ring, the dust number density can be assumed to follow a certain distribution with distance. The flux thermally emitted as a function of wavelength λ from the dust population is:

$$\Phi_{th}(\lambda) = \frac{1}{4\pi d^2} \int_{a_{min}}^{a_{max}} \pi B_\lambda(T_p(a,r)) 4\pi a^2 n(a,r) Q_{abs}(\lambda, N(\lambda), a)\, da \tag{21}$$

observed at distance d from the star and where $\mathrm{n(a, r)}$ is the number density for the size distribution and the density distribution. It is assumed that thermal emission from the dust particles are radiated isotropically. Assuming that the size distribution is only a function of size and that the density distribution is only a function of distance, can simplify calculations. This means that the size distribution does not change with distance and that the distribution itself and all the parameters remains the same for all distances. The same applies to the density distribution, i.e. that it is assumed identical for all sizes. Although these assumption make the calculations easier, whether it turns out to be a reasonable approximation or not should be considered more thoroughly in future work, since it is thought that the size distribution changes with distance for dust around Vega (Wyatt 2009). To further simplify the calculations, an average temperature was estimated separately, providing only one temperature for the Planck's function in equation *(*21). The density distribution was only used for calculating an average temperature, since it was assumed that the temperature is the only parameters which varies with distance. In addition, an average absorption efficiency was found separately. Despite all the simplifications, equation *(*21*)* can provide a model for SEDs of dust around a star in a certain range of wavelengths, where the total thermal emission is found by adding together the contribution from each dust grain. In the following sections, all the different terms in equation *(*21*)* and how they were calculated will be explained in more details.

3.3.2 Dust size distribution

The dust size distribution can be described by a power law where $n(a) \propto a^{-k}$ (Mennesson et al. 2013) and a probability density function (PDF) for this distribution can be defined as:

$$p(a) = C_{nom} a^{-k}, \qquad a_{min} \leq a \leq a_{max}$$

where $\mathrm{C_{nom}}$ is a normalization constant, the PDF is truncated between $\mathrm{a_{min}}$ and $\mathrm{a_{max}}$, a is assumed to be a continuous variable and δ is the size distribution power index. In order to ensure that the PDF integrates to 1, as required by a PDF, the normalization constant can be calculated in the following way:

$$C_{nom} \int_{a_{min}}^{a_{max}} a^{-\delta}\, da = 1$$

$$C_{nom} \left[\frac{1}{1-\delta} a^{1-\delta} \right]_{a_{min}}^{a_{max}} = C_{nom} \frac{a_{max}^{1-\delta} - a_{min}^{1-\delta}}{1-\delta} = 1$$

$$C_{nom} = \frac{1-\delta}{a_{max}^{1-\delta} - a_{min}^{1-\delta}}$$

and the PDF can be expressed as:

$$p(a) = \frac{1-\delta}{a_{max}^{1-\delta} - a_{min}^{1-\delta}} a^{-\delta} \tag{22}$$

(Lebreton et al. 2013).

The moments are:

$$\langle a^m \rangle = \int_{a_{min}}^{a_{max}} a^m p(a)\, da = C_{nom} \int_{a_{min}}^{a_{max}} a^{m-\delta}\, da = C_{nom} \left[\frac{1}{m+1-\delta} a^{m+1-\delta} \right]_{a_{min}}^{a_{max}}$$

$$\langle a^m \rangle = C_{nom} \frac{a_{max}^{m+1-\delta} - a_{min}^{m+1-\delta}}{m+1-\delta}$$

Then, the mean can be given by:

$$m = 1: \ \mu = C_{nom} \frac{a_{max}^{2-\delta} - a_{min}^{2-\delta}}{2-\delta} \tag{23}$$

and the standard deviation is:

3.3.3 Total emission surface

Equation *(*21*)* requires the calculations of the emission surface for a population of dust particles. The following derivations are similar to the ones done by (Zender 2013) and (Dohnanyt 1969). The total emission surface will be proportional to total mass of the dust. The surface area increases in size if the number of smaller particles are higher since these have a higher surface to volume ratio. In order to find the total emission surface, a total mass of the dust has to be assumed, that is to say the total mass of the dust is the parameter which will be fixed to find all the other parameters. Then, if the mass density is known, the volume of the dust V_{dust} can be found by:

$$V_{dust} = \frac{m_{dust}}{\rho} \tag{24}$$

where ρ is the mass density and m_{dust} is the total mass of the dust, given as:

$$m_{dust} = AM_{earth} \tag{25}$$

where A is a constant which can be adjusted and M_{earth} is the mass of the Earth, which was set equal to 5.974×10^{24} (Karttunen et al. 2006). The dust mass is given as fraction of the mass of the Earth in order to compare it to the derivation in (Su et al. 2013). The total of volume of the dust is:

$$V_{tot} = \int_{a_{min}}^{a_{max}} V(a) n(a)\, da = \frac{4\pi}{3} \int_{a_{min}}^{a_{max}} a^3 n(a)\, da \tag{26}$$

Again, the dust particles are assumed to be spherical. As can be seen, an expression for the size distribution $n(a)$ is needed. $n(a)$ gives the number of dust particles with radius a and can be found by expressing the PDF as:

$$p(a) = \frac{number\ of\ favorable\ outcomes}{number\ of\ possible\ outcomes} = \frac{n(a)}{N_{tot}} \tag{27}$$

where the total number of dust particles is integrated over all possible sizes and is given by:

$$N_{tot} = \int_{a_{min}}^{a_{max}} n(a)\, da \tag{28}$$

(Zender 2013). By setting equation *(*22*)* equal to equation *(*27*)* and solving for $n(a)$, gives:

$$n(a) = C_{nom} a^{-\delta} N_{tot} \tag{29}$$

and the total emission surface can be stated as:

$$\sigma_{tot} = \int_{a_{min}}^{a_{max}} \sigma(a) n(a)\, da = 4\pi \int_{a_{min}}^{a_{max}} a^2 n(a)\, da = 4\pi C_{nom} N_{tot} \int_{a_{min}}^{a_{max}} a^{2-\delta}\, da$$

$$\sigma_{tot} = 4\pi C_{nom} N_{tot} \left[\frac{1}{3-\delta} a^{3-\delta}\right]_{a_{min}}^{a_{max}} = 4\pi C_{nom} N_{tot} \frac{a_{max}^{3-\delta} - a_{min}^{3-\delta}}{3-\delta} \tag{30}$$

where the dust particles are assumed to radiate isotropically on a spherical surface. An expression for N_{tot} can be derived from equation *(26)*:

$$V_{tot} = \frac{4\pi}{3} C_{nom} N_{tot} \left[\frac{1}{4-\delta} a^{4-\delta}\right]_{a_{min}}^{a_{max}} = \frac{4\pi}{3} C_{nom} N_{tot} \frac{a_{max}^{4-\delta} - a_{min}^{4-\delta}}{4-\delta}$$

$$N_{tot} = \frac{(4-\delta) 3 V_{tot}}{4\pi C_{nom} \left(a_{max}^{4-\delta} - a_{min}^{4-\delta}\right)} \tag{31}$$

This expression can be inserted into equation *(30)* to find the total emission surface, which gives:

$$\sigma_{tot} = \frac{(4-\delta) 3 V_{tot}}{\left(a_{max}^{4-\delta} - a_{min}^{4-\delta}\right)} \frac{a_{max}^{3-\delta} - a_{min}^{3-\delta}}{3-\delta}$$

If all the dust particles are assumed to have the same radius, i.e. a distribution like a delta function, the total volume will be:

$$V_{tot} = \sum_{n=1}^{N} \frac{4\pi}{3} a_n^3 = \frac{4\pi}{3} a_1^3 + \frac{4\pi}{3} a_2^3 + \cdots + \frac{4\pi}{3} a_N^3 = N_{tot} \frac{4\pi}{3} a^3$$

where $a_1 = a_2 = \cdots = a_N$. Rearranging the expression yields:

$$N_{tot} = \frac{3 V_{tot}}{4\pi a^3} \tag{32}$$

and the total emission surface is:

$$\sigma_{tot} = 4\pi a^2 N_{tot} \tag{33}$$

3.3.4 Average temperature and absorption efficiency

In order to calculate the average temperature for different sizes and distances, the following equation was utilized:

$$\langle T_p \rangle = \frac{\int_{\vec{r}_{min}}^{\vec{r}_{max}} \int_{a_{min}}^{a_{max}} T_p(\vec{r}, a) n(a) n(\vec{r})\, da\, d\vec{r}}{\int_{\vec{r}_{min}}^{\vec{r}_{max}} \int_{a_{min}}^{a_{max}} n(a) n(\vec{r})\, da\, d\vec{r}}$$

where $\vec{\mathbf{r}} = \mathbf{r}(\mathrm{r}, \theta, \varphi)$ is the distance between the dust and the star in spherical polar coordinates. To simplify calculations the temperature is assumed to only vary in the radial direction r, and because it is assumed that the stellar photon flux is radiated isotropically and only is dependent on r. The average temperature can then be given as:

$$\langle T_p \rangle = \frac{\int_{r_{min}}^{r_{max}} \int_{a_{min}}^{a_{max}} T_p(r, a) n(a) n(r)\, da\, dr}{\int_{r_{min}}^{r_{max}} \int_{a_{min}}^{a_{max}} n(a) n(r)\, da\, dr} \tag{34}$$

The PDF for the density distribution is assumed to follow a power law, taking the form:

$$p(r) = \frac{1-\delta}{r_{max}^{1-\delta} - r_{min}^{1-\delta}} r^{-\delta} r \tag{35}$$

i.e. the same as equation *(*22*)*, but as a function of the radial distance between the dust and the star. An average for the absorption efficiency was calculated as:

$$\langle Q_{abs} \rangle = \frac{\int_{a_{min}}^{a_{max}} Q_{abs}(a,\lambda) n(a)\, da}{\int_{a_{min}}^{a_{max}} n(a)\, da} \tag{36}$$

by using the size distribution and calculated between a minimum size and maximum size. With a size and density distribution index of -3.5 (Su et al. 2013), the average temperature tend to be inclined towards the values of the smallest particles and at the distance closest to the star and the absorption efficiency will be dominated be smallest particles. This is because for a power law distribution with an index of 3.5 or larger, all the parameters like temperature and absorption efficiency will be dominated by the smallest particles, since these are more numerous. If the power index is increased, the size distribution will be even more dominated by the smallest particles, which means that the largest dust particles does not make any significant contributions. With an power index of 1 there is a more uniform distribution among the different distances. Figure 4 is an illustration of power law distributions with different power indices, where the panel to the right shows a size distribution and the panel to the right shows a density distribution.

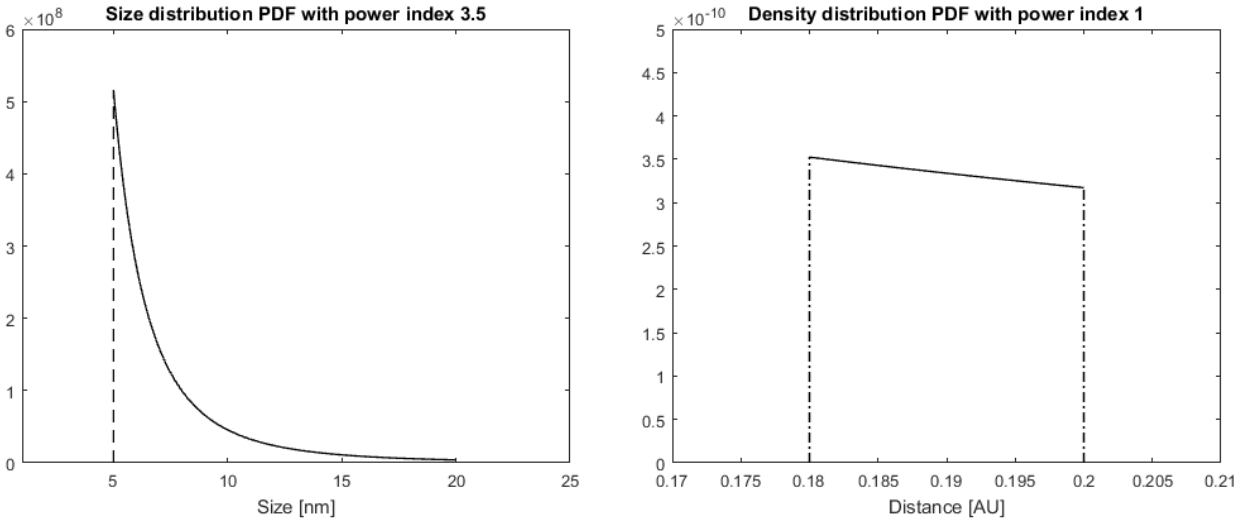

Figure 4: PDFs (probability density distribution) with different power indices. To the left: A size distribution with a minimum radius of 5 nm and a maximum of 20 nm. This figure $(\propto a^{-3.5})$ *is clearly dominated by the smallest dust particles. To the right: A density distribution for a ring between 0.18 and 0.2 AU. For this figure, the number density* $(\propto r^{-1})$ *is distributed more uniformly among the different distances. If the PDFs are integrated for all the possible sizes, the total area is equal to 1, as required.*

3.3.5 Calculating the thermal emission brightness

With all the simplifications in mind, model calculation of spectral energy distribution as expressed in equation *(*21*)* can now be given as:

$$\Phi_{th}(\lambda) = \frac{\pi B_\lambda(\langle T_p \rangle) \langle Q_{abs} \rangle \sigma_{tot}}{d^2} \tag{37}$$

with units of $\frac{W}{m^2 Hz}$ or $10^{-26}\frac{W}{m^2 Hz}$, known as Jansky (Jy).

3.4 Additional considerations

In this section, some additional consideration related to dust around star will be discussed. This includes the sublimation lifetime of dust around a star and whether the dust cloud is optically thin or thick.

3.4.1 Sublimation lifetime

This section follows the description by Lebreton et al. (2013) and Wurz (2012). Cosmic dust can be eroded by different processes, among others sputtering and sublimation. These processes are more important for smaller particles since the erosion takes place at the surface of a particle. Smaller particles have a larger surface to volume ratio compared to larger objects. Sublimation is a phase transition where a material goes directly from solid to gas without passing through a liquid phase.

Generally, sublimation occurs at low pressure and at certain temperatures and the rate of sublimation will increase when the temperature rises. Since the dust is located in the vacuum of empty space, the density of any surrounding gas and the pressure will in practice be zero. Most materials in space will therefore sublimate. If any fragments from the surface of a materials sublimates, there are no possibilities for them to condensate at the surface again. These fragments will be lost into space. Sublimation lifetimes of a dust particle can be estimated if the vapour pressure and the rate of evaporation are known, where the rate of evaporation gives an indication on the tendency of particles to escape from a solid material and the vapour pressure depends strongly on the temperature of a material. The sublimation lifetime will vary with distance from the star since the dust temperature is a function of distance and the temperature is expected to decrease with increasing distance from the star. Calculations on sublimation lifetimes are important because they give an indication of how close to the star the dust can survive without sublimating. The distance where the rate of sublimation of ice becomes negligible compared to the other erosion processes, is known as the snow-line.

Sputtering is a process where the impact of solar wind ions upon the surface of a material leads to the release of atoms or molecules from the material. Both sputtering and sublimation can restrict the lifetime of cosmic dust. In addition, the dust can be destroyed in collisions with other particles.

3.4.2 Optically thickness

The theory considered in this section is applicable for an optically thin dust cloud. It will be shown that the dust disk is optically thin.

If the calculations on the thermal emission brightness are to be fully valid, the dust ring must be optically thin, otherwise the calculations will be an approximation. A dust disk can be assumed to be optically thin if that the total surface area of the dust is much smaller than the surface area of the dust disk. In order to estimate whether or the dust disk is optically thin or not, the surface area of the dust is assumed to be the geometric cross-section, i.e. the dust is viewed pole-on (from above) and the area of the dust disk is assumed to be a ring with an inner radius and an outer radius. These areas are then compared to check if the disk is optically thin.

Given that the dust disk is optically thin, all the dust grains can in practice be observed since the probability of the dust grains overlapping is low. Being optically thin, it can also be assumed that the light from the star is only scattered once by a dust grain and that the thermal emission from a dust grains is not scattered or absorbed by another dust grain and that all dust grains are fully exposed to star light (Evans 1993). If the disk is optically thick, the dust particles might be overlapping. Therefore the estimated mass of the dust might be lower than what it really is, since some of the thermal emission will not be fully observed.

4 Method

This chapter introduces the optical constant which were used in the computing Mie efficiencies, the testing of a Matlab Mie code and its comparison to two different Fortran code, one from Bohren and Huffman (1983) and the other as used by Li and Greenberg (1997) and the computations of dust temperature. The last part in this chapter explains how the thermal emission brightness of the dust was computed.

4.1 Optical constants

A material's optical constant as a function of wavelength is required to derive Mie parameters. In the calculations, the optical constants, or refractive indices, for the following materials were used: amorphous carbon, astronomical silicate, ice and organic refractory from Li and Greenberg (1997) and a mixture of 60 % magnesium oxide (MgO) and 40 % iron oxide (FeO) from Henning et al. (1995). Astronomical silicate is represented as amorphous olivine, $MgFeSiO_4$, in Li and Greenberg (1997) and the astronomical organic refractory is supposedly the outcome of exposing an ice mantle on a silicate core to ultraviolet radiation, which then accumulates in a molecular cloud. It can be noted that amorphous means that a material does not have crystalline structure.

4.2 Testing Mie code

This section discusses the testing of a Matlab program for computations on Mie scattering and absorption and its comparison to two different Fortran programs, one from Bohren and Huffman (1983) and the other from Li and Greenberg (1997). The objective is to examine if the Mie parameters calculated with the Matlab program provide similar results as those from the Fortran programs. If the results from the Matlab program are considered acceptable, they will be used to derive the absorption efficiency, which is needed to calculate the temperature of the dust and the thermal emission brightness. Other Mie parameters can be derived if needed. The reason for using Matlab instead of FORTRAN is that it is user-friendly and has well-developed plotting routines. Different Matlab programs were found, but the most promising program was one from Mätzler (2002), since the documentation in the public domain for this program was comprehensive in comparison to the other programs. The Matlab program from Mätzler (2002) can compute the scattering coefficients from equation *(5)* and *(6)*, efficiencies for scattering, extinction, absorption from equation *(7)*, *(8)* and *(9)*, respectively, as well the asymmetry parameters given in equation *(11)* and two parameters known as the angular scattering functions. Requirements for the Matlab functions is that the sphere is homogenous and dielectric, meaning that the sphere has to be an electric insulator with no flow of free electric charges. As input, the Matlab program need the complex refractive index of the sphere relative to the surrounding medium and the size parameters, as defined in section 3.1 about Mie theory.

4.2.1 Compare to Bohren and Huffman (1983)

The first test run on the Matlab function from Mätzler (2002) was comparing it to Fortran code for a homogeneous sphere from appendix A in Bohren and Huffman (1983) at page 477-482. Running the Matlab programs with the same input parameters as the Fortran program gave the results which are listed in Table 2, Table 3 and Table 4. The input parameters were: refractive index of surrounding medium $N_2 = 1$, refractive index of sphere $N_1 = 1.5500 + 0i$, radius of sphere $a = 0.525\ \mu m$, wavelength $\lambda = 0.6328\ \mu m$ and size parameter $x = 5.213$. In Table 2, Table 3 and Table 4 the Mie parameters which were computed include the scattering efficiency, extinction efficiency, backscattering efficiency, the Stokes parameters S11, S33, S34 and the ratio POL between the Stokes parameters S12 and S11. Only the absorption efficiency and extinction efficiency were used in the

calculations on dust temperature and thermal emission, the other parameters were calculated only to check the code, since they were conveniently given in Bohren and Huffman (1983). As can be seen, there are no differences between the results calculated by the code from Matlab and the code from Fortran for all the Mie parameters in Table 2, Table 3 and Table 4. In Bohren and Huffman (1983), the calculations were done for angles from 0 to 180 degrees, while in the table only angles from 0 to 54 degrees are included. The results for the missing angles computed with the code from Matlab and the code from Fortran were identical.

Table 2: Mie efficiencies from Matlab code compared to Fortran code.

Efficiency	**Matlab**	**Fortran**
Q_{sca}	3.10543	3.10543
Q_{ext}	3.10543	3.10543
Q_{back}	2.92534	2.92534

Table 3: Mie parameters as a function of scattering angle computed with Matlab code.

Angle	**S11**	**POL**	**S33**	**S34**
0	1	0	1	0
9	0.785390	-0.00459811	0.999400	0.0343261
18	0.356897	-0.0458541	0.986022	0.160184
27	0.0766119	-0.364744	0.843603	0.394076
36	0.0355355	-0.534997	0.686967	-0.491787
45	0.0701845	0.00959953	0.959825	-0.280434
54	0.0574313	0.0477927	0.985371	0.163584

Table 4: Mie parameters as a function of scattering angle computed with Fortran code.

Angle	**S11**	**POL**	**S33**	**S34**
0	1	0	1	0
9	0.785390	-0.00459811	0.999400	0.0343261
18	0.356897	-0.0458541	0.986022	0.160184
27	0.0766119	-0.364744	0.843603	0.394076
36	0.0355355	-0.534997	0.686967	-0.491787

45	0.0701845	0.00959953	0.959825	-0.280434
54	0.0574313	0.0477927	0.985371	0.163584

Then, there was an attempt at reproducing scattering coefficients given at page 114 in Bohren and Huffman (1983). These results are given in Table 5 and Table 6, showing that the scattering coefficients computed with the Matlab and Fortran program are not equal.

Table 5: Scattering coefficients computed with Matlab code.

$\boldsymbol{n}$	$\frac{\boldsymbol{2n+1}}{\boldsymbol{n(n+2)}}$	$\boldsymbol{a_n}$	$\boldsymbol{b_n}$
1	$2/3$	0.50069 + 0.49999i	0.73469 + 0.44149i
2	$5/6$	0.33009 + 0.47024i	0.36867 + 0.48244i
3	$7/12$	0.043461 + 0.20389i	0.0078835 + 0.088438i
4	$9/20$	0.00088478 + 0.029732i	0.000056169 + 0.0074943i
5	$11/30$	0.0000074275 + 0.0027253i	0.00000022246 + 0.00047164i

Table 6: Scattering coefficients computed with Fortran code.

$\boldsymbol{n}$	$\frac{\boldsymbol{2n+1}}{\boldsymbol{n(n+2)}}$	$\boldsymbol{a_n}$	$\boldsymbol{b_n}$
1	$2/3$	0.51631 + 0.49973i	0.73767 + 0.43990i
2	$5/6$	0.34192 + 0.47435i	0.40079 + 0.49006i
3	$7/12$	0.048467 + 0.21475i	0.0093553 + 0.096269i
4	$9/20$	0.0010346 + 0.032148i	0.000068810 + 0.0082949i
5	$11/30$	0.0000090375 + 0.0030062i	0.00000028309 + 0.00053204i

Differences between the Matlab and Fortran program will be explored in order to find out why the scattering coefficients are not the same. The Fortran program will be discussed first, followed by the Matlab program.

In the Fortran program, the equations for the scattering coefficients in *(*5*)* and *(6)* are simplified to:

$$a_n = \frac{m\psi_n(mx)\psi_n'(x) - \psi_n(x)\psi_n'(mx)}{m\psi_n(mx)\xi_n'(x) - \xi_n(x)\psi_n'(mx)} \tag{38}$$

$$b_n = \frac{\psi_n(mx)\psi_n'(x) - m\psi_n(x)\psi_n'(mx)}{\psi_n(mx)\xi_n'(x) - \mathrm{m}\xi_n(x)\psi_n'(mx)} \tag{39}$$

where the permeability of the sphere and the surrounding medium is taken to be the same and to further simplify the scattering coefficients, Riccati-Bessel functions are used:

$$\psi_n(\rho) = \rho j_n\rho, \qquad \xi_n(\rho) = \rho h_n^{(1)}(\rho)$$

Calculating the scattering coefficients can be challenging. This is because the required number of terms n for convergence can be quite large and the scattering coefficients are complex functions involving spherical Bessel functions and the derivatives of these functions. In addition, there can be an accumulation of round-off errors due to the representation of a number with an infinite number of digits as one with a finite precision. Equation *(*38*)* and *(*39*)* is not that well suited for computations and therefore the scattering coefficients can be rewritten as:

$$a_n = \frac{[D_n(mx)/m + n/x]\psi_n(x) - \psi_{n-1}(x)}{[D_n(mx)/m + n/x]\xi_n(x) - \xi_{n-1}(x)} \tag{40}$$

$$b_n = \frac{[mD_n(mx) + n/x]\psi_n(x) - \psi_{n-1}(x)}{[mD_n(mx) + n/x]\xi_n(x) - \xi_{n-1}(x)} \tag{41}$$

where

$$D_n(\rho) = \frac{d}{d\rho} ln\big(\psi_n(\rho)\big)$$

is the logarithmic derivate. In the Fortran program, D_n was calculated by downward recurrence where lower orders are generated from higher orders, justified by the fact that D_n is more numerically stable for downward recurrence. Furthermore, ψ_n and ξ_n were computed by upward recurrence where higher orders are generated from lower orders. For computations, the infinite series of the scattering coefficients has to be truncated after a certain number of terms. The number required for convergence can be given by: $x + 4x^{1/3} + 2$ where x is the size parameter and the series is terminated after n_{max} terms (Bohren and Huffmann 1983 p.477). Including more terms can lead to round-off errors because calculation on ψ_n by upward recurrence is unstable. In the Matlab code, these expressions for the scattering coefficients were used:

$$a_n = \frac{m^2 j_n(mx)[xj_n(x)]' - j_n(x)[mxj_n(mx)]'}{m^2 j_n(mx)\left[xh_n^{(1)}(x)\right]' - h_n^{(1)}(x)[mxj_n(mx)]'} \tag{42}$$

$$b_n = \frac{j_n(mx)[xj_n(x)]' - j_n(x)[mxj_n(mx)]'}{j_n(mx)\left[xh_n^{(1)}(x)\right]' - h_n^{(1)}(x)[mxj_n(mx)]'} \tag{43}$$

where $\mu = \mu_1$ and built-in Matlab functions were used for calculations of the Bessel functions.

However, it is not clear whether forward or upward recurrence were used to compute the spherical Bessel functions j_n and h_n. In order to truncate the series, the same condition as in the Fortran code was applied. As a summary, the main difference between the two programs is that they use a different expression for the scattering coefficients, but otherwise there are no obvious differences.

4.2.2 Compare to Li and Greenberg (1997)

In addition, the Matlab code was additionally compared to a Fortran program from Li and Greenberg (1997). The results are shown in Figure 5 for a mixture of 60 % MgO and 40 % FeO with a size of 5 and 20 nm. By viewing Figure 6, it is apparent that the difference between the two codes is less than 0.04 %.

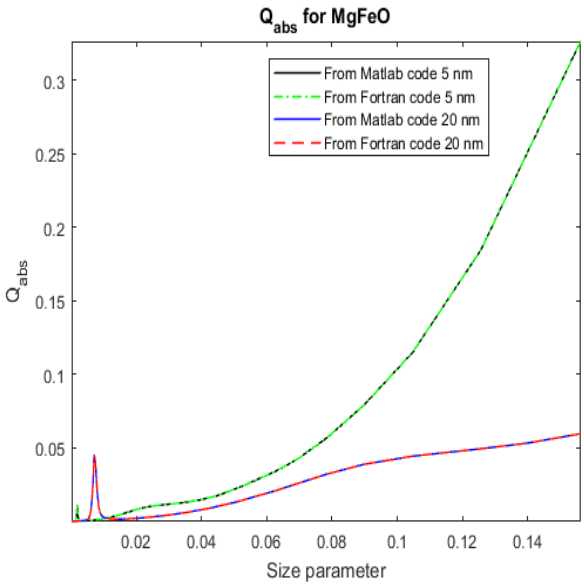

Figure 5: Comparison of absorption efficiencies derived with a program from Matlab and Fortran for a dust particle consisting of a mixture of MgO and FeO with a size of 5 and 20 nm.

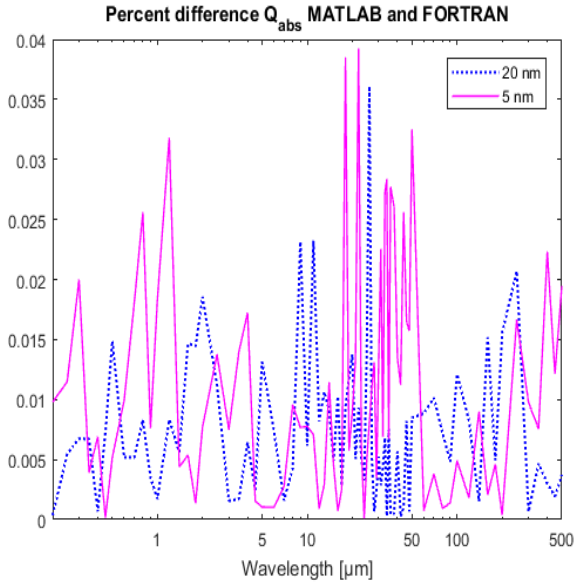

Figure 6: Percent difference between Q_{abs} derived with Matlab and Fortran program for MgO/FeO with a radius of 5 and 20 nm.

4.2.3 Conclusion

All in all, the Matlab program performs well. The only case where the results computed by the Matlab program differed significantly from those computed by the Fortran program was for the scattering coefficients. The difference was likely caused by the use of different equations for the scattering coefficients. For the most important parameters, which are the scattering and absorption efficiency, the Matlab code provides satisfactory results. Therefore, it is concluded that the Matlab program can be applied to calculate the Mie parameters.

4.3 Calculating dust temperature

The temperature of dust was computed by implementing equation *(20)*. This was done with two different programs, both developed in Matlab. These two programs have different input and output. The first program, called input_temperature, takes dust temperature as an input and gives the corresponding distance from the star as an output, while the other program, named input_distance takes distance from the star as an input and gives dust temperature as an output. Developing two

separate programs made it possible to compare them to each other to see if the computed dust temperatures were similar. The two programs were also compared to an analytical solution.

The temperatures were calculated for the materials mentioned in section 4.1, such as astronomical silicate, amorphous carbon, ice, organic refractory and a mixture of MgO and FeO with a radius of 5, 20, 100 nm and 1 μm in a dust ring between 0.18-0.2 AU. A dust ring around 0.99-1.01 AU was tested for Vega and a ring at 1 AU for Fomalhaut, as a comparison. For the Sun, the temperature was computed for a distance of 0.01 to 2 AU as part of testing the two Matlab temperature programs mentioned previously. This was done with a radius of 10 nm, 100 nm and 1 μm for all the materials, except MgO/FeO which was computed for 5, 20, 100 nm and 1 μm. In equation *(*18*)*, for the calculated absorbed power, the effective temperature and radius of the star from Table 1 were used. Additionally, for the Sun the dust temperature was calculated by using a black body spectrum and a real spectrum. This was not done for Vega and Fomalhaut since it was challenging to find a real spectrum for these stars for a wide range of wavelengths. The three following sections describe the two Matlab dust temperature programs and also the processing of data for a real spectrum of the Sun, which were used as input for the Matlab function input_distance. All computations on dust temperature use absorption efficiencies derived by Mie theory.

4.3.1 Matlab dust temperature program

The Matlab program input_temperature was the first to be developed for computing dust temperature. As inputs, it needs dust temperatures, absorption efficiency as a function of wavelength, distances from the star and a spectrum for the star, assumed to be black body in all the calculations. The program works by looping through all the input dust temperatures, taking in one dust temperature one at time, calculating the emitted power of the dust particle. It also computes the absorbed power for all the input distances. In the loop, there is an attempt at finding the distance were the absorbed power is as identical as possible to the emitted power, since it is assumed that the absorbed power is equal to the emitted power. This was done by subtracting the absorbed power from the emitted power and looking for the minimum value of this subtraction. Ideally this minimum value should be zero, but since the calculations are done numerically, this will not be the case. The minimum value should be reasonably small, though. When the index of the distance which gives the minimum value is found, the corresponding distance is given as an output. If there is no good match between the input dust temperatures at a certain input distances due to low resolution of the input distance, or that the temperature is out of range, the resulting output distance will be inaccurate. For example, if the input dust temperature is from 100-1000 K for the Sun and the input distance is 0.01-1 AU, there might be no good match between the dust temperatures at a distance. The suitable interval varies with material and size. In order for the output distance to be accurate, the input distance need to have a large range with a high resolution, which slows down the program. Due to this, the program is somewhat impracticable to use and it was not used to find the dust temperature for Vega and Fomalhaut, it was only tested for the Sun.

Figure 7 shows the input dust temperature plotted together with black body temperatures calculated with Stefan-Boltzmann law at the distances given as output from the function input_temperature. In Figure 8, the error between these two temperatures is displayed. The top panel in Figure 8 shows the fractional difference between these two temperatures, while the bottom panel shows the difference where the two temperatures have been subtracted. For higher temperatures, i.e. closer to the star, the error seem to increase, which may be caused by a faster rise in temperature closer to the star and here

the resolution for the distance used as an input should probably be higher compared to further from the star. At these distances, outward of 0.1 AU, the temperature increases more slowly, as can be seen in Figure 7.

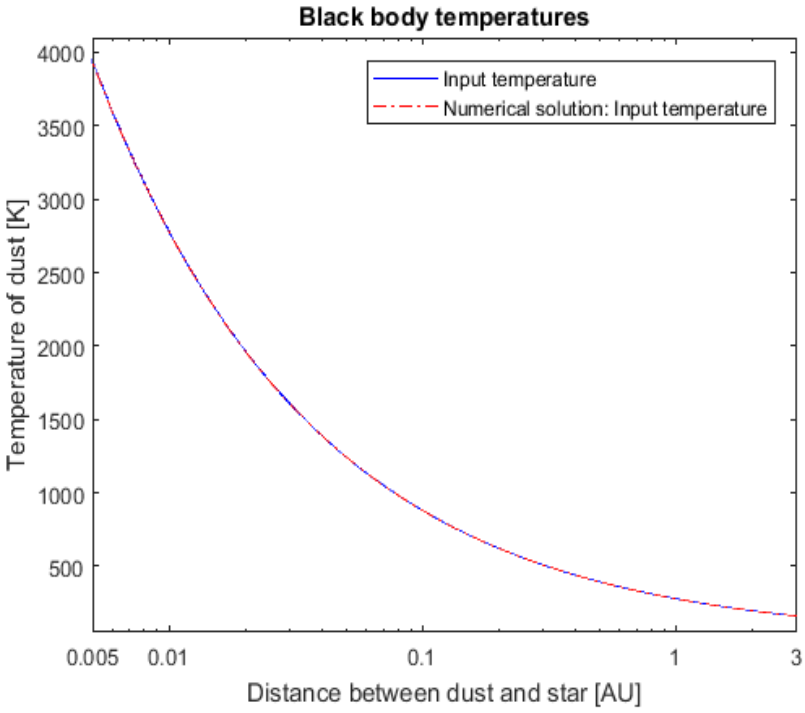

Figure 7: Comparison between the temperatures which were used as input and a black body temperature at the distances given as outputs from the Matlab function input_temperature.

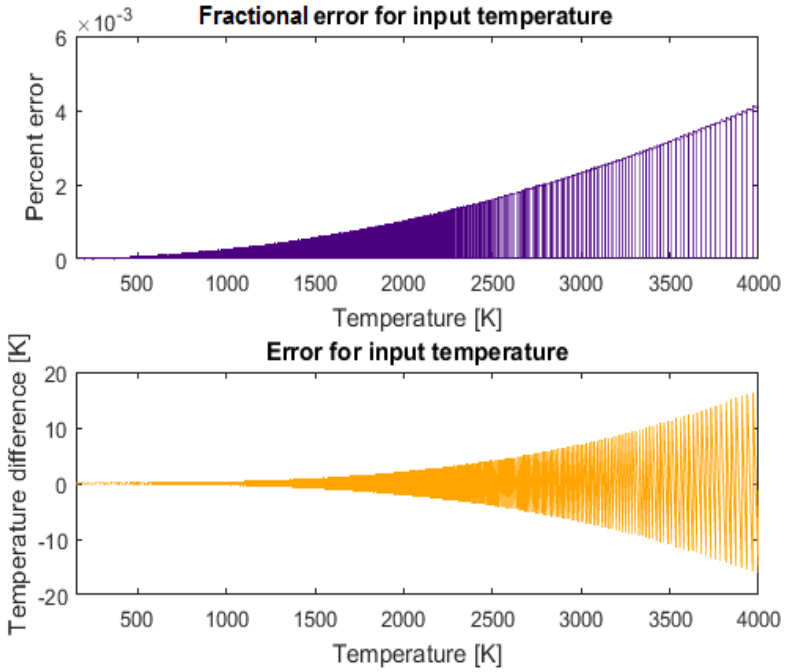

Figure 8: Fractional error (top panel) and error (bottom panel) between input dust temperature and black body temperature at output distance. In the top panel, the error is less than 0.6 %.

In this part, there will be a discussion on the testing of the Matlab function input_distance, which calculates the temperature for a given material at an arbitrary distance from the star. The idea for this program is inspired by Aasmus et al. (2014), where an iterative scheme was used to derive the temperature of a spherical particle. The authors of the article compute the temperature for mesospheric dust particles. In the initial step of the programme, the temperature is set to be equal to the ambient atmospheric temperature, using the temperature in a previous step to derive the temperature. Then, the iteration is terminated when the dust temperature reaches an asymptotic value. Modifying the iteration scheme and using a different way of terminating made it possible to derive the temperature of dust around a star. The function needs the absorption efficiency and the radius of the dust particle as an input. The output is dust temperature as a function of distance. It also needs an initial temperature, i.e. a temperature in the initial step of the iteration, which for simplicity was set to be the black body temperature at a given distance. In this program, the absorbed power is calculated by using the effective temperature of the star. The emitted power is found by inserting the start temperature and iterating one distance at a time through a loop; the function looks for a temperature of the dust for which the emitted power is approximately equal to the absorbed power, i.e. it is assumed that the dust particle is in thermal equilibrium. The iteration is terminated when the absorbed power is the same as the emitted power.

The emitted power will never be exactly equal to the absorbed power due to round-off errors, however. A stop value was therefore included, which means that the function will stop when the difference between the emitted power and the absorbed power is very small. If the stop value is set too low, the function will be very slow, but if it is too high, the estimated temperature of the dust can be inaccurate. Therefore, the stop value was chosen so that there was a balance between speed and accuracy. In order to find the desired temperature, a small value was added or subtracted from the start temperature, depending on whether the emitted power was too high or too low compared to the absorbed power. At first, this value was set too low and because of this, the program was exceedingly slow. When this value was adjusted to be higher, the program worked a lot faster. This value cannot be too high though, since the emitted power may then turn out to be too high or too low and the difference between the emitted power and the absorbed power will always be larger than the stop value. It will cause the loop to never finish, jumping back and forth between temperatures of the dust that is either too high or too low, i.e. the program will be stuck in an infinite loop.

Figure 9 shows the difference between a numerical solution of the dust temperature calculated with the function input_distance and an analytical solution, where the analytical solution is the temperature of a black body, derived with Stefan-Boltzmann law. As described in Figure 8, the top panel in Figure 10 shows the error in percent and the bottom panel shows the error where the numerical solution has been subtracted from the analytical solution. It can be seen in Figure 10 that the error between the numerical solution and the analytical solution is quite low, less than 10^{-5} %. The start temperature used in these calculations was $\pm\ 100\ K$ of black body temperature.

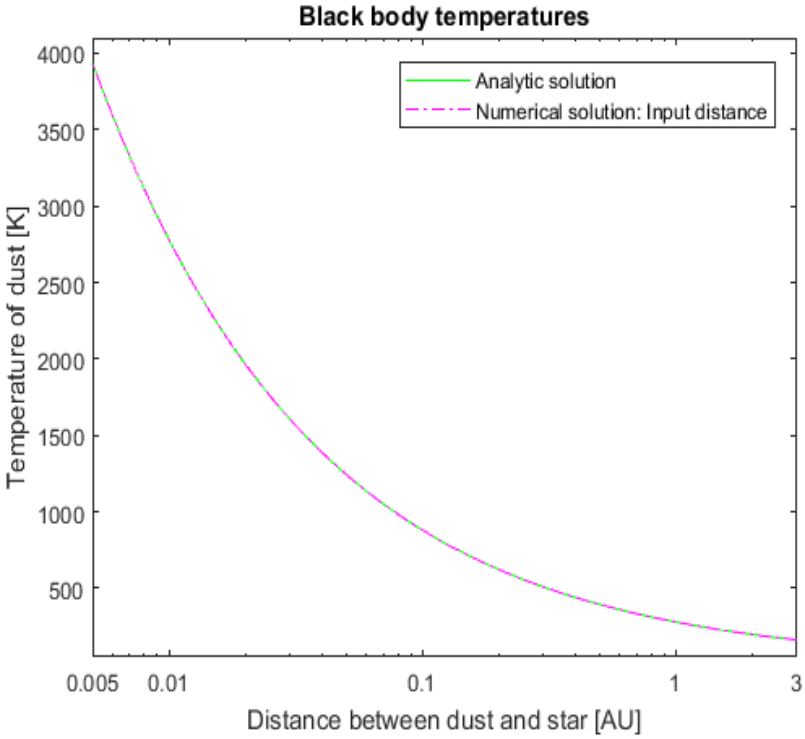

Figure 9: Plot of an analytical solution for a black body computed with Stefan-Boltzmann law and a numerical solution computed with the MATLAB function input_distance.

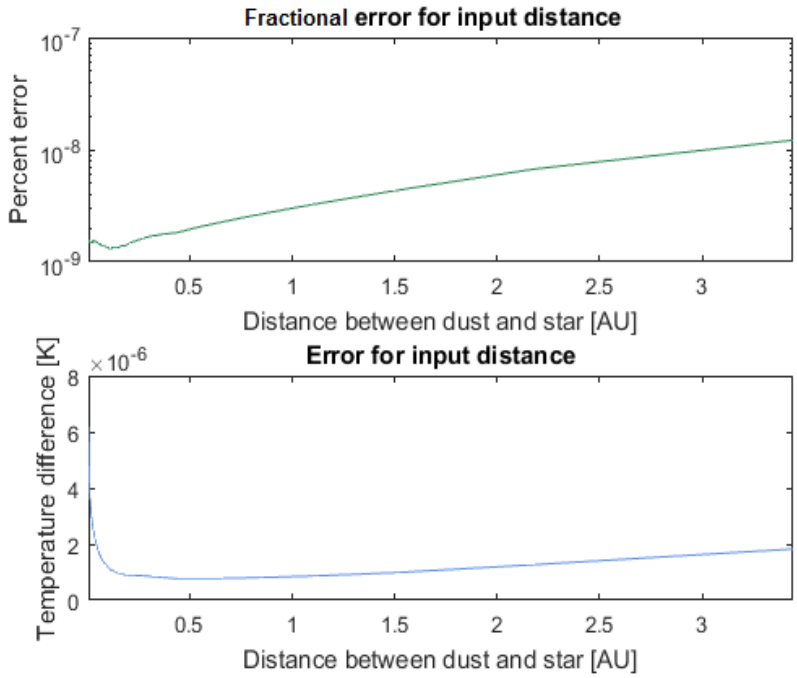

Figure 10: Fractional error (top panel) and error (bottom panel) between analytical solution and numerical solution, as described in Figure 9. The error is less than 1e-5 %.

In order to test the performance of the Matlab function input_distance, the dust temperature was estimated by trying different start temperatures. Putting in a negative start temperature gave erroneous result of a factor $\sim 10^{11}$, the same was the case for a start temperature 400 K higher than a black body temperature. These errors only occurred farther away from the star at about 2-3 AU, but increasing the start temperature resulted in shifting the erroneous temperature closer to the star. It can be concluded that the program does not perform well when the start temperature is negative or too high, but it is not entirely clear yet why this is happening. This should in any case be explored further. Adding an error message for dust temperature higher or equal to the effective temperature of the star has been done in order to be warned when erroneous dust temperatures occur. In some ways it can be viewed as fortunate that the erroneous dust temperatures are so large, since they will then be easier to spot. It can be concluded that the temperature program needs a reasonable input temperature, in this case the black body temperature at the same distance as the dust particle. The temperature program works well within certain limits and it has worked well for the calculations in this work.

Computing dust temperatures with a larger size than 1 μm was also tested. When calculating the dust temperature of a particle with a radius of 10 μm, the estimated temperature of a dust particle consisting of ice turned out to be wrong with a factor $\sim 10^{11}$. The temperature of the other materials for a 10 μm dust particle appears to be correct since they were not too low or too high compared to black body temperatures. One explanation for the erroneous temperature of ice may be that the absorption efficiencies are incorrect. As mentioned before, the absorption efficiencies were computed with a Mie code in Matlab, which mainly has been tested for particles ≤ 1 μm and the code works well for dust particles with these sizes. So, whether the Matlab Mie code works for particles with a radius of 10 μm has not yet been tested thoroughly. It can be noted that the Mie code did not seem to work for 1 mm particles. Mätzler (2002) stated that the code performs poorly for large size parameters. All in all, the dust temperature for a 10 μm ice particle may be incorrect due to the absorption efficiencies, but this is not a major concern since dust particles with this size are not the main focus and were only computed for comparison.

4.3.2 Real solar spectrum

Using a real spectrum for the Sun made it possible to compare dust temperature with a black body spectrum and a real spectrum. Data for the spectrum of the Sun was downloaded from LISDR (Lasp interactive solar irradiance datacentre). A spectrum during solar minimum (2009) and solar maximum (2015) were chosen for comparison. The data was converted to SI units with the wavelength in meters and the irradiance in [W/m^{2}m] since this simplifies the calculations and reduce the risk of errors due to units. Negative value and NaN (not a number values) for the irradiance were removed. Between 39.5 nm and 115.5 nm there was a gap in the spectrum from 2009 and 2015. Data for this gap was retrieved from LISDR. The missing wavelengths and irradiances were then put into the spectrum from 2009 and 2015. Since the refractive indices started on a longer wavelength compared the real spectrum, the real spectrum was cut at approximately 92 nm for astronomical silicate, amorphous carbon, ice and organic refractory and at 200 nm for MgO/FeO in order to avoid extrapolating the refractive indices. There was no data at wavelengths longer than 2 μm for the real spectrum, but there was data for the refractive indices here. A black body spectrum was used for the missing wavelengths. The irradiance of the real spectrum had to be derived as a function of distance from the Sun and therefore the power at the photosphere was computed since the irradiance of the real spectrum was at 1 AU. Lastly, the refractive indices were interpolated so that the resolution of the real spectrum and the refractive indices were the same. Figure 11 displays the spectrum from 2009 at solar minimum and from 2015 at

solar maximum compared with a black body spectrum. Additionally, where the spectrum was cut is also shown in Figure 11, here shown at 200 nm which was at the wavelength where the refractive indices for MgO/FeO started.

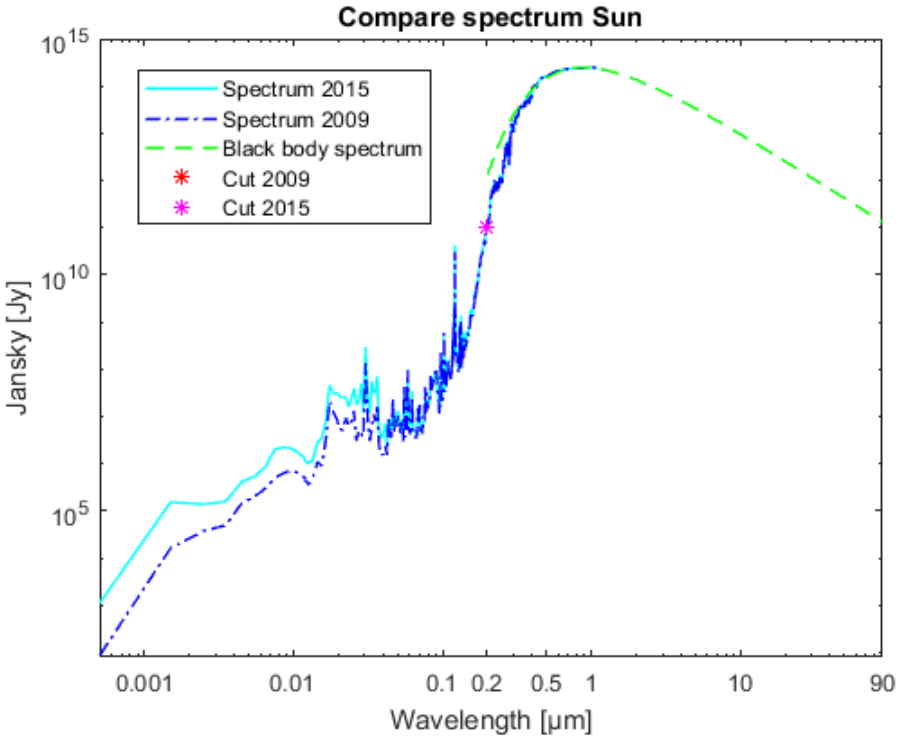

Figure 11: Real spectrum of the Sun from solar minimum (2009) and solar maximum (2015) compared with a black body spectrum. The red/magenta point shows were the spectrum was cut in order to avoid extrapolating the refractive indices, here shown for the refractive indices of MgO/FeO which started at 200 nm.

4.4 Thermal emission brightness

This section discusses how the thermal emission of dust was derived. As mentioned in section 4.1, the optical constants were obtained from Henning et al. (1995) and Li and Greenberg (1997) and these were used to compute absorption efficiencies with the Mie code mentioned in section 4.2 from Mätzler (2002) for dust particles with a radius of 5, 20, 100 nm and 1 µm. In the sections below, there will be a discussion on which size and density distribution power indices that were chosen for the different stars. There will be a discussion on how the average absorption efficiency, average dust temperature and total emission surface were computed and what observation constraints that were put on the modelling of SEDs.

4.4.1 Size and density distribution power index

For Vega and Fomalhaut, the size distribution power index was set to be -3.5 like Su et. al. (2013). The density distribution power law index for Vega and Fomalhaut is supposedly less than -3 (Su et al. 2013). In the solar system, the number density decreases farther away from the Sun and follows r^{-1} outward of 0.3 AU, concentrated at the ecliptic plane. Inward of 0.3 AU there are no firm number density due to lack of observations (Mann et al. 2003). Therefore, the density distribution power index was simply set to -1 for Sun and the size distribution index was set to -3.5.

4.4.2 Average absorption efficiency and average dust temperature

By using equation *(36)*, an average absorption efficiency was found for a size distribution between 5 and 20 nm. This was done in Matlab with trapezoidal numerical integration. Figure 12 shows a plot of the absorption efficiency for a dust particle with a radius of 5 and 20 nm and an average absorption efficiency between these sizes. Also shown in Figure 12, as a comparison for the derived average absorption efficiency, is the absorption efficiency of the mean radius which was computed by using equation *(23)*. With a minimum radius of 5 nm and a maximum radius of 20 nm and a size distribution power index of -3.5 (Su et al. 2013), gives a mean $\mu \approx 7.53$ nm. In Figure 12 it can be seen that the average absorption efficiency is the same as the absorption efficiency of the mean radius.

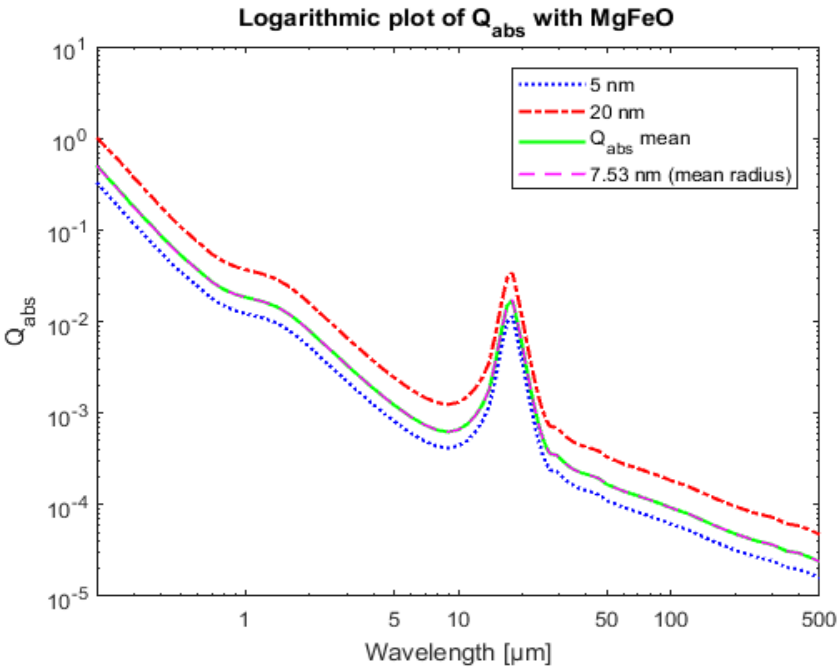

Figure 12: Absorption efficiency of a dust particle with radius 5, 7.53 and 20 nm, as well an average absorption efficiency between 5 and 20 nm. The radius of 7.53 nm is a mean radius. Q_{abs} is dimensionless.

The average temperature was found with equation *(34)*, again with trapezoidal numerical integration in Matlab, by using the size distribution in equation *(22)* and the density distribution in equation *(35)*. First, the temperature could be integrated with respect to distance so that the temperature's dependence on distance disappeared, then it could be integrated with respect to size, if needed. Integrating the temperature with respect to size and distance separately, had the advantage that calculations were simplified when the temperature was only dependent on size or distance. Due to the size distribution, the average temperature was inclined towards the temperature of the smallest particles at the distance closest to the star, in this case the 5 nm particles at 0.18 AU, as mentioned before.

4.4.3 Total emission surface

Calculations on the total emission surface of the dust population was done by using equation *(30)* for 5 to 20 nm with a size distribution power index of -3.5 (Su et al. 2013) or equation *(33)* where all the dust particles are assumed to have the same size. This was done for the Sun, Vega and Fomalhaut. The total emission surface was derived by first assuming a total mass of the dust with the use of equation

(25) and then computing the total volume of the dust with equation *(24)*. Computing the total volume requires that the mass density of the material is known. For ice, carbon, astronomical silicate and MgO/FeO the mass density was assumed to be 1000 kg/m^3, 1850 kg/m^3 and 3300 kg/m^3 (Köhler and Mann 2002), and 4800 kg/m^3 (Su et al. 2013), respectively. When the total volume of the dust is known, the total number of dust particles can be calculated with equation *(31)* or *(32)*, which is needed in order to compute the total emission surface. The mass of the dust was derived in units of number of Halley comets, since this is presumed easier to comprehend than the dust mass in units of kilos or tons.

4.4.4 Computations on thermal emission brightness

The dust population will thermally emit a flux observed at a distance d from Earth and the spectral energy distribution can be computed with equation *(37)*. For Vega and Fomalhaut, the distance d was assumed to be 7.76 parsec and 7.69 parsec, respectively (Köhler and Mann 2002). Deciding on a distance d for dust observations around the Sun was not so straightforward, since this will depend on where the dust is observed. The dust can be observed from ground-based telescopes or by satellites in orbit around the Earth or the Sun and so on. For all the calculations on thermal emission from dust around the Sun, it was simply assumed that the dust was observed from a distance of 1 AU.

4.4.5 Observational constraints

Below are the observational constraints that were included for the modelling of SED from hot dust emission around Vega and Fomalhaut.

Vega:
K-band (FLUOR): 2.12 µm (Absil et al. 2006).
H-band (IONIC): 1.65 µm (Defrère et al. 2011)
Blinc: 10.6 µm (Defrère et al. 2011)
All these interferometric observations have sampled a specific part of the inner disk of Vega, but with different instruments (FLUOR, BLINC, IONIC).

Fomalhaut:
K-band: 2.18 µm (Absil et al. 2009).
N-band: 8.25-12.69 µm (Mennesson et al. 2013).
Spitzer/MIPS: 23.68 µm (Lebreton et al. 2013).
Herschel/PACS: 70 µm (Lebreton et al. 2013).

The total mass of dust around Vega and Fomalhaut was adjusted so that the absolute brightness of the spectral energy distribution fit into the K-band, since both stars conveniently had measurements in this band. Due to lack of observation around the Sun, the dust mass was assumed to be equivalent to one Halley comet. All the measurements of mid-infrared excess around Vega is mentioned in Defrère et al. (2011) as a fraction in percent of the flux from the Vega. Unfortunately, for the interesting wavelengths, which are 1.65, 2.12 and 10.6 µm, the flux of Vega is not given. The same applies to the measurements of an excess around Fomalhaut in Mennesson et al. (2013). Here, the excess is given as a fractional excess, but the flux of Fomalhaut is not given. Therefore, due to a lack of data for the spectrum of Vega and Fomalhaut, a black body spectrum was assumed for these stars, which was then multiplied by the fractional excess to find the brightness of the dust at in given bands. In Mennesson et al. (2013), the observations in the N-bands were done over four different nights and because of this,

there are four different measurements for each of the wavelengths. By using equation *(51)* for a weighted mean and equation *(52)* for the corresponding uncertainty, the fractional excess at each of the wavelengths in the N-band was computed with the four different measurements in Mennesson et al. (2013). Equation *(51)* and *(52)* are given in appendix 9.1.

4.5 Beta-values

Beta-values were computed with equation *(15)*. All the stellar parameters which were used in the computations are listed in Table 7. These stellar parameters are the same as in Köhler and Mann (2002), which make comparison easier since this article shows calculated beta-values for the Sun, Vega and Fomalhaut. The mass density for the different materials are the same as listed in section 4.4. A black body spectrum was assumed for the stellar brightness. The radiation pressure efficiency was derived with equation *(11)* by using Mie theory. It was assumed that the dust particles are spherical and the geometric cross-section and volume was therefore assumed to be πa^2 and $4\pi a^3/3$, respectively. The mass was determined with $m = \rho V$. Integrating the expression in equation *(15)* from a minimum to a maximum wavelength was done in Matlab with trapezoidal numerical integration. Computed beta-values were compared to the large particle limit, which is an approximation, given in equation *(16)* and equation *(17)*.

Table 7: Stellar parameters used in computations for the beta-values. Source: Köhler and Mann (2002):

Star	**Temperature [K]**	**Mass** $[M_{Sun}]$	**Radius** $[R_{Sun}]$
The Sun	5800	1.0	1.0
Vega	9553	2.5	2.0
Fomalhaut	8760	2.3	1.7

5 Results and analysis

This chapter presents the results of calculations on dust temperature around the Sun, Vega and Fomalhaut with different composition and sizes and at different distances. The dust composition includes ice, amorphous carbon, astronomical silicate, organic refractory and a mixture of MgO/FeO and the sizes ranges from 5 nm to 1 µm. In addition, computations on sublimation lifetimes will be presented. There will also be a presentation of derived spectral energy distribution for thermal emission by dust. Finally, calculated beta-values will be presented.

5.1 Dust temperature

In this section, a selection of figures showing dust temperature will be presented. The rest of the figures will be presented in appendix 9.2.1. First, dust temperature around the Sun will be discussed, followed by Vega and Fomalhaut. Additionally, temperatures computed with a real solar spectrum will be compared to those computed with a black body spectrum for the Sun.

Figure 13 shows the temperature of astronomical silicate, distributed in a dust belt between 0.01-2 AU around the Sun for dust particles with a radius of 10 nm, 100 nm and 1 µm compared with temperature of a black body. In Li and Mann (2012), the equilibrium temperature of silicate dust with a radius of 5 nm at a distance of 1 AU from the Sun was 282 K. The computed dust temperature of astronomical silicate with a radius of 5 nm (not shown in Figure 13) at 1 AU around the Sun was found to be 286 K, corresponding to a difference of 1.4 %. Inward of 2 AU, the dust temperatures shown in Figure 13 are higher than black body for all the different sizes. Farther away from the Sun, moving towards 2 AU, the dust temperatures seem to be approaching black body temperature. Figures of dust temperature for the rest of the materials are displayed in appendix 9.2.1.

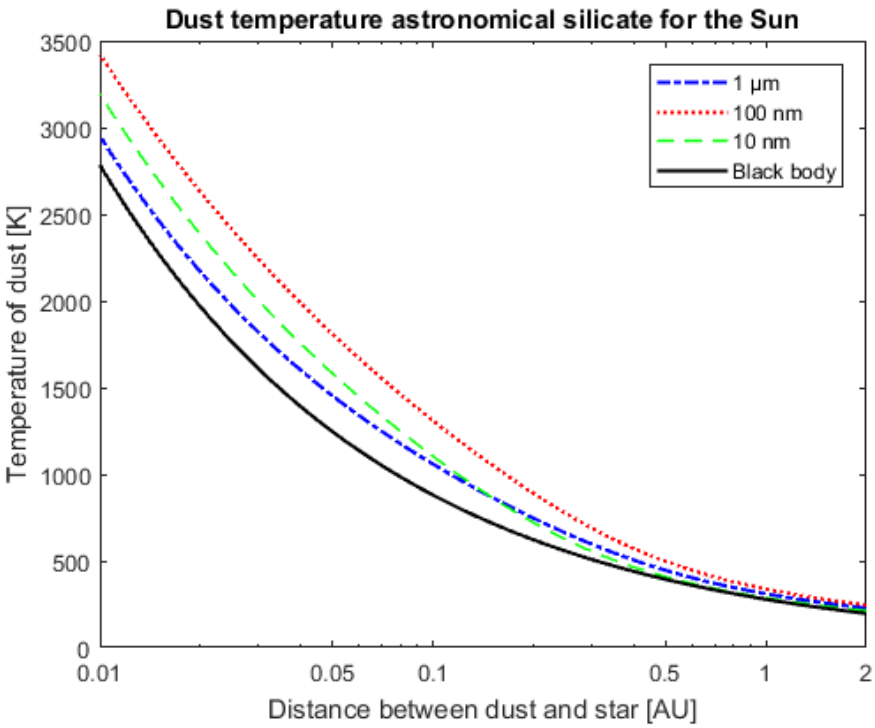

Figure 13: Temperature of dust consisting of astronomical silicate with a radius of 10 nm, 100 nm and 1 µm from a distance of 0.01-2 AU from the Sun. Also shown is the temperature of black body as a comparison.

From these figures, it is noticeable that dust temperature varies greatly with dust composition and size, but also with distance from the Sun. For instance, dust composed of ice with sizes 10 nm, 100 nm and 1 µm around the Sun have a temperature which is lower than black body. Generally, dust particles composed of amorphous carbon, a mixture of MgO/FeO or organic refractory with a size less than 1 µm have a temperature which is higher than black body, while larger dust particles have a temperature which is lower or higher than black body depending on the distance from the Sun.

Figure 14 shows the temperature of astronomical silicate dust with a size of 5 nm computed with an assumed black body spectrum for the solar brightness, compared with the temperature calculated with a real spectrum at solar minimum in 2009 and solar maximum in 2015. In Figure 14, dust temperature computed with a real solar spectrum seems to be lower than the dust temperature computed with a black body spectrum for the Sun. This is also the case for dust particles consisting of astronomical silicate with a size of 20 nm and 100 nm. For a size of 1 µm the dust temperatures computed with a real and a black body spectrum for the Sun are similar, see appendix 9.1. On the other hand, it has been taken into account that the solar spectrum was cut at 92/200 nm and therefore a lot of the variation between a real solar spectrum and a black body spectrum for the Sun may have been removed. Due to this, drawing conclusion on how the dust temperature differs by using a real solar spectrum and a black body spectrum should be done with care. Ideally, the solar intensity at shorter wavelength should be included in the calculations on dust temperature, but this requires that the refractive indices of a material have been derived at shorter wavelengths. If there are no available data for the refractive indices at shorter wavelengths, the data could possibly be estimated by extrapolating. Though, if the knowledge of how the refractive indices behaves at shorter wavelengths is inadequate, the extrapolation will have a large uncertainty and it will be guesstimation.

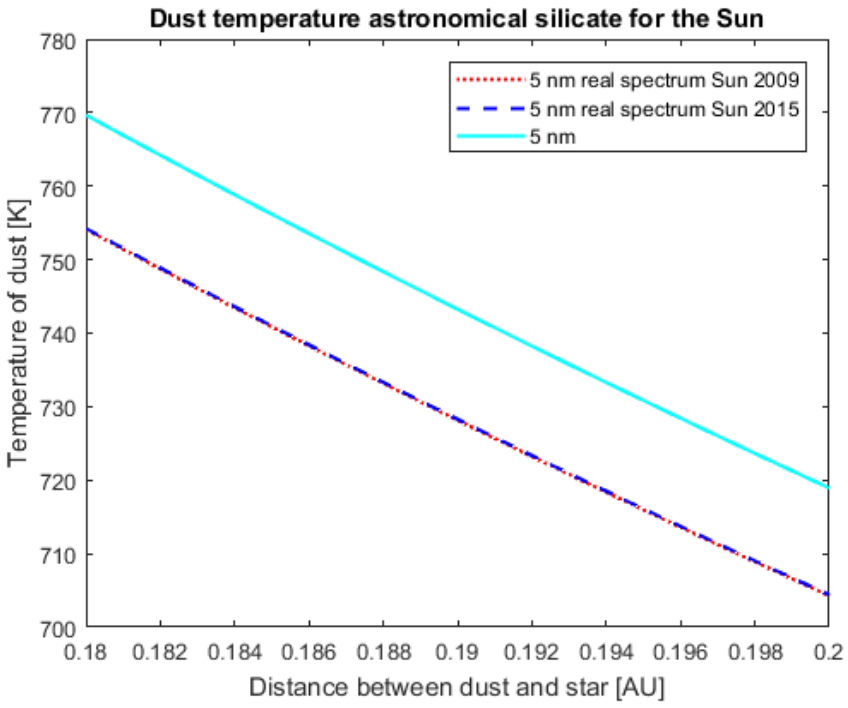

Figure 14: Dust temperature of astronomical silicate with a radius of 5 nm in a ring between 0.18-0.2 AU computed with a black body spectrum and a real spectrum for the Sun.

When it comes to the difference between dust temperatures derived with a solar spectrum at minimum and maximum, in Figure 14 the difference seems to be small. Looking at Figure 11 reveals that the most significant differences in intensity between a solar spectrum at minimum and maximum is at wavelengths from 0.001-0.1 µm (1-100 nm) in the UV, which is not included in the derivation of dust temperatures. Whether dust temperature will vary by using a solar spectrum at minimum or maximum is not entirely clear and this is something that should be explored further.

In Figure 15 and Figure 16, dust temperatures around Vega and Fomalhaut for dust particles consisting of a mixture of MgO/FeO are presented. It is apparent that the dust temperatures in Figure 15 and Figure 16 are significantly higher than dust temperatures around the Sun with dust particles consisting of MgO/FeO, shown in Figure 35 in appendix 8.2.1. For Vega, the temperatures reach almost 3000 K, for Fomalhaut the highest temperatures are around 2300 K and for the Sun ~1200 K. The dust temperatures of the other materials, ice, astronomical silicate, amorphous carbon and organic refractory, are in general highest around Vega. Fomalhaut has a lower temperature than Vega, where the temperatures are 600-800 K lower than those for dust around Vega. For the Sun, the dust temperatures are less than half of the temperatures around Vega. Why the dust temperatures are significantly higher around Vega and Fomalhaut can be explained by looking at the expression for the absorbed power, which is given in equation (18). Here it is shown that the absorbed power is proportional to the radius of the star squared. From Table 1, one can see that the radius of Vega at the equator is nearly three times as large as the radius of the Sun, while the radius for Fomalhaut is approximately twice as large as the radius for the Sun. This means that the amount of absorbed power is sensitive to the radius of the star and will increase with a larger radius, which can contribute to why the dust temperatures are higher around these stars, especially around Vega with its large radius at the equator. In addition, the higher stellar flux around Vega and Fomalhaut compared to the Sun will also contribute to an increase in dust temperatures around these stars.

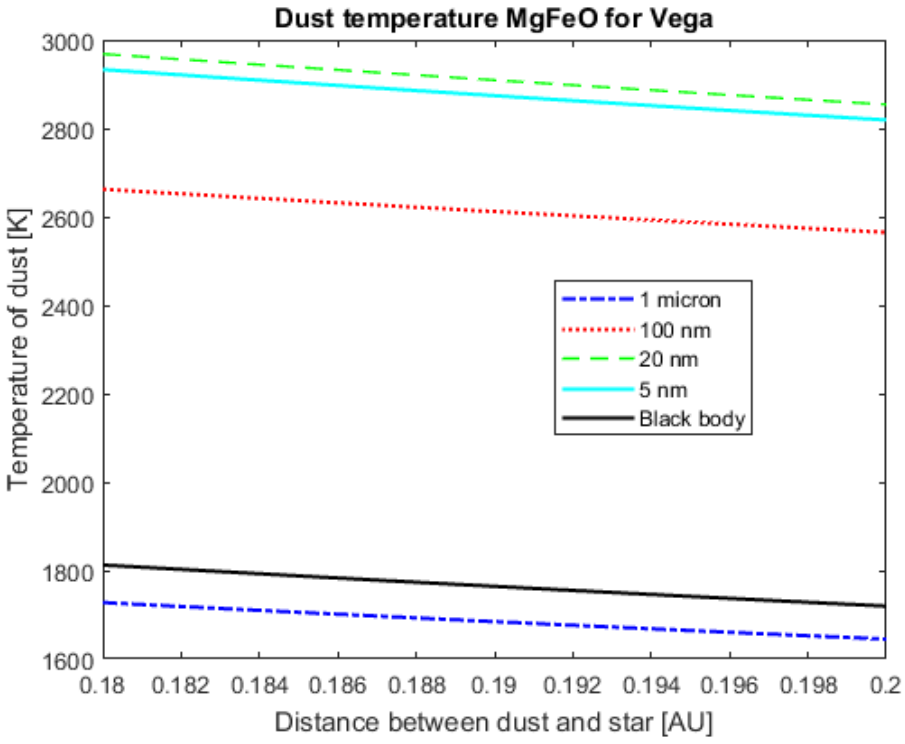

Figure 15: Dust temperatures around Vega with dust particles consisting of a mixture of MgO/FeO.

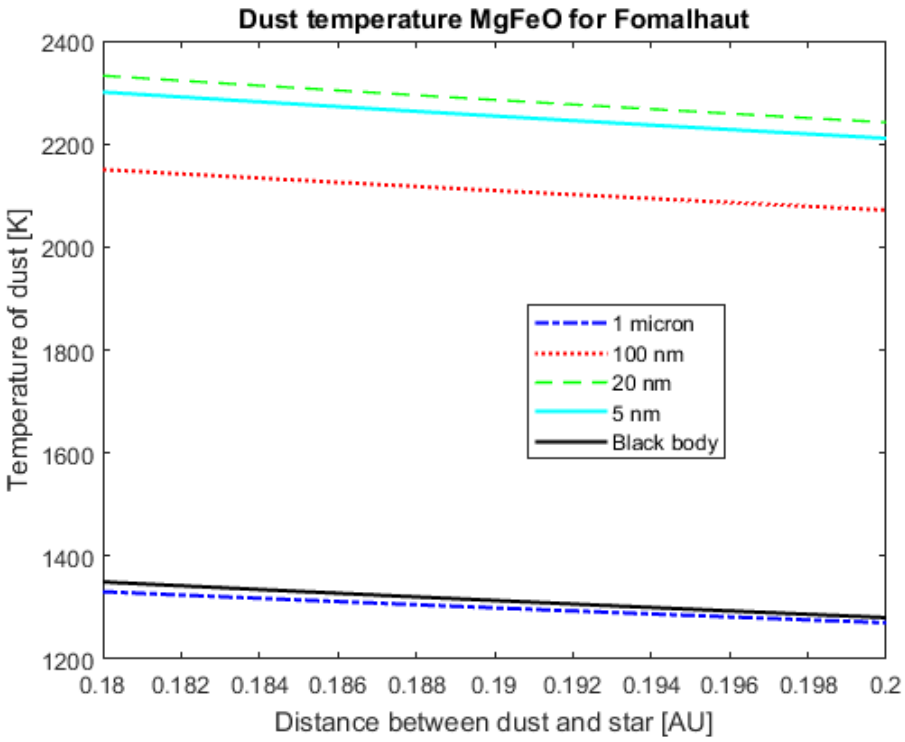

Figure 16: Dust temperatures around Fomalhaut with dust particles consisting of a mixture of MgO/FeO.

Su et al. (2013) computed temperatures for dust particles consisting of a mixture of MgO/FeO, located in a narrow ring between 0.18-0.2 AU around Vega. They found that the dust temperatures reach ~2400 K. These dust temperatures are ~600 K higher than those displayed in Figure 15. The dust temperatures which Su et al. (2013) calculated were found by using a stellar model computed by Aufdenberg et al. (2006). In the article by Aufdenberg et al. (2006), the spectral energy distribution of Vega as viewed from its equatorial plane was predicted with interferometric measurements. Thus, the difference between the temperatures computed by Su et al. (2013) and those shown in Figure 15 may be due to the use of a different stellar spectrum, since the dust temperatures in Figure 15 were calculated with a black body spectrum for Vega.

In general, dust with various compositions and sizes have a temperature which is different from a black body. Whether the temperature is higher or lower than black body is dependent on composition, size and distance from the star. In Yamamoto and Mukai (1998), it was found that dust particles composed of pure olivine with a size less than 1 µm have a temperature which is higher than black body, while those larger than 1 µm have a lower temperature. Wyatt (2009) stated that small dust particles can have a temperature which is notably higher than black body since these particles emit less efficiently at longer wavelengths, but this will depend on the composition of the dust. Looking at Figure 17 , it is apparent that the dust particles with a radius of 5 nm emits less efficiently at longer wavelengths compared to dust particles with a radius of 1 µm. Generally, small dust particles have an emission efficiency which is different from blackbody.

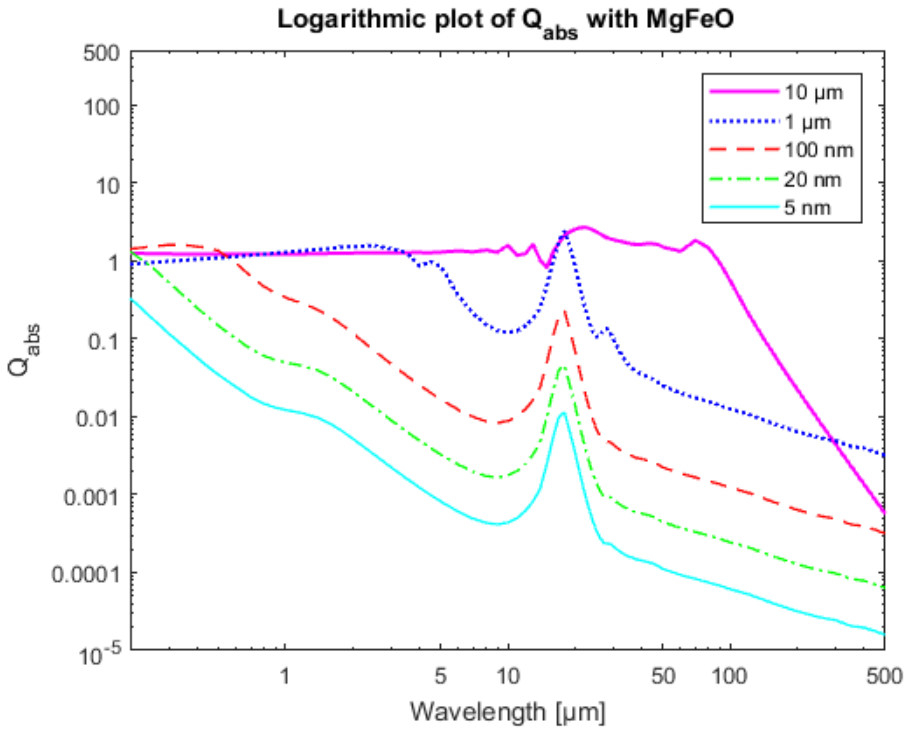

Figure 17: Absorption efficiency as a function of wavelength for a mixture of MgO and FeO with a radius of 5 nm, 10 nm, 100 nm, 1 µm and 10 µm.

For dust with the same composition, the variation of dust temperature with size can be due to a difference in absorption and emission efficiency. If the absorption efficiency has a peak at a wavelength where the stellar spectrum is high, the dust particle will absorb more energy. This means that the amount of energy absorbed by a dust particle will be dependent on the shape of the stellar spectrum. The emission spectrum of the different sizes will be determined by their temperature. Given that the dust particle emits poorly where this spectrum has its peak, determined by the dust particle's emission efficiencies, less energy will be emitted. Dust particles which absorbs energy more efficiently and emits energy less efficiently will have a higher temperature. This can explain why dust temperature varies with size, since different sizes have absorption and emission efficiencies which are not the same.

5.2 Thermal emission brightness

In this section, the spectral energy distribution of thermal emission from dust will be presented. Only the figures that are considered to be most relevant will be shown, while the rest of the figures will be presented in appendix 9.2.3. First, some hopefully interesting aspects of dust emission around the Sun, Vega and Fomalhaut will be discussed, which include comparing thermal emission brightness computed with dust composed of different materials and discussing some prominent features seen in the thermal emission of astronomical silicate and a mixture of MgO/FeO. Then, dust emission around Vega and Fomalhaut will be discussed. For Vega and Fomalhaut, the objective was to investigate which sizes, materials and distances from the star provided a spectral energy distribution which fits observations. The total dust mass was adjusted so that the absolute brightness of the SEDs fit to observations in the K-band. If the curve of the spectral energy distribution was within the uncertainty of the observations, this was considered to be a fit.

For the Sun, the dust mass was set to be equivalent to the mass of one Halley comet. Since the dust mass is the same for a population of dust particles composed of different materials, the thermal emission brightness of these materials can therefore be compared. This shows that the brightness of amorphous carbon, astronomical silicate and a mixture of MgO/FeO in a ring between 0.18-0.2 AU are within the same range, having a magnitude of around $2 \times 10^{10} - 6 \times 10^{10}$ Jansky. The brightness of ice is smaller than the other materials with a magnitude of about 3×10^{9} Jansky, which is expected because ice is colder. The brightness of astronomical silicate and a mixture of MgO/FeO at 1 AU around the Sun are lower than at 0.18-0.2 AU. This is to be expected due to a lower temperature at distances further away from the Sun. The figures of amorphous carbon, a mixture of MgO/FeO and ice, are displayed in appendix 8.2.3, while astronomical silicate is shown in Figure 18 and Figure 19.

There is a prominent feature at ~10 μm which can be seen in the thermal emission brightness of astronomical silicate for dust particles with a size of 1 μm or less. It can be seen both at 0.18-0.2 AU and 1 AU for the Sun, which is shown in Figure 18 and Figure 19, respectively, at 0.18-0.2 AU for Vega and 0.18-0.2 AU and 0.99-1.01 AU for Fomalhaut. The absolute brightness of this feature is higher at 0.18-0.2 AU compared to around 1 AU, but the location of the feature (i.e. at which wavelength the feature is located) does not change with distance, that is to say it remains at ~10 μm for both 0.18-0.2 AU and around 1 AU. This feature disappears for a 10 μm dust particle. In addition, there is a prominent feature at ~18 μm for MgO/FeO both at 0.18-0.2 AU and around 1 AU for the Sun, Vega and Fomalhaut. As for astronomical silicate, the brightness of the feature is lower around 1 AU, the location of the feature remains at the same place at ~18 μm when the distance of the dust is changed and the features disappears for a 10 μm dust particle. No prominent features are seen in the thermal emission of amorphous carbon and the curve resembles a black body spectrum. If observation reveals a distinct flux at ~10 μm, this may indicate that astronomical silicate with a size of 1 μm or less is responsible for the emission or given that the flux is at ~18 μm, a mixture of MgO/FeO with a size of 1 μm or less may be responsible.

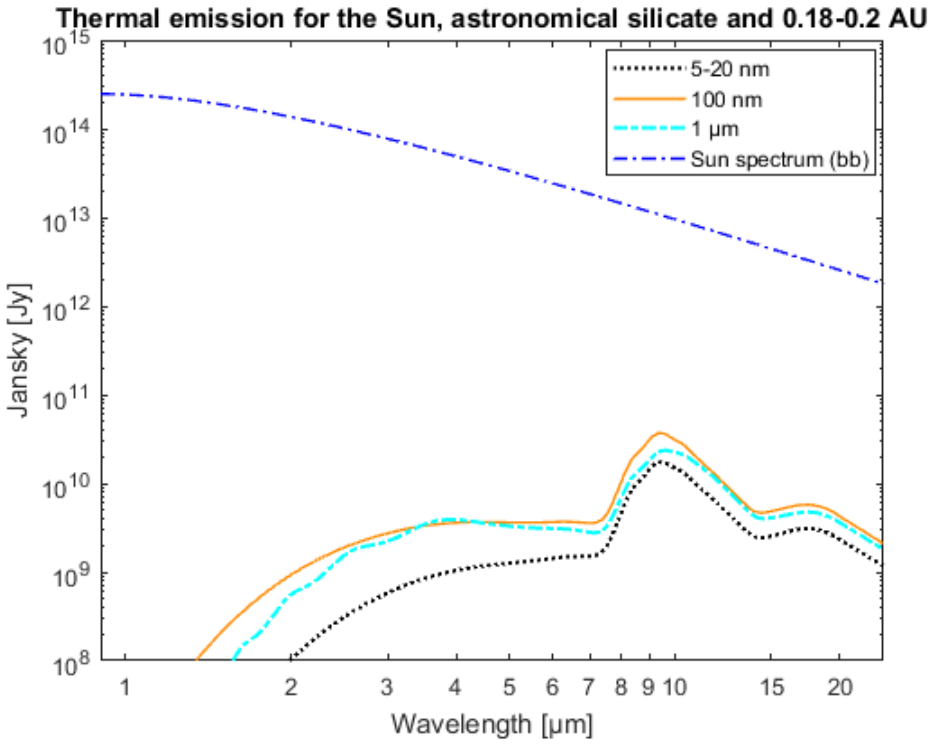

Figure 18: Thermal emission brightness for dust around the Sun with dust particles consisting of astronomical silicate where the dust is distributed in a narrow ring between 0.18-0.2 AU.

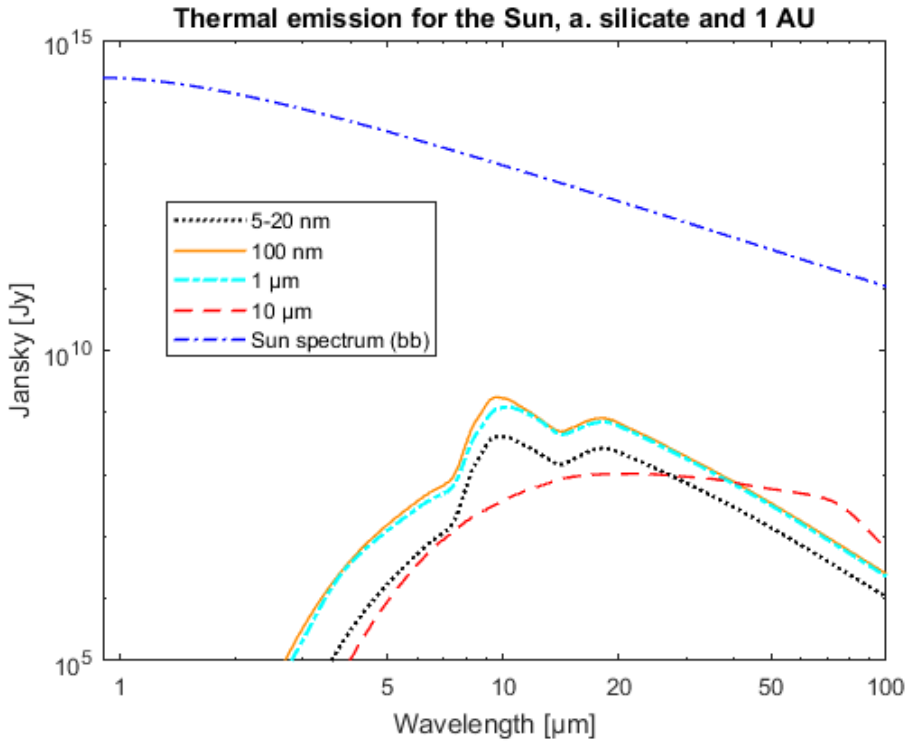

Figure 19: Thermal emission brightness for dust around the Sun with dust particles consisting of astronomical silicate where the dust is at 1 AU.

Vega

There were three observational constraints on the modelling of SEDs around Vega, where one measurement was in the H-band at 1.65 µm, the other in the K-band at 2.12 µm and the last one at 10.6 µm, referred to as Blinc in the figures, which is the name of the instrument measuring the flux. With these constraints in mind, it is apparent that the following materials and sizes are not a good fit:

- Dust particles consisting of ice with a size of 1 µm, 100 nm, and 5-20 nm and at distance of 0.18-0.2 AU from Vega. It does not fit within the uncertainty of the flux in the H-band and at 10.6 µm (Blinc). Shown in Figure 58 in appendix 9.2.3.
- Dust particles consisting of amorphous carbon with a size of 1 µm and at distance of 0.18-0.2 AU from Vega. It does not fit within the uncertainty of the flux in the H-band. Shown in Figure 20.
- Dust particles consisting of a mixture of MgO/FeO with a size of 1 µm and at distance of 0.18-0.2 AU from Vega. It does not fit within the uncertainty of the flux in the H-band. Shown in Figure 21.
- Dust particles consisting of astronomical silicate with a size of 1 µm, 100 nm, and 5-20 nm and at distance of 0.18-0.2 AU from Vega. It does not fit within the uncertainty of the flux at 10.6 µm (Blinc). Shown in Figure 59 in appendix 9.2.3.
- Dust particles consisting of a mixture of MgO/FeO with a size of 5-20 nm and at distance of 0.99-1.01 AU from Vega. It does not fit within the uncertainty of the flux at 10.6 µm (Blinc). Shown in Figure 23.

The following materials and sizes fit within the uncertainty of all the observations:

- Dust particles consisting of amorphous carbon with a size of 100 nm and 5-20 nm and at distance of 0.18-0.2 AU from Vega. Shown in Figure 20.
- Dust particles consisting of a mixture of MgO/FeO with a size of 100 nm and 5-20 nm and at distance of 0.18-0.2 AU from Vega. Shown in Figure 21.

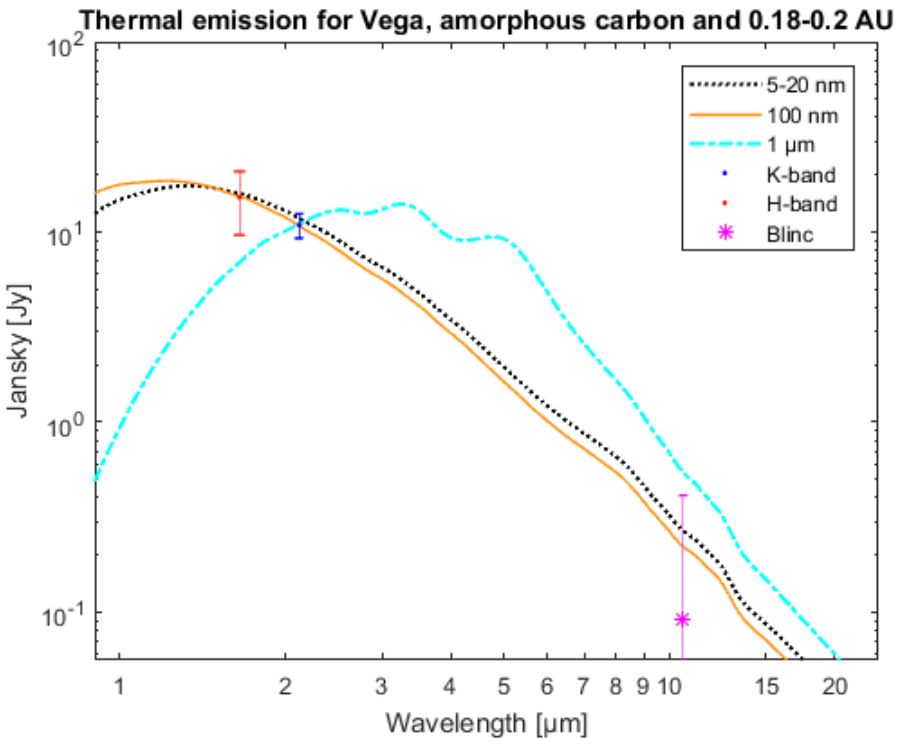

Figure 20: Thermal emission brightness for dust around Vega with dust particles consisting of amorphous carbon where the dust is distributed in a narrow ring between 0.18-0.2 AU.

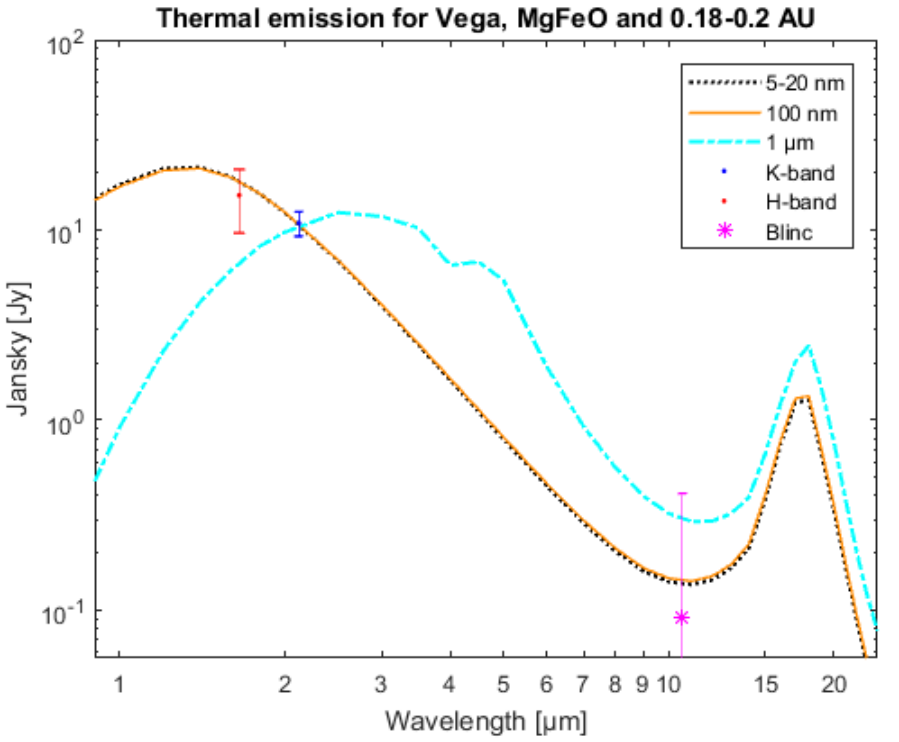

Figure 21: Thermal emission brightness for dust around Vega with dust particles consisting of a mixture of MgO/FeO where the dust is distributed in a narrow ring between 0.18-0.2 AU.

As mentioned before in this section, the dust mass was adjusted to fit within the K-band. The amount of dust mass for the different sizes and materials are listed in Table 8 in units of Halley comets. For MgO/FeO with a size of 5-20 nm at 0.99-1.01 AU, the dust mass was equivalent to 470 Halley comets, not shown in Table 8. The dust mass required for ice is higher than the other, but this most likely because the brightness is lower for ice. For amorphous carbon and MgO/FeO with a size of 5-20 nm and 100 nm, the smallest amount of dust mass is required. The amount of dust mass required for the various materials is not the same. This is most likely because the dust temperature, the absorption efficiency and the total emission surface are different. When it comes to the total emission surface, the mass density was needed to compute the total volume of the dust and the mass density varies for the materials, causing the total emission surface to differ.

Table 8: Dust mass in units of Halley comets for dust particles consisting of MgO/FeO, amorphous carbon, astronomical silicate or ice at 0.18-0.2 AU with a size of 1 µm, 100 nm and 5-20 nm around Vega.

	5-20 nm	100 nm	1 µm
MgO/FeO	56	50	146
Amorphous carbon	34	21	60
Astronomical silicate	235	144	157
Ice	913	2348	33913

In the two following sections, there will be a discussion on the testing of different dust temperatures for the SED of amorphous carbon and MgO/FeO with a size of 5-20 nm. The testing was performed to check if changing the dust temperature resulted in a fit or a non-fit to observations in the H-band, K-band and at 10.6 µm. Only a size of 5-20 nm was tested since the SED of 100 nm and 5-20 nm dust particles were similar. This testing was considered important since there was indication that MgO/FeO and amorphous carbon would sublimate at a distance of 0.18-0.2 AU and the objective was to see if the dust ring could be located further away from Vega, i.e. where the dust temperature is lower.

The average dust temperature for a mixture of MgO/FeO with a size 5-20 nm distributed in a ring between 0.18-0.2 AU was derived to 2878 K. As a comparison, a dust temperature of 1948 K with the same size and at the same distance was also tested in the modelling of SEDs, where the dust mass required to fit the curve into the K-band was equivalent to 196 Halley comets. Even with the lower temperature at 1948 K, the SED of MgO/FeO at 0.18-0.2 AU with a size of 5-20 nm still fitted within all the observations. On the hand, the SED of MgO/FeO at 0.99-1.01 AU with a size of 5-20 nm does not fit within the flux at 10.6 µm (Blinc). It had an average dust temperature of 1547 K and the required dust mass was 470 Halley comets. This can be interpreted in the direction that the SED of MgO/FeO with a size of 5-20 nm can be fitted within the uncertainty of the observation for a temperature between about 1950 K to as a high as almost 2900 K. Looking at data for dust temperature of MgO/FeO between 0.18-0.9 AU, shows that a dust particle of 5-20 nm has a temperature of 1950 K at around 0.55 AU. So from these results, there is an indication that a dust ring with MgO/FeO and a size of 5-20 nm can be as far out as 0.55 AU from Vega and still fit within the uncertainty of the observations. At 0.99-1.01, the temperature is too low and the curve does not fit, but whether there is a fit between 0.55 and 0.99 remains to be investigated.

In addition, the same method was tested for amorphous carbon. The SED of amorphous carbon with a size of 5-20 nm was calculated with an average dust temperature of 2687 K. An average dust temperature of 1793 K was also tested, requiring a dust mass equivalent to 117 Halley comets to fit within the uncertainty of the K-band. With a temperature of 1793 K, the SED of amorphous carbon did not fit within the uncertainty of the observation at 10.6 µm. Again, looking at data for dust temperature, indicate that a dust temperature of ~1790 K with amorphous carbon corresponds to around 0.5-0.6 AU from Vega. However, the SED with amorphous carbon computed with a temperature of 1793 K was only slightly higher than the uncertainty of the observation at 10.6 µm, so the SED with amorphous carbon will probably fit with a temperature which is higher than 1793 K. This means that a dust ring with amorphous carbon can probably be located inward of 0.5 AU and still fit to observations, but this must be studied in more detail.

Since the radius and temperature of Vega varies from the pole to the equator, and the observational dust brightness was computed as a fraction of the stellar spectrum of Vega, the polar and equatorial parameters of Vega was tested to see if this made a difference. Using a polar or equatorial for the radius and temperature, did not result in a significant difference for the observational dust brightness. This can be seen in Figure 22, where the use of a polar or equatorial radius and temperature only increases the lower uncertainty in the H-band and the K-band. The SED of MgO/FeO and carbon with a size of 5-20 nm and 100 nm still fits within the uncertainty in the H-band, K-band and at 10.6 µm.

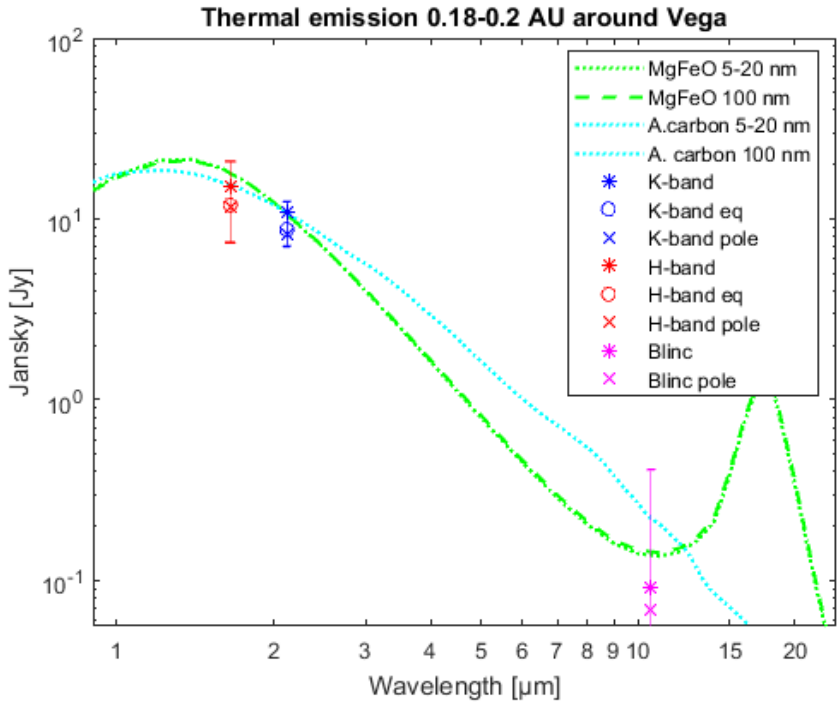

Figure 22: Comparison of observational dust brightness in H-band, K-band and at 10.6 µm computed with an equatorial and a polar temperature and radius for Vega, where the observational dust brightness is a fraction of the stellar spectrum. The circle (eq) and the cross (pole) represents the relative flux of the dust with respect to the stellar photosphere, computes with a equatorial and polar effective temperature/radius of Vega, respectively, by assuming a black body spectrum for the star. The blue circle and cross is the flux in the K-band, the red circle and cross is the flux in the H-band and the pink cross is the flux at 10.6 µm.

In Figure 23, there is a comparison of SEDs computed with a dust ring at 0.18-0.2 AU and another at 0.99-1.01. A dust ring where the dust continuously distributed from 0.18-1.01 AU is also shown in this figure. The dust in these rings is composed of MgO/FeO and has a size of 5-20 nm. As for the all the SEDs, the SEDs of the two rings were computed with an average dust temperature. The ring at 0.18-0.2 AU is computed with a certain temperature, while the one at 0.99-1.01 is computed with another, which was lower since the dust is located further away from the star. The thermal emission from dust distributed continuously from 0.18-1 AU is computed with only one temperature, found by calculating an average temperature based on the density distribution as a function of distance. This average temperature is inclined towards the temperature of the smallest particles and towards the distance of the particles that are closest to the star, i.e. the temperature of a 5 nm dust particle at 0.18 AU. Together, the curves of the two rings displays a distinct feature due to the location of the peaks, while dust distributed from 0.18-1 AU only have one peak. Given that these results are computed accurately, observing a distinct feature for a SED may indicate that there are two separate dust rings giving rise to the thermal emission. These two peaks can most likely only be observed if they are far apart since they otherwise will overlap. So, distinguishing between two dust belts which are located close to each other and dust which is continuously distributed in a belt may not be possible. In any case, observing two dust belts can be interesting since the gap has to be maintained, for instance by having planets present in the gap. Whether the SED in Figure 23 reflect reality, remains to be checked. A better representation of the SEDs would perhaps be to compute the thermal emission brightness as a function of temperature and add all the contributions from dust particle of different sizes and at different distances together, instead of using an average temperature. This could provide SEDs that are more realistic, but it would be more time-consuming and complicated.

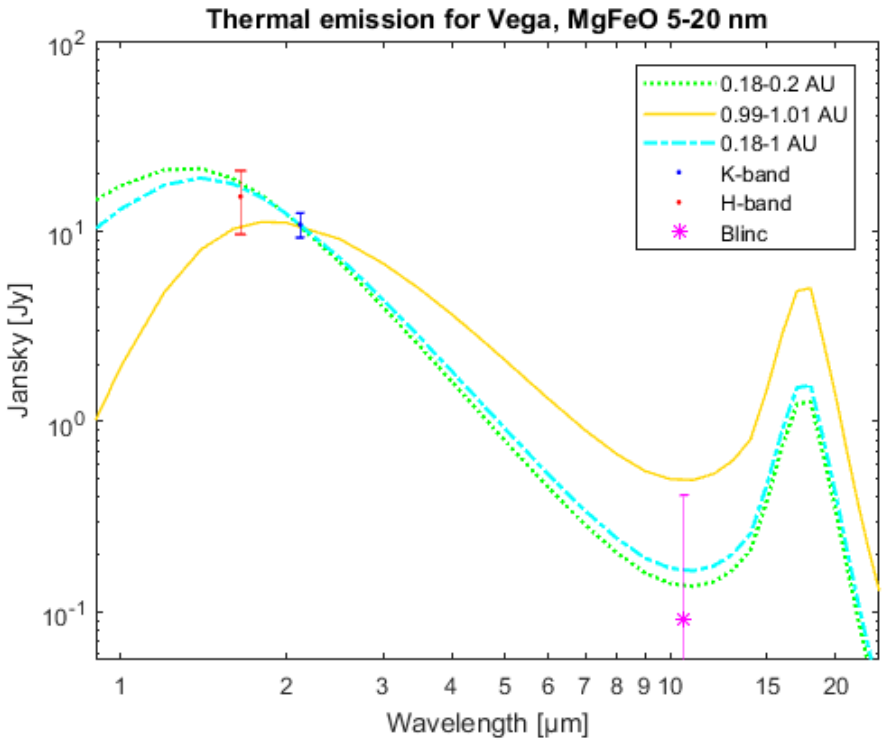

Figure 23: Comparison of MgO/FeO with a size of 5-20 nm in a ring at 0.18-0.2 AU and another ring at 0.99-1.01 AU and dust distributed continuously from 0.18-1 AU.

In Table 9 and there is a summary of whether the SEDs at 0.18-0.2 AU around Vega fit or not to the observations. The SED for dust consisting of MgO/FeO with a size of 5-20 nm at 0.99-1.01 AU around Vega, not shown in Table 9, does not fit to observation at 10 μm and a large amount of dust mass is required in order to fit the SED to the K-band.

Table 9: Summary of different aspect related to the SED of different materials and sizes at 0.18-0.2 AU around Vega.

	5-20 nm	100 nm	1 μm
MgO/FeO	Fits well to observations. Little dust mass required.	Fits well to observations. Little dust mass required.	Does not fit in the H-band. Much dust mass required.
Amorphous carbon	Fits well to observations. Little dust mass required	Fits well to observations. Little dust mass required	Does not fit in the H-band. Much dust mass required.
Astronomical silicate	Does not fit at 10.6 μm. Much dust mass required.	Does not fit at 10.6 μm. Much dust mass required.	Does not fit at 10.6 μm. Much dust mass required.
Ice	Does not fit in the H-band and at 10.6 μm. Large amount of dust mass required.	Does not fit in the H-band and at 10.6 μm. Large amount of dust mass required.	Does not fit in the H-band and at 10.6 μm. Large amount of dust mass required.

Fomalhaut

For Fomalhaut, there were two observational constraints, one in the K-band at 2.18 μm and one in the N-band between 8.25-12.69 μm. These were the SEDs that did not fit:

- Dust particles consisting of ice with a size of 1 μm, 100 nm, and 5-20 nm and at a distance of 0.18-0.2 AU from Fomalhaut. It does not fit within the uncertainty of the flux in the N-band. Shown in Figure 60 in appendix 9.2.3.
- Dust particles consisting of a mixture of MgO/FeO with a size of 100 nm and 5-20 nm and at a distance of 0.18-0.2 AU from Fomalhaut. It does not fit within the uncertainty of the N-band. Shown in Figure 25.
- Dust particles consisting of astronomical silicate with a size of 1 μm, 100 nm, and 5-20 nm and at a distance of 0.18-0.2 AU from Fomalhaut. It does not fit within the uncertainty of the N-band. Shown in Figure 61 in appendix 9.2.3.
- Dust particles consisting of amorphous carbon with a size of 1 μm, 100 nm, and 5-20 nm and at a distance of 0.99-1.01 AU from Fomalhaut. It does not fit within the uncertainty of the flux in the N-band. Shown in Figure 62 in appendix 9.2.3.
- Dust particles consisting of a mixture of MgO/FeO with a size of 1 μm, 100 nm, and 5-20 nm and at a distance of 0.99-1.01 AU from Fomalhaut. It does not fit within the uncertainty of the flux in the N-band. Shown in Figure 63 in appendix 9.2.3.
- Dust particles consisting of astronomical silicate with a size of 1 μm, 100 nm, and 5-20 nm and at a distance of 0.99-1.01 AU from Fomalhaut. It does not fit within the uncertainty of the N-band. Shown in Figure 64 in appendix 9.2.3.

The other SEDs fitted partially:

- Dust particles consisting of amorphous carbon with a size of 1 μm and at a distance of 0.18-0.2 AU from Fomalhaut. There is a fit between 12.2 to 12.69 μm in the N-band. It does not fit within the uncertainty of the flux in the N-band from 8.25 to 11.72 μm. Shown in Figure 24.
- Dust particles consisting of amorphous carbon with a size of 100 nm and at a distance of 0.18-0.2 AU from Fomalhaut. It fits in the N-band between 9.2 to 9.72 μm, but it does not fit between 8.25 to 8.74 μm and between 10.22 to 12.69 μm. Shown in Figure 24.
- Dust particles consisting of amorphous carbon with a size of 5-20 nm and at a distance of 0.18-0.2 AU from Fomalhaut. It fits in the N-band between 8.25 to 8.74 μm, but it does not fit between 9.2 to 12.69 μm. Shown in Figure 24.
- Dust particles consisting of a mixture of MgO/FeO with a size of 1 μm and at a distance of 0.18-0.2 AU from Fomalhaut. There is a fit from 11.21 to 12.69 μm in the N-band, but not from 8.25 to 10.68 μm. Shown in Figure 25.

Additionally, there were two observations at longer wavelengths, one at 23.68 μm and the other 70 μm. None of the SEDs fitted to these observations, but the curve of the spectral energy distribution of amorphous carbon at 0.99-1.01 AU with a size of 1 μm seems to follow the slope of the observations. The dust emission responsible of these observations is perhaps due to a dust ring located farther away from Fomalhaut and habited by larger dust particles. This is beyond the scope of the thesis since the focus is dust particles of 1 μm or less and which is close to the star.

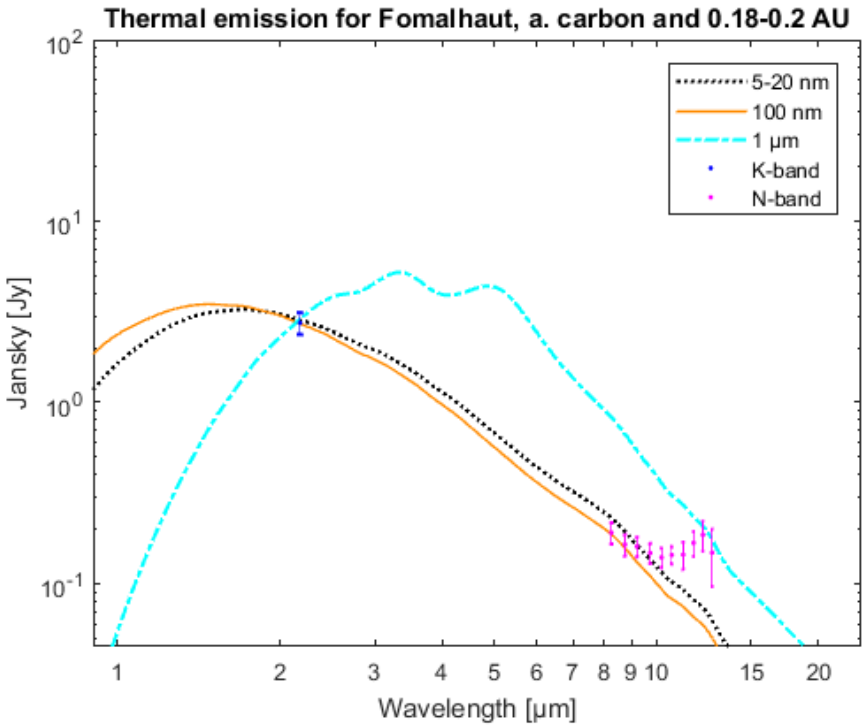

Figure 24: Thermal emission brightness for dust around Fomalhaut with dust particles consisting of amorphous carbon where the dust is distributed in a narrow ring between 0.18-0.2 AU.

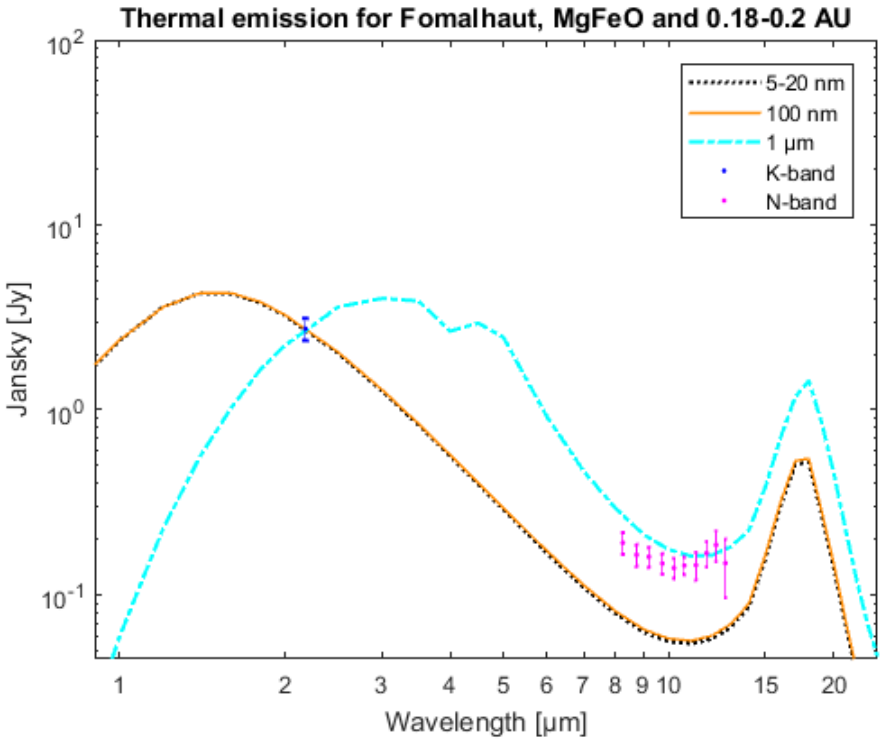

Figure 25: Thermal emission brightness for dust around Fomalhaut with dust particles consisting of a mixture of MgO/FeO where the dust is distributed in a narrow ring between 0.18-0.2 AU.

As for Vega, the dust mass was adjusted to fit within the uncertainty of the K-band and the amount of dust required is listed in Table 10 and Table 11, where the dust mass is given in units of Halley comets. In general, the dust mass required is larger at 0.99-1.01 AU compared to 0.18-0.2 AU, which might be related to the fact that the dust temperatures are lower at 0.99-1.01. By viewing Table 10 and Table 11, it is apparent that the dust mass required varies with both dust composition and the size. Figuring out why these variations occur, can be complicated. This is because the SEDs are computed with different temperatures and absorption efficiencies. In addition, the total surface emission varies because it is calculated for dust particles with different sizes and also by using different equation, i.e. a power law size distribution for 5-20 nm, while for 100 nm and 1 μm it was assumed that the all dust particles have the same size. Though, the amount of dust mass for 5-20 nm with MgO/FeO, amorphous carbon and astronomical silicate is suspiciously high compared to 100 nm and 1 μm, and it cannot be ruled out that there might be an error somewhere in the calculations. This can be investigated further.

Table 10: Dust mass in units of Halley comets for dust particles consisting of MgO/FeO, amorphous carbon, astronomical silicate or ice at a distance of 0.18-0.2 AU with a size of 1 μm, 100 nm and 5-20 nm around Fomalhaut.

	5-20 nm	100 nm	1 μm
MgO/FeO	30	26	117
Amorphous carbon	18	10	52
Astronomical silicate	157	78	117
Ice	3391	9130	156520

Table 11: Dust mass in units of Halley comets for dust particles consisting of MgO/FeO, amorphous carbon, astronomical silicate or ice at a distance of 0.99-1.01 AU with a size of 1 μm, 100 nm and 5-20 nm around Fomalhaut.

	5-20 nm	100 nm	1 μm
MgO/FeO	391	32	170
Amorphous carbon	339	15	97
Astronomical silicate	17113	300	222

None of the SEDs fitted exactly within the uncertainty of all the observations. It can be noted that the uncertainty in the N-band is one standard deviation (1σ), meaning that 68.2 % of the measurements are expected to fall within the confidence interval between -1σ and 1σ, assuming a normal distribution. So, if the curve of the spectral energy distribution is only slightly below or above the uncertainty, drawing conclusion on whether there is a fit or not is a bit uncertain. If the curve of the SED is far from the uncertainty, the conclusion that the curve does not fit is more robust. This means that the materials and sizes which were listed as a non-fit, are unlikely to be responsible for the emission since they were far from the uncertainty in the N-band.

On the other hand, the shape of the curve for the SED of MgO/FeO with a size of 1 µm, 100 nm and 5-20 nm seem to fit to the slope of the observations in the N-band. At 0.18-0.2 AU, the curve for MgO/FeO with a size of 100 nm and 5-20 is below the measurements in the N-band, where a dust temperature of 2112 K (100 nm) and 2258 K (5-20 nm) was used. For a dust ring at 0.99-1.01AU the curve is above these measurements with a temperature of 1183 K (100 nm) and 1230 K (5-20 nm). The question then is if the curve will fit within the uncertainty of the N-band by using a temperature between ~2000 K and ~1200 K, corresponding to about 0.2-0.9 AU. This should probably be tested. When it comes to MgO/FeO with a size of 1 µm, deciding on whether there is a fit or not is difficult since there are no observations in the H-band for Fomalhaut, unlike Vega. Around Vega, a 1 µm consisting of MgO/FeO at 0.18-0.2 AU did not fit in the H-band. If a 1 µm particle with MgO/FeO at 0.18-0.2 AU around Fomalhaut fits to observation, remains an open question at the moment.

In addition, the shape of the curve for the SED of amorphous carbon with a size of 100 nm and 5-20 nm at 0.18-0.2 AU seems to fit from 8.25 to 10.22 µm and it fits in the K-band at 2.18 µm. This is similar to the findings of Mennesson et al. (2013), which concluded that the data from 2-11 µm in the N-band was consistent with a ring around ~0.1 AU with dust particles composed of carbon-rich material and that the dust particles are in the size range of 10-300 nm. They suggested that the data at longer wavelengths could be due to a second dust ring located further out from Fomalhaut at about 0.4-1 AU and that the grains could consist of silicate and have a larger size of a few microns.

In Table 12 and Table 13, there is a summary of whether the SEDs around Fomalhaut fitted or not to the observations.

Table 12: Summary of different aspect related to the SED around Fomalhaut of different materials and sizes at 0.18-0.2 AU.

	5-20 nm	100 nm	1 µm
MgO/FeO	Does not fit in the N-band. Little dust mass required.	Does not fit in the N-band. Little dust mass required.	Partially fit in the N-band. Much dust mass required.
Amorphous carbon	Partially fit in the N-band at shorter wavelengths. Little dust mass required.	Partially fit in the N-band at shorter wavelengths. Little dust mass required.	Partially fit in the N-band at longer wavelengths. Much dust mass required.
Astronomical silicate	Does not fit in the N-band. Much dust mass required.	Does not fit in the N-band. Much dust mass required.	Does not fit in the N-band. Much dust mass required.
Ice	Does not fit in the N-band. Large amount of dust mass required.	Does not fit in the N-band. Large amount of dust mass required.	Does not fit in the N-band. Large amount of dust mass required.

Table 13: Summary of different aspect related to the SED around Fomalhaut of different materials and sizes at 0.99-1.01 AU.

	5-20 nm	100 nm	1 µm
MgO/FeO	Does not fit in the N-band. Much dust mass required.	Does not fit in the N-band. Little dust mass required.	Does not fit in the N-band. Much dust mass required.
Amorphous carbon	Does not fit in the N-band. Much dust mass required.	Does not fit in the N-band. Little dust mass required.	Does not fit in the N-band. Much dust mass required.
Astronomical silicate	Does not fit in the N-band. Large amount of dust mass required.	Does not fit in the N-band. Much dust mass required.	Does not fit in the N-band. Much dust mass required.

5.3 Beta-values

In this section, computed beta-values will be presented. They were computed as a side-project and were used in trajectory calculations for dust around Vega and Fomalhaut by Johann Stamm (master thesis in preparation).

In Figure 26 beta-values for dust particles around the Sun are shown, where dust with sizes larger than 500 nm has beta-values smaller than 0.5 and dust with sizes between 100-500 nm has beta-values larger than 0.5. For dust sizes less than 500 nm the beta-values are larger than 0.5 for dust composed of amorphous carbon and MgO/FeO and the beta-values are smaller than 0.5 for astronomical silicate and ice.

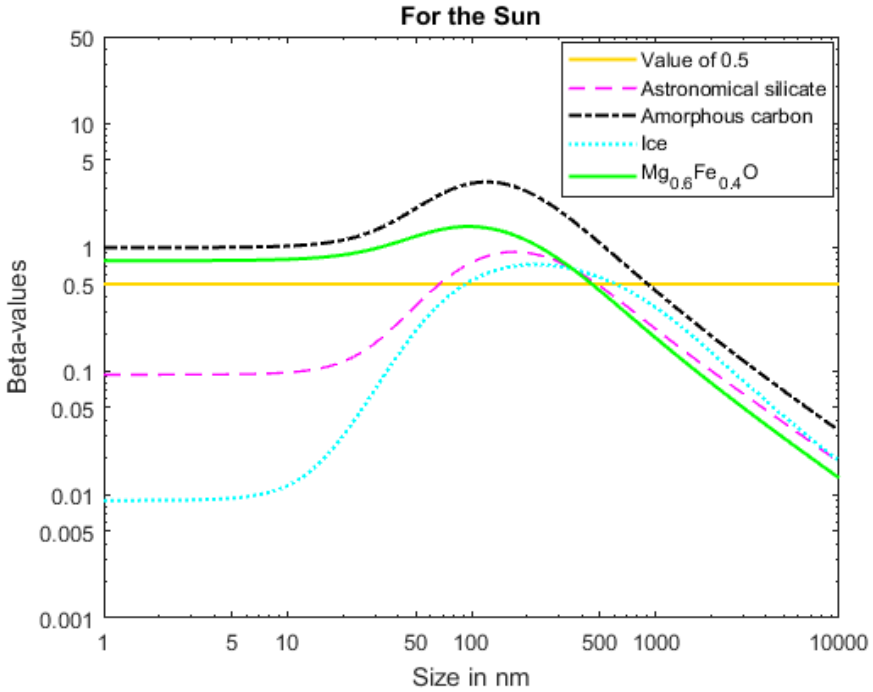

Figure 26: Computed beta-values for dust particles around the Sun.

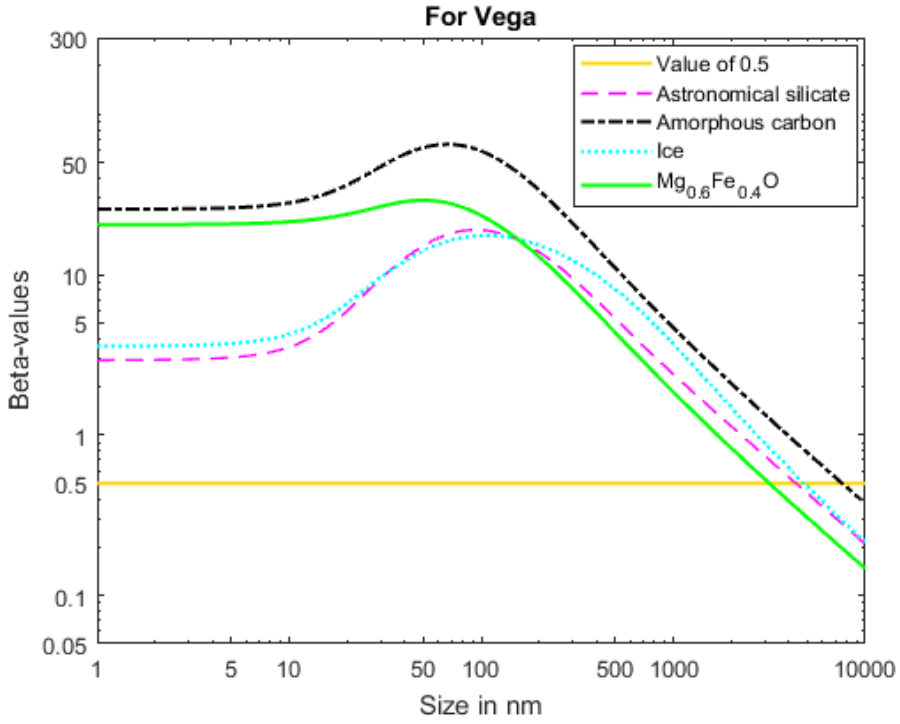

Figure 27: Computed beta-values for dust particles around Vega.

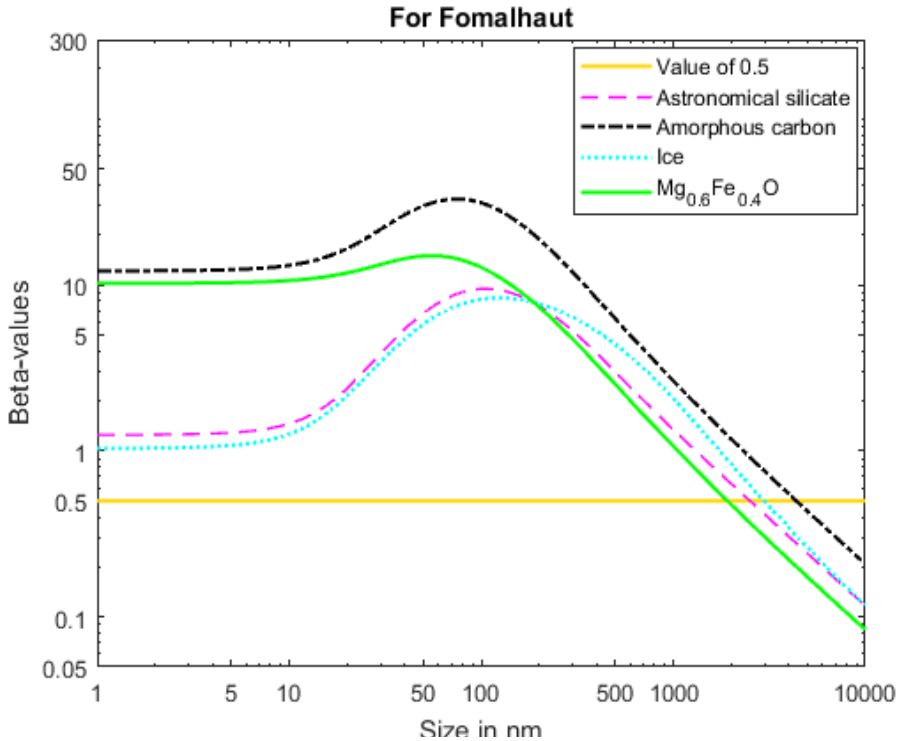

Figure 28: Computed beta-values for dust particles around Fomalhaut.

Figure 27 shows the beta-values for Vega. For dust with a size of ~3000 nm and larger, the beta-values are smaller than 0.5 and for dust with sizes smaller than 300 nm, the beta-values are larger than 0.5 for all materials considered. In Figure 28, the beta-values for Fomalhaut are presented. As for Vega, sizes of ~3000 nm have a beta-value smaller than 0.5, while dust with a size less than 3000 nm have a beta-values larger than 0.5 Beta-values larger than 0.5 indicate that the dust particles will be influenced by radiation pressure and that they can be ejected from the stellar system. This means that for Vega and Fomalhaut, all dust particles less than 3000 nm can be ejected due to radiation pressure.

Shown in Figure 29 is the comparison between beta-values for MgO/FeO computed by using Mie theory and by using an approximation for particles which are much larger than the incident wavelength, i.e. geometric optics. It can be seen that this approximation is not valid for the smallest particles with a size less than 100 nm and for this size-range, Mie theory must be applied. Meanwhile, for the smallest particles, those approximately less than 10 nm, Rayleigh theory can possibly be used.

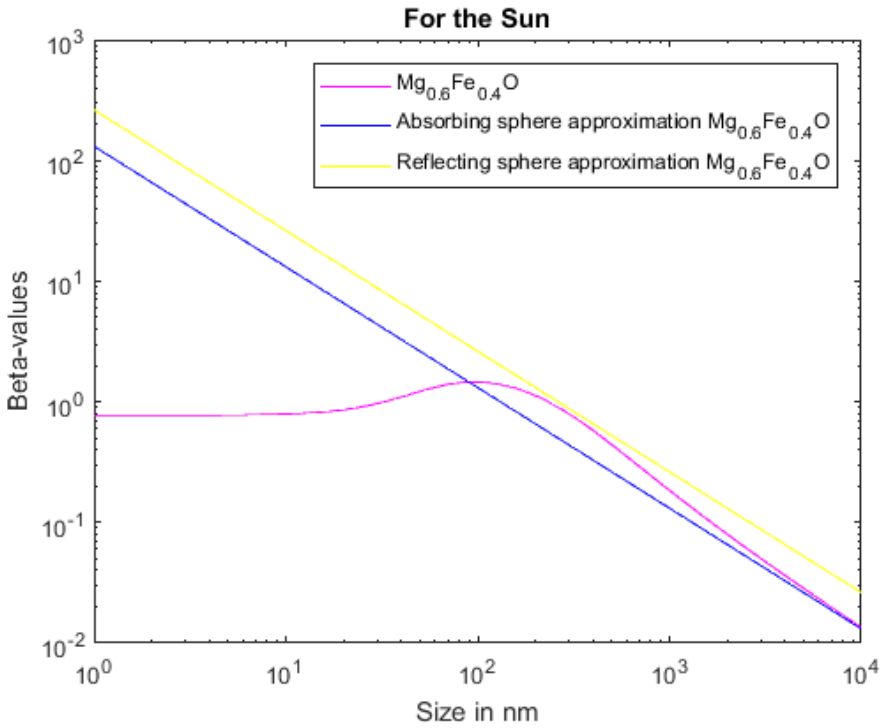

Figure 29: Beta-values for MgO/FeO computed with Mie theory (purple) and with an absorbing sphere approximation (blue) and reflecting sphere approximation (yellow), which is the large particle limit.

5.4 Additional considerations

5.4.1 Sublimation lifetime

The sublimation lifetimes in this section was computed by Carsten Baumann and Jan Fredrik Aasmundtveit. Dust temperatures as a function of size, material and distance from the star were needed for these computations and they were provided by the author of this thesis. First, there will be a comparison between the sublimation lifetimes of different materials. Then, how the sublimation lifetime varies between the Sun, Vega and Fomalhaut will be discussed, followed by comparing the sublimation lifetime of dust particles with different sizes. The figures of astronomical silicate dust around the Sun and MgO/FeO dust around Vega and Fomalhaut are shown in this section, while the rest of the figures are presented in appendix 9.2.2.

In this part, the sublimation lifetime of different materials will be compared to see how the sublimation lifetimes varies and the comparison will be done for a size of 5 nm and for dust consisting of MgO/FeO, amorphous carbon and astronomical silicate. Dust particles with a size of 5 nm were compared since particles in the nano-range are the focus of this thesis. In Table 14, the comparison of sublimation lifetimes for the different materials at 0.18 AU for the Sun and 0.3 AU for Vega and Fomalhaut for a dust particle of 5 nm are presented. The difference in sublimation lifetime between the different materials may in part be due to a difference in dust temperature. The dust temperatures of these materials are presented in Table 15 for the Sun at 0.18 AU and for Vega and Fomalhaut at 0.3 AU for a 5 nm dust particle. Even though MgO/FeO is slightly hotter than astronomical silicate and amorphous carbon, the difference in dust temperature between these materials is not so high that it alone can explain why the sublimation lifetimes differs considerably. Therefore, it may be that the sublimation lifetimes are different because the vapour pressures vary for these materials. Looking at the data for the vapour pressure around Vega and Fomalhaut for the given materials, show that the vapour pressure for MgO/FeO is notably higher compared to the vapour pressure of amorphous carbon and astronomical silicate. It can be noted that amorphous carbon has a very low vapour pressure compared to MgO/FeO. This may partially explain why amorphous carbon has a higher sublimation lifetime. Apparently, the values for the vapour pressure were found experimentally and the method is unknown and thus, the uncertainty of the vapour pressure is at the moment not certain. The vapour pressure apparently has some relation to the chemical bonding between the molecules and the crystal structure of a material. Since Mg^{2+} and O^{2-}/ Fe^{2+} and O^{2-} are held together by ionic bonding and has a cubic crystal structure like a salt, it may be that this material is more volatile compared to amorphous carbon. Amorphous carbon does not have crystal structure and the molecules are bound together by electron-pair bonding. Thus, perhaps amorphous carbon is significantly more refractory compared to MgO/FeO.

Table 14: Sublimation lifetimes for dust particles with a size of 5 nm consisting of different materials around the Sun, Vega and Fomalhaut. The sublimation lifetime for dust around the Sun is at 0.18 AU, while for Vega and Fomalhaut the sublimation lifetime for dust is at 0.3 AU.

	MgO/FeO	Amorphous carbon	Astronomical silicate
The Sun	$\sim 0.2\ s$	$\sim 9 \times 10^{21}\ s$	$\sim 2.5 \times 10^{5}\ years$
Vega	$\sim 0.0003\ s$	$\sim 33\ s$	$\sim 0.005\ s$
Fomalhaut	$\sim 0.08\ s$	$\sim 116\ days$	$\sim 116\ s$

Table 15: Temperatures in Kelvins of dust with a size of 5 nm of MgO/FeO, amorphous carbon and astronomical silicate for the Sun, Vega and Fomalhaut. The dust temperatures around the Sun are at 0.18 AU and for dust around Vega and Fomalhaut at 0.3 AU.

	MgO/FeO	Amorphous carbon	Astronomical silicate
The Sun	$\sim 1200\ K$	$\sim 1100\ K$	$\sim 800\ K$
Vega	$\sim 2400\ K$	$\sim 2200\ K$	$\sim 2200\ K$
Fomalhaut	$\sim 1900\ K$	$\sim 1700\ K$	$\sim 1600\ K$

It is also possible to do a comparison to see how the sublimation lifetime varies around the Sun, Vega and Fomalhaut. For dust consisting of MgO/FeO, astronomical silicate and amorphous carbon, the sublimation lifetime is consistently much longer around Fomalhaut compared to Vega, varying from about 300 to 30000 times longer around Fomalhaut. This is most likely due to higher dust temperatures around Vega compared to Fomalhaut. In addition, the vapour pressure of these materials is significantly higher around Vega compared to Fomalhaut, which means that the materials will sublimate faster. The longest sublimation lifetime is seen around the Sun when compared to Vega and Fomalhaut. This can be expected, since Vega and Fomalhaut are much brighter than the Sun.

By comparing dust particles with different sizes, shows that in general, the smallest particles with a size ≤ 100 nm, sublimates considerably faster than dust particles with a size of 1 µm. Again, this is probably caused by a difference in dust temperature since 1 µm particles are colder than the smaller particles.

This section considers the sublimation lifetime of dust particles with a size of 1 µm. With a size of 1 µm, dust particles consisting of all the materials listed in Table 16 seems to survive outward of 0.18 AU around the Sun and outward of 0.3 around Vega and Fomalhaut, except for MgO/FeO and astronomical silicate around Vega. These materials only survives for a relatively short time at 0.3 AU, but survives significantly longer at 0.9 AU, which means that the sublimation lifetime rises steeply between 0.3-0.9 AU. The sublimation lifetime of dust consisting of different materials between 0.18-0.2 AU for the Sun and between 0.3-0.9 AU for Vega and Fomalhaut are summarized in Table 16 and conclusion on whether it is likely that a certain material will survive, is summarized in Table 17. In Table 17, the categories are defined as:

- If the dust particles survives less than three days, the particles is categorized as: unlikely to survive.
- If the dust particles survives between three days and up to a year, the particles are categorized as: less likely to survive.
- If the particles survives for a year or longer, the particles are categorized as: Survives
- If the sublimation lifetime varies significantly, i.e. from seconds or hours to many years, between 0.18-0.2 AU for the Sun and between 0.3-0.9 AU for Vega and Fomalhaut, the particles are categorized as: Varies significantly with distance.
- If the sublimation lifetime varies, i.e. from days to many years, between 0.18-0.2 AU for the Sun and between 0.3-0.9 AU for Vega and Fomalhaut, the particles are categorized as: Varies with distance.

Table 16: Sublimation lifetime in various units of dust particles with a radius of 1 μm around the Sun at 0.18-0.2 AU and around Vega and Fomalhaut at 0.3-0.9 AU.

	MgO/FeO	Amorphous carbon	Astronomical silicate
The Sun	$64\,000 - 950\,000$ years	$6 \times 10^{37} - 2 \times 10^{38}$ years	$6 \times 10^{6} - 5 \times 10^{8}$ years
Vega	106 hours to 1.6×10^{7} years	$2.5 \times 10^{8} - 3 \times 10^{27}$ years	~7000 seconds to 1×10^{6} years
Fomalhaut	$250 - 3 \times 10^{13}$ years	$4 \times 10^{17} - 6 \times 10^{40}$ years	$8 - 9 \times 10^{14}$ years

Table 17: Results for different materials with a size 1 μm and conclusion on whether the material can survive between 0.18-0.2 AU for the Sun and 0.3-0.9 AU for Vega and Fomalhaut.

	MgO/FeO	Amorphous carbon	Astronomical silicate
The Sun	Survives	Survives	Survives
Vega	Varies significantly with distance	Survives	Varies significantly with distance
Fomalhaut	Survives	Survives	Survives

In this part, dust particles with a size ≤ 100 nm are considered. It should be noted that the discussion in this section only considers sublimation and not sputtering. From the results shown in the figures for the sublimation lifetime, it appears that dust particles which consist of astronomical silicate can survive outward of 0.18 AU around the Sun since the sublimation lifetime is approximately 3 years. Around Vega and Fomalhaut, the sublimation lifetime of astronomical silicate varies from 0.005 seconds to 55 hours for Vega and from 20 seconds to 18 million years for Fomalhaut, both at a distance between 0.3-0.9 AU. It seems like astronomical silicate is not capable of surviving around Vega at a distance between 0.3-0.9 AU, at least not for long. The sublimation lifetime of astronomical silicate around Fomalhaut obviously varies a lot between 0.3-0.9 AU. The dust can most likely survive outward of 0.6-0.7 AU, where the sublimation lifetime is around 1 years. Inward of 0.6 AU, the sublimation lifetime of astronomical silicate decreases and thus the likelihood of it surviving is reduced and it is unlikely that it would survive close to 0.3 AU.

Around the Sun, amorphous carbon survives for a long time between 0.18-0.2 AU, while for Vega, amorphous carbon is likely to survive outward of 0.6 AU where the sublimation lifetime is ~1 year. It is unlikely that amorphous carbon will survive at 0.3 around Vega since the sublimation lifetime is only 33 seconds. Amorphous carbon can survive for outward of 0.3-0.4 AU around Fomalhaut since the sublimation lifetime is approximately 1 year.

When it comes to dust particles consisting of MgO/FeO, the results indicate that this material cannot survive around the Sun at 0.18-0.2 AU, since the sublimation lifetime is low, varying from 0.2 to 5 seconds. Whether the dust can survive further out, needs to be investigated further. For Vega, the sublimation lifetime of MgO/FeO ranges from 0.0003-1400 seconds between 0.3-0.9 AU and this indicates that MgO/FeO cannot survive at these distances. On the other hand, the sublimation lifetime for MgO/FeO around Fomalhaut is longer compared to Vega, varying from less than a second to around one day. It appears that MgO/FeO cannot survive around Fomalhaut between 0.3-0.9 AU. The results are summarized in Table 18 and Table 19. The categories in Table 19 is defined in the same way as in Table 17.

Table 18: Results of sublimation lifetime for different materials with a size ≤ 100 *nm between 0.18-0.2 AU for the Sun and 0.3-0.9 AU for Vega and Fomalhaut.*

	MgO/FeO	Amorphous carbon	Astronomical silicate
The Sun	0.2-5 seconds	$3 \times 10^{11} - 9 \times 10^{15}$ years	$3 - 4 \times 10^{7}$ years
Vega	0.0003-1400 seconds	33 seconds to 6000 years	0.005 seconds to 55 hours
Fomalhaut	0.08 seconds to 23 hours	100 days to 1×10^{12} years	20 seconds to 2×10^{7} years

Table 19: Results for different materials with a size ≤ 100 *nm and conclusion on whether the material can survive between 0.19-0.2 AU for the Sun and 0.3-0.9 AU for Vega and Fomalhaut.*

	MgO/FeO	Amorphous carbon	Astronomical silicate
The Sun	Unlikely to survive	Survives	Survives
Vega	Unlikely to survive	Varies significantly with distance	Unlikely to survive
Fomalhaut	Unlikely to survive	Varies with distance	Varies significantly with distance

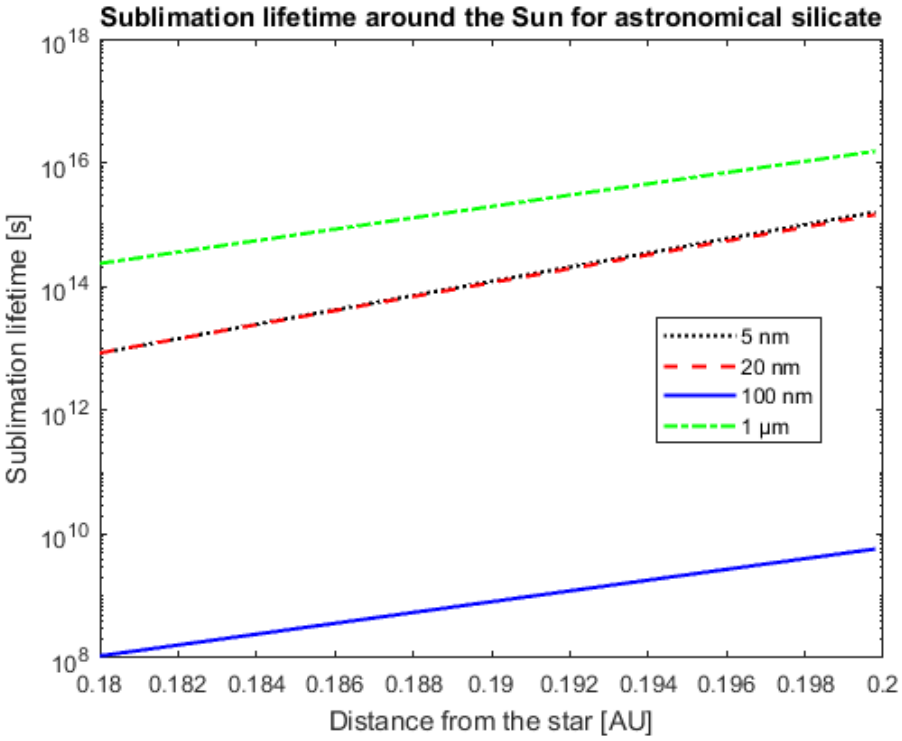

Figure 30: Sublimation lifetime in units of seconds around the Sun for dust particles consisting of astronomical silicate.

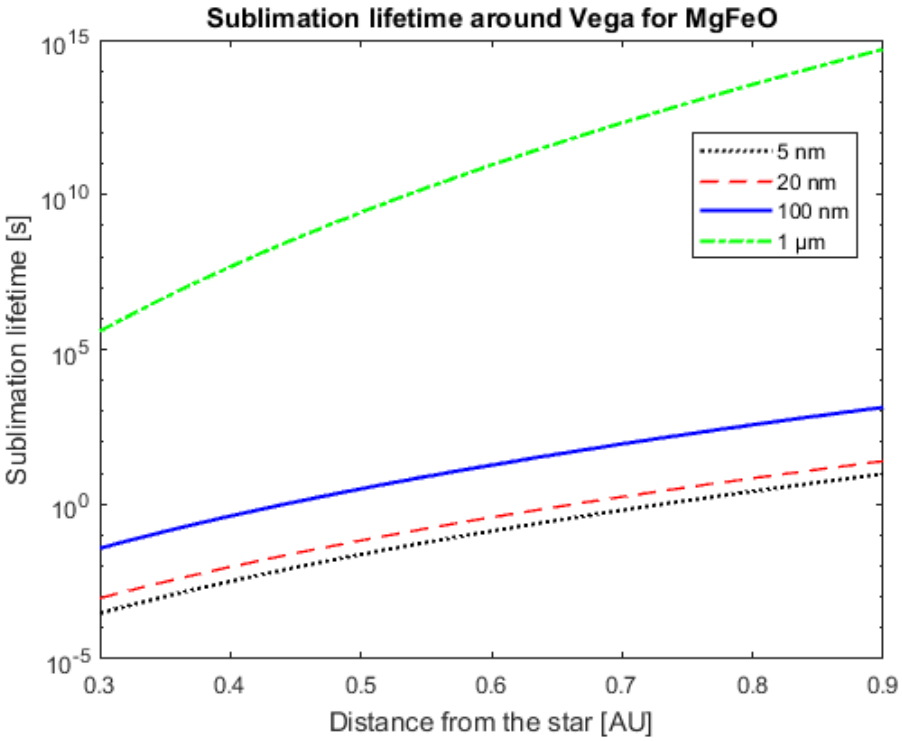

Figure 31: Sublimation lifetime in units of seconds around Vega for dust particles consisting of a mixture of MgO/FeO.

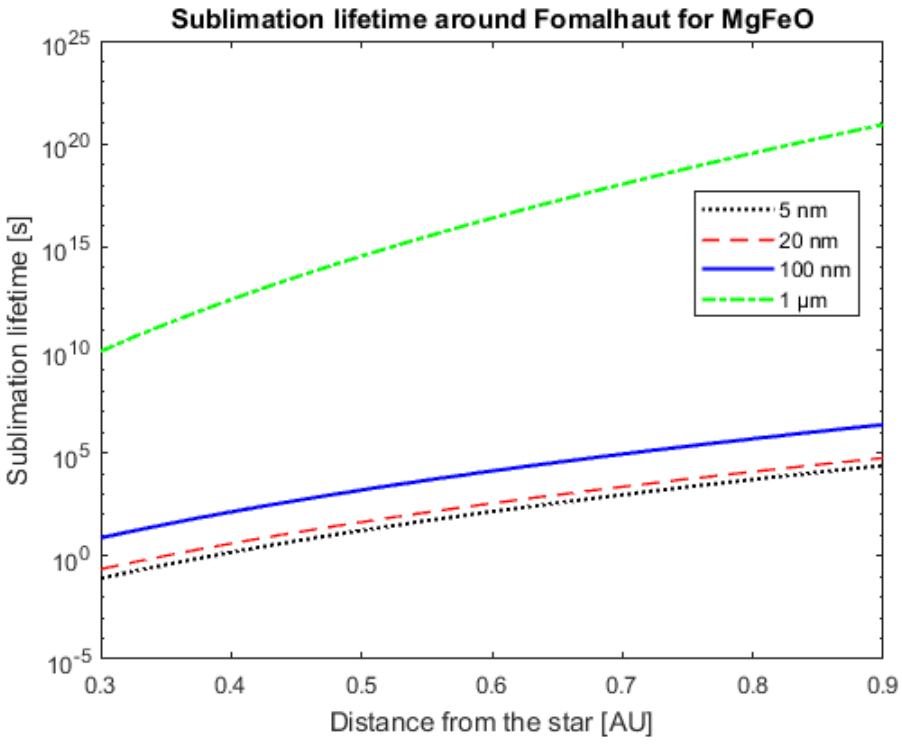

Figure 32: Sublimation lifetime in units of seconds around Fomalhaut for dust particles consisting of a mixture of MgO/FeO.

5.4.2 Optically thickness

The calculations of the thermal emission brightness were made by simple integration of single particle emission. Multiple scattering or absorption within the dust disk was not taken into consideration. This is a reasonable description if the dust disk is optically thin. Vega can be viewed pole-on, while the Fomalhaut system is inclined by 67º (Su et al. 2013). The calculations on optically thickness were done by assuming that the stellar system is viewed pole-on. This assumption was made since there are no available observational data on the height of the dust disk. Computations on total dust mass showed that Vega contains more dust mass compared to Fomalhaut, making Fomalhaut more likely to be optically thin.

The total surface area of a dust disc between 0.18-0.2 AU was $5.3 \times 10^{20}\ m^2$. For dust particles consisting of MgO/FeO in a size distribution between 5-20 nm, the total surface area of the geometric cross-section was $2.0 \times 10^{20}\ m^2$. The total dust mass was equivalent to 56 Halley comets. With a total dust mass equivalent to 10 Halley comets and with dust particles consisting of amorphous carbon where the size is 100 nm, the total surface area of the geometric cross-section was $3.7 \times 10^{18}\ m^2$. This shows that the cross-section of the dust is smaller than the surface area of the dust disk, and therefore, the dust cloud can be considered to be optically thin.

6 Discussion

Dust particle with a size of 1 µm or less which are composed of a mixture of iron oxide and magnesium oxide or astronomical silicate have a prominent feature at ~18 µm or ~10 µm in their model SEDs, respectively. This feature disappears for a 10 µm dust particle. If measurements are performed in the close vicinity of the Sun and a prominent feature is observed at these wavelengths, this may indicate that a mixture of iron oxide and magnesium oxide or astronomical silicate with a size of 1 µm or less is present. Though, around the Sun, MgO/FeO dust with a size of 100 nm or smaller is less likely to be observed inward of 0.2 AU since calculated sublimation lifetime indicates that it sublimates within seconds. MgO/FeO with a size of 1 µm and astronomical silicate with a size of 1 µm or less have significantly longer sublimation lifetimes. These sublimation lifetime varies from a couple of years to thousands of years, making it more probable to be observed.

By just considering the computed SEDs, MgO/FeO and amorphous carbon are the materials that fit to observations around Vega and Fomalhaut. For Vega, MgO/FeO with a size of 5-20 nm and 100 nm and amorphous carbon with a size of 5-20 nm and 100 nm at 0.18-0.2 AU fits very well to the observations. These materials and sizes are therefore likely candidates to give rise to the excess emission observed around Vega. Authors of other articles concluded that the dust size ranges from 10-200 nm, see section 1.2, and this in accordance with the finding for Vega, where dust particles with a size of 1 µm did not fit to observations. For Fomalhaut, drawing precise conclusion is more difficult. None of the model SEDs fitted exactly within the observational uncertainties in the N-band. Amorphous carbon with a size of 5-20 and 100 nm at 0.18-0.2 AU could be responsible for the excess emission, but this requires the presence of another dust ring located further out, since it did not fit the observation in the N-band at longer wavelengths. A mixture of MgO/FeO with a size of 5-20 nm or 100 nm at 0.18-0.2 AU could possibly fit to the observations if the dust ring is located further away from Fomalhaut, although this has not yet been tested. On the other hand, dust particles of 1 µm consisting of MgO/FeO around Fomalhaut almost fit to observations in the N-band. Due to a lack of measurements at shorter wavelengths in the H-band, this conclusion is less certain than for Vega, which have observations in the H-band. Generally, the SEDs for a dust ring located at ~1 AU did not fit to observations around Vega and Fomalhaut. For Vega, dust particles distributed in a ring at 0.99-1.01 AU did not fit to observations, but this was only tested for MgO/FeO with a size of 5-20 nm, so whether other materials and sizes at 0.99-1.01 AU fit to observations remains untested. For a dust ring located between 0.99-1.01 AU around Fomalhaut none of the materials or sizes that were tested fit to observations. The findings that the dust is located inward of a distance of ~0.2 AU from the star are in accordance with the results found in other articles by Mennesson et al. (2011) and Lebreton et al. (2013).

In summary, around Vega there is a good fit for the SEDs, while for Fomalhaut the SEDs fit less good, but generally the dust ring has to be located close to the star, inward of 0.2 AU, the dust size is in the nano-range and materials like MgO/FeO and amorphous carbon explains the SEDs better compared to the other materials. In reality, there will be other materials present in a dust ring as well, i.e. there will be a mixture of materials, but a high percentage of the dust might consist of MgO/FeO or/and amorphous carbon. Since there are few observations, there are many ways to reproduce the SEDs, so other materials than those that were tested in this work might fit to observations around Vega and Fomalhaut, or in a combination of materials might also fit to observations.

To fit the SEDs to Vega's observations, a total dust mass is required that is equivalent to the mass of 20-60 Halley comets. For Fomalhaut, the total dust mass required is equivalent to 10-30 Halley comets. The mass of one Halley comet is 2.2×10^{14} kg (Cevolani et al. 1987) and the mass of 60 Halley comets is 1.3×10^{16} kg. As a comparison, the mass of Earth is 5.974×10^{24} kg (Karttunen et al. 2006), as mentioned before, and the mass of Jupiter is 1.9×10^{27} kg (JPL Solar System Dynamics 2009). If a dust mass equivalent to 60 Halley comets has to be replenished per year and the mass equivalent to Jupiter was available, the dust would last for:

$$\frac{1.9 \times 10^{27}\ kg}{1.3 \times 10^{16}\ kg/year} = 1.5 \times 10^{11}\ years$$

The age of Vega is 455 Myr (Yoon et al. 2010) or 4.5×10^{8} years and the age of Fomalhaut is 400 Myr (Mamajek 2012) or 4.4×10^{8} years, which means that the dust could be replenished every year with 60 Halley comets and it would last for longer than the age of Vega and Fomalhaut. Consequently, if the dust survives for a year, a total dust mass equivalent to 10-60 Halley comets is quite reasonable, even more so if the dust mass is compared to the total mass of a planetary debris disk.

Looking at dust loss mechanisms is therefore important, so that the dust replenishing rate can be estimated. These loss mechanism includes sublimation or loss because the dust particles are blown away from the star by radiation pressure. If the dust is lost, it has to be replenished in order to give rise to an emission. This dust mass can come from sublimating comets which are dynamically perturbated from the warm and cold belt around Vega and Fomalhaut. It can also come from dust that are transported inward due to Poynting-Robertson drag and which are then fragmented into smaller dust particle due to collisions (Mennesson et al. 2011). As stated by Defrère et al. (2011) and Lebreton et al. (2013), both Vega and Fomalhaut are currently undergoing major dynamical activity, similar to the late heavy bombardment in the solar system. The observed excess emission around Vega and Fomalhaut and the possibly high dust production rate can perhaps be explained by this dynamical restructuring. How high the replenishing rate has to be, will depend on the sublimation lifetime and the ejection rate due to radiation pressure and electromagnetic forces.

Sublimation lifetimes indicate that MgO/FeO is severely affected by sublimation between 0.18-0.9 AU around Vega and Fomalhaut, since it only survives for about a thousand seconds around Vega and around one day around Fomalhaut. If MgO/FeO supposedly is giving rise to the excess emission, it would require that the dust replenishing rate is very high. Amorphous carbon with a size of 100 nm and 5-20 nm is perhaps a more probable candidate since it has a longer sublimation lifetime compared to MgO/FeO, requiring a lower replenishing rate. Both for Vega and Fomalhaut there were indications that amorphous carbon with a size of 100 nm or less could be located outward of 0.2 AU and still fit to observations. In that case, the replenishing rate can be even lower. Comparing a dust replenishing rate with 60 Halley comets per second to the mass of Jupiter, as done in the section above, gives:

$$\frac{1.9 \times 10^{27}\ kg}{1.3 \times 10^{16}\ kg/second} = 1.5 \times 10^{11}\ seconds = 4756\ years$$

i.e the dust can last for 4756 years with a mass equivalent to Jupiter at hand. Based on present knowledge, it is unknown if the observed excess emission only is a transient event, triggered by the dynamical activity around Vega and Fomalhaut. It may be that the excess emission will not continue to be observable in the future, and if this is the case, then MgO/FeO and amorphous carbon could

explain the excess emission around Vega and Fomalhaut, since it is only a transient phenomenon. The question which remains is: For how many years can the dust be observed?

There have been many articles that have discussed the observed excess emission at ~2 μm around A-type stars and thermal emission by dust has been viewed as the best explanation for this emission. Other explanation which has been proposed includes scattering of stellar light by dust or emission by optically thin gas (Rieke et al. 2016). The total emission by dust will contain a component of scattered light by dust (Lebreton et al. 2013). SEDs of scattered stellar light by dust has a peak around the same wavelengths as the SED of the star since the light has only been refracted. It falls of steeply at longer wavelengths and it is considerably lower at ~2 μm compared to the SEDs of thermal emission by dust. (Mennesson et al. 2013). Therefore, the scattered stellar light by dust does not contribute significantly at ~2 μm, which is where the observed flux is, i.e. in the K-band and the H-band. If these observations around Vega are to be explained by scattering of starlight by dust, the total dust mass has to be much larger in order to give a high enough brightness so that it fits to observations. This makes emission from scattered star light by dust a less probable candidate compared to thermal emission by dust. On the other hand, if a dust ring scattering stellar light is located further away from the star, the dust will be less affected by sublimation and the replenishing rate can be lower. When it comes to emission by gas, it is presently unknown whether the gas can explain the observed excess emission. The gas may be present in abundance since sublimating dust produces gas. Another scenario could be that the excess emission is caused by scattered light from electrons in the K-corona for Vega and Fomalhaut, which could be investigated further. The excess emission around Vega and Fomalhaut was supposedly found by subtracting a model of the stellar photosphere from observations, but it is unclear if the stellar corona was included in this subtraction.

Around A-type stars, the problem has been that the radiation pressure is strong for dust in the nano-range. These dust particles are likely to be ejected from the stellar system. The computed beta-values showed that for dust less than about 3 μm, the beta-values are larger than 0.5 and they are likely to be ejected. If the dust is charged by the stellar wind or the photoelectric effect, the dust particles could possibly be trapped by the magnetic field. Rieke et al. (2016) showed that dust particles in the nano-range could be retained close to the stars for weeks by trapping in the stellar magnetic field. On the other hand, Johann Stamm (master thesis in preparation), showed that all charged dust particles, regardless of size, would be ejected from the stellar system, despite the influence of electromagnetic forces in the stellar wind. So, whether charged dust particles can be magnetically trapped around Vega and Fomalhaut remains unclear, but given that they are trapped, the dust replenishing rate can be lower.

All in all, the hot dust still remains a bit of a mystery. It is possible that thermal emission from dust consisting of amorphous carbon, and perhaps MgO/FeO, with a size in the nano-range is responsible for the excess emission around Vega and Fomalhaut. The SEDs may fit to observations if the dust ring is located further away from the stars and here, the sublimation lifetime will be longer, but the dust can still be lost through ejection by radiation pressure. Anyhow, this would require a high production rate. Perhaps the excess emission is only a transient event? Or maybe it is caused by something else?

Some of the questions related to dust can possibly be answered by two upcoming space mission, the Solar Orbiter, which has an optical instrument on board and which can measure scattered light by dust, and the Parker Solar probe. Both space missions can possibly measure dust impact. From these space

missions, one can learn about dust composition near the Sun, how close it is to the Sun, the size as a function of distance from the star and in general, learn about dust size distribution.

7 Conclusion

Computed dust temperatures around the Sun, Vega and Fomalhaut vary with dust composition, size and distance from the star and is different from the temperature of a black body. For the dust materials considered in this work, calculations showed that dust particles with a size of 100 nm or less can have a temperature which is significantly higher than black body.

SEDs of MgO/FeO and amorphous carbon with a size of 100 nm and 5-20 nm at 0.18-0.2 AU fit to observations in the H-band, K-band and at 10.6 µm around Vega. The total dust mass is equivalent to less than 60 Halley comets around Vega. For Fomalhaut, none of the spectral energy distributions fitted exactly within the observations in the K-band and the N-band, but MgO/FeO with a size of 100 nm and 5-20 nm could possibly fit if the dust ring is located further away than 0.2 AU from Fomalhaut, while amorphous carbon with a size of 100 nm and 5-20 nm can possibly fit if there are two dust ring, one located at 0.18-0.2 AU and located one further out. For Fomalhaut, the total dust mass is equivalent to less than 30 Halley comets.

Around Vega and Fomalhaut, MgO/FeO is influenced by sublimation inward of 0.9 AU, leaving amorphous carbon as a more likely candidate to be responsible for the excess emission, since it has a longer sublimation lifetime. Dust consisting of amorphous carbon could possibly be located further out, but within ~1 AU, where the sublimation lifetime will be higher, while still fit to the observations. This may also be the case for MgO/FeO. In addition, dust with a size in the nano-range will be exposed to a strong radiation pressure around Vega and Fomalhaut and computed beta-values indicate that dust particles with a size of 1 µm or less is ejected from the stellar system.

Whether thermal emission from dust is responsible for the excess emission observed around Vega and Fomalhaut is still not resolved, even though the SEDs fits to observations, because the dust can be lost quickly through sublimation and due to radiation pressure, requiring that the replenishing rate is very high, perhaps too high to be realistic. It is also not clear if the excess emission is only a transient event and if it can be observed in the future. Other sources for the excess emission can also be possible.

7.1 Future work

Future work can include testing dust with other materials, sizes and distances around Vega and Fomalhaut. When computing the SEDs, many simplifications were made. The SEDs were regarded as adequate since only a small set of observations were available. If more observations are measured, it might be worthwhile to estimate the SEDs more accurately. This can be done by adding Planck functions together at each distance or by having the size and density distribution as a function of both size and distance and so on. In addition, it is possible to look at other possible explanations for the observed excess emission around Vega and Fomalhaut, and possibly other stars. For example, look at scattering by gas or scattering by electrons in the corona.

8 References

Absil, O., E. di Folco, A. Mérand, J.-C. Augereau, V. Coudé du Foresto, J. P. Aufdenberg et al. (2006): *Circumstellar material in the Vega inner system revealed by CHARA/FLUOR*. Astronomy & Astrophysics, 452, pp. 237-244.

Absil, O., B. Mennesson, J. B. Le Bouquin, E. Di Folco, P. Kervella and J. C. Augereau (2009): *An interferometric study of the Fomalhaut inner debris disc. I. Near-infrared detection of hot dust with VLTI/VINCI.* The Astrophysical Journal, 704, pp. 150-160.

Asmus, H., H. Wilms, B. Strelnikov and M. Rapp (2014): *On the heterogeneous nucleation of mesospheric ice on meteoric smoke particles: Microphysical modelling.* Journal of atmospheric and solar-terrestrial physics, 118, pp. 180-189. http://dx.doi.org/10.1016/j.jastp.2014.03.009.

Aufdenberg, J. P., A. Mérand, V. Coudé du Foresto, O. Absil, E. Di Folco, P. Kervella, S. T. Rigdway et al. (2006): *First results from the CHARA array. VII. Long-baseline interferometric measurements of Vega consistent with a pole-on, rapidly rotating star.* The Astrophysical Journal, 645, pp. 664-675.

Bohren, C. F. and D. R. Huffmann (1983): *Absorption and scattering of light by small particles.* New York: John Wiley & Sons.

Brekke, A. (2013): *Physics of the upper polar atmosphere*. Second edition. Heidelberg: Springer.

Brown. G. *NASA renames Solar probe mission to honour pioneering physics Eugene Parker.* [Read: 02.05.2018]. https://www.nasa.gov/feature/goddard/2017/nasa-renames-solar-probe-mission-to-honor-pioneering-physicist-eugene-parker.

Cevolani, G., G. Bortolotti and A. Hajduk (1987): *Halley, comet's mass loss and age.* II Nuovo Cimento C. Italian Physical Society, 10(5), pp. 587-591.

Defrère, D., O. Absil, J. C. Augereau, E. Di Folco, J. P. Berger, V. Coudé du Foresto, P. Kervella et al. (2011): *Hot exozodiacal dust resolved around Vega with IOTA/IONIC.* Astronomy & Astrophysics, 534, A5.

Dohnanyt, J.S. (1969): *Collisional model of asteroids and their debris.* Journal of Geophysical Research, 74, 10, pp. 2531-2555.

Evans, A. (1993): *The dusty universe*. England: Ellis Horwood Limited.

Gulliver, A. F., G. Hill and S. J. Adelman (1994): *Vega: A rapidly rotating pole-on star*. The Astrophysical Journal, 429 (2), L81-L84.

Henning, Th., B. Begeman, H. Mutschke and J. Dorschner (1995): *Optical properties of oxide dust grains.* Astronomy & Astrophysics, Suppl. Ser., 112, pp. 143-149.

JPL Solar system Dynamics (2009): *Astrodynamic Constants.* [Read: 06.05.2018]. https://ssd.jpl.nasa.gov/?constants

Karttunen, H., P. Kroger, H. Oja, M. Poutanen and K. J. Donner (eds.) (2006): *Fundamental astronomy*. Fifth edition. Berlin: Springer.

Köhler, M. and I. Mann (2002): *Model calculations of dynamical forces and effects on dust in the circumstellar debris disk.* Berlin: Proceedings of asteroids, comets, meteors (ACM 2002), 29 July-2 August 2002. http://adsabs.harvard.edu/abs/2002ESASP.500..771K

Lebreton, J., R. van Lieshout, J. C. Augereau, O. Absil, B. Mennesson, M. Kama, C. Dominik et al. (2013): *An interferometric study of the Fomalhaut inner debris disk. III. Detailed models of the exozodiacal disk and its origin.* Astronomy & Astrophysics, 555, A146.

Li, A. (2009): *Optical properties of dust.* I: Mann, I., A. M. Nakamura and T. Mukai (eds.) (2009): *Small bodies in planetary systems*. Berlin: Springer.

Li, A. and J. M. Greenberg (1997): *A unified model of interstellar dust.* Astronomy & Astrophysics, 323, pp. 566-584.

Li, A. and I. Mann (2012): *Nanodust in the interstellar medium in comparison to the solar system.* I: Mann, I., N. Meyer-Vernet and A. Czechowki (eds.) (2012) *Nanodust in the Solar System: Discoveries and interpretations.* Heidelberg: Springer. DOI 10.1007/978-3-642-27543-2.

LISIRD (2018a): *Source Solar Spectral Irradiance - Spectrum.* [Read: 02.05.2018]. http://lasp.colorado.edu/lisird/data/sorce_ssi_l3/

LISIRD (2018b): *Timed SEE EGS SSI- Level 2 - Spectrum.* [Read: 02.05.2018]. http://lasp.colorado.edu/lisird/data/timed_see_egs_ssi_l2/

Mann, I., D. A. Biesecker, B. T. Tsuritani, E. Grün, B. McKibben, J. C. Liou, R. M. McQueen et al. (2003). *Dust near the Sun*. Netherlands: Kluwer Academic Publisher.

Mann, I., M. Köhler, H. Kimura, A. Cechowski and T. Minato (2006): *Dust in the solar system and in extra-solar planetary systems.* Springer-Verlag. DOI 10.1007/s00159-006-0028-0.

Mamajek, E. E., A. Prsa, G. Torres, P. Harmanec, M. Asplund, P. D. Bennett, N. Capitaine et al. (2015): *Resolution B3 on recommended nominal conversion constants for selected Solar and planetary properties*. arXiv:1510.07674 [astro-ph.SR].

Mamajek, E. E. (2012): *On the age and bimarity of Fomalhaut*. The Astrophysical Journal Letters, 754, L20.

Menneson, B., O. Absil, J. Lebreton, J. C. Augereua, E. Serabyn, M. M. Colavita, R. Millan-Gabet et al. (2013): *An interferometric study of the Fomalhaut inner debris disk. II. Keck Nuller mid-infrared observations.* The Astrophysical Journal, 763, 119.

Mennesson, B., E. Serabyn, C. Hanot, S.R. Martin, K. Liewer, and D. Mawet (2011): *New constraints on companions and dust within a few AU of Vega.* The Astrophysical Journal, 736, 14.

Mätzler, C. (2002): *Matlab Functions for Mie scattering and absorption.* [Read: 21.09.2017] https://omlc.org/software/mie/maetzlermie/Maetzler2002.pdf

Nakamura, A. M. and P. Michel (2009): *Asteroids and their collisional disruption.* I: Mann, I., A. M. Nakamura and T. Mukai (eds.) (2009): *Small bodies in planetary systems*. Berlin: Springer.

NASA (2018a): *Parker Solar probe.* [Read: 02.05.2018]. http://parkersolarprobe.jhuapl.edu/

NASA (2018b): *Solar Orbiter.* [Read: 02.05.2018]. https://science.nasa.gov/missions/solar-orbiter/

Rieke, G. H., A. Gáspár and N. P. Ballering (2016): *Magnetic grain trapping and the hot excess around early-type stars.* The Astrophysical Journal, 816, 50.

Smithsonian Institution (2018): *PIA12192: Iron-nickel meteorite from Texas with triangle-pattern texture.* [Read: 02.05.2018]. https://photojournal.jpl.nasa.gov/catalog/PIA12192

Su, K. Y. L. and G.H. Rieke, R. Malhotra, K. R. Stapelfeldt, A. Meredith Hughes, A. Bonsor, D. J. Wilner et al. (2013): *Asteroid belts in debris disk twins: Vega and Fomalhaut*. The Astrophysical Journal, 763, 118.

Taylor, J. R. (1982): *An introduction to error analysis.* Mill Valley: Oxford University Press.

Wilck, M and I. Mann (1995): *Radiation pressure forces on "typical" interplanetary dust grains.* Planet. Space science, 44, 5, pp. 493-499.

Wurz, P. (2013): *Erosion processes affecting interplanetary dust grains.* I: Mann, I., N. Meyer-Vernet and A. Czechowski (eds): *Nanodust in the Solar systems. Discoveries and interpretations.* Heidelberg: Springer.

Wyatt, M. C (2009): *Dynamics of small bodies in planetary systems.* I: Mann, I., A. M. Nakamura and T. Mukai (eds.) (2009): *Small bodies in planetary systems*. Berlin: Springer.

Yamamoto, S. and T. Mukai (1998): *Thermal radiation from dust grains in Edgeworh-Kuiper Belt.* Earth Planets Space, 50, pp. 531-537.

Yoon, J., D. M. Peterson, R. L. Kurucz and R. J. Zagarello (2010): *A new view of Vega's composition, mass and age*. The Astrophysical Journal, 708 (1), pp. 71-79.

Zender, C. (2013): *Particle size distribution: Theory and applications to aerosols, clouds and soils.* [Read 31.01.2017] http://dust.ess.uci.edu/facts

9 Appendix

9.1 Weighted mean

The computations in this section follows the reasoning by (Taylor 1982). When comparing model calculation of spectral energy distributions, as stated in equation *(37)*, to observation of an excess emission, a mean value can be used if there are more than one measurements for each wavelength, where each of the measurements has its own uncertainty. Finding an average for these measurements can be done by weighting them based on their uncertainty. This is called a weighted mean and the measurements with the lowest uncertainty, i.e. the most accurate ones, will weighted the most. With two different measurements and the corresponding uncertainty:

$$Case\ 1: m = m_1 + \sigma_1, \qquad Case\ 2: m = m_1 + \sigma_1 \tag{44}$$

where the objective is to find a mean and its assumed that these measurements represents values which are normally distributed around a unknown, true value M. The probability for measuring the value in case 1 and 2 is, assuming that they are normally distributed:

$$P_M(m_1) \propto \frac{1}{\sigma_1} e^{-(m_1-M)^2/2\sigma_1}, \qquad P_M(m_2) \propto \frac{1}{\sigma_2} e^{-(m_2-M)^2/2\sigma_2} \tag{45}$$

Assuming that case 1 and 2 are independent, the joint probability for case 1 and 2 can be given by:

$$P_M(m_1, m_2) = P_M(m_1)P_M(m_2) \propto \frac{1}{\sigma_1\sigma_2} e^{-\chi^2/2} \tag{46}$$

where

$$\chi^2 = \left(\frac{m_1 - M}{\sigma_1}\right)^2 + \left(\frac{m_2 - M}{\sigma_2}\right)^2 \tag{47}$$

The best estimate for the unknown, true value M is where the probability of $P_M(m_1, m_2)$ has its maximum, or equivalently where χ^2 has its minimum, which can be found by differentiate χ^2 with respect to M and setting the derivative equal to zero:

$$\frac{\partial\chi^2}{\partial M} = -2\left(\frac{m_1 - M}{\sigma_1^2}\right) - 2\left(\frac{m_2 - M}{\sigma_2^2}\right) = 0 \tag{48}$$

Solving equation *(48)* for M gives the best estimate for the mean:

$$m_{best} = \frac{\frac{m_1}{\sigma_1^2} + \frac{m_2}{\sigma_2^2}}{\frac{1}{\sigma_1^2} + \frac{1}{\sigma_2^2}} \tag{49}$$

By defining:

$$w_1 = \frac{1}{\sigma_1^2}, \qquad w_2 = \frac{1}{\sigma_2^2}$$

gives the weighted mean:

$$m_{best} = \frac{w_1 m_1 + w_2 m_2}{w_1 + w_2} \tag{50}$$

With N separate measurements, equation *(50)* can be given as:

$$m_{best} = \frac{\sum_{i=1}^{N} w_i m_1}{\sum_{i=1}^{N} w_i} \; for \; i = 1,2,\ldots,N \tag{51}$$

and the uncertainty is:

$$\sigma_{mbest} = \left(\sum_{i=1}^{N} w_i \right)^{-1/2} \tag{52}$$

9.2 Figures

9.2.1 Dust temperatures

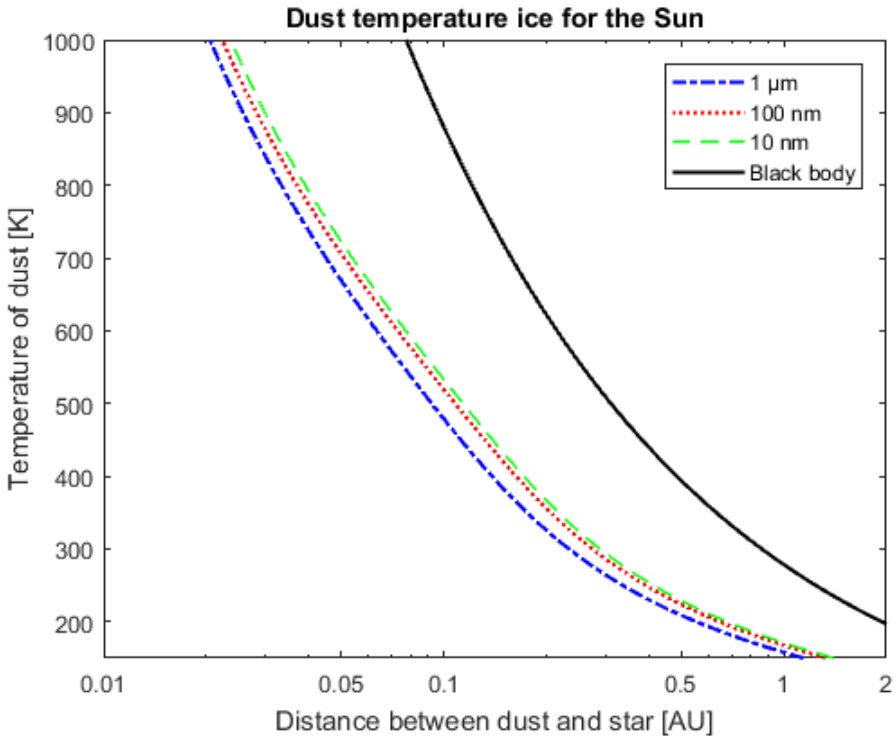

Figure 33: Temperature of dust particles consisting of ice around the Sun.

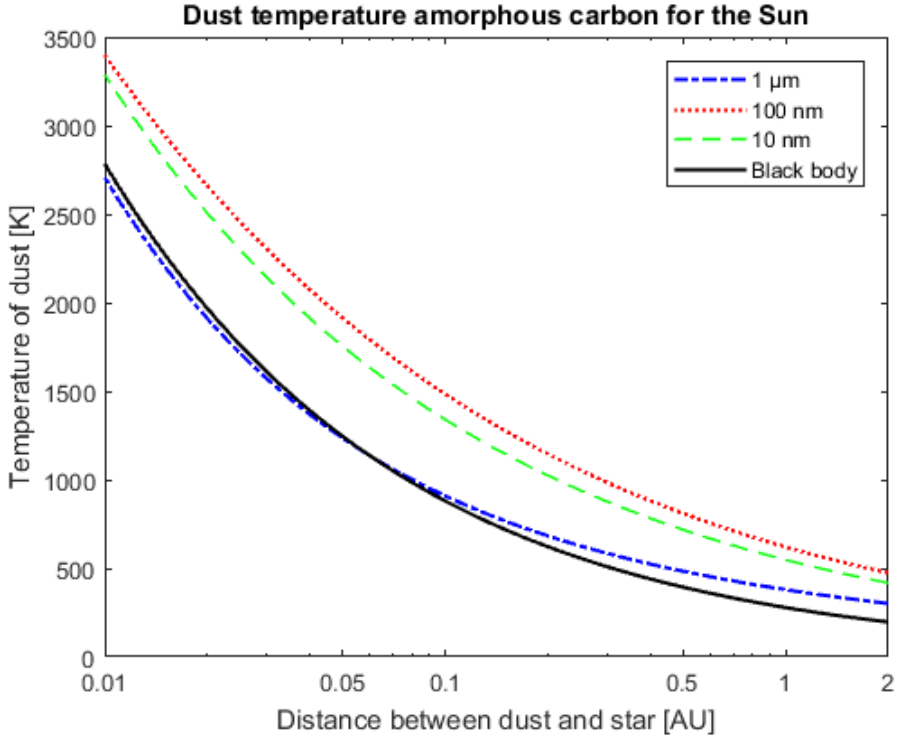

Figure 34: Temperature of dust particles consisting of amorphous carbon around the Sun.

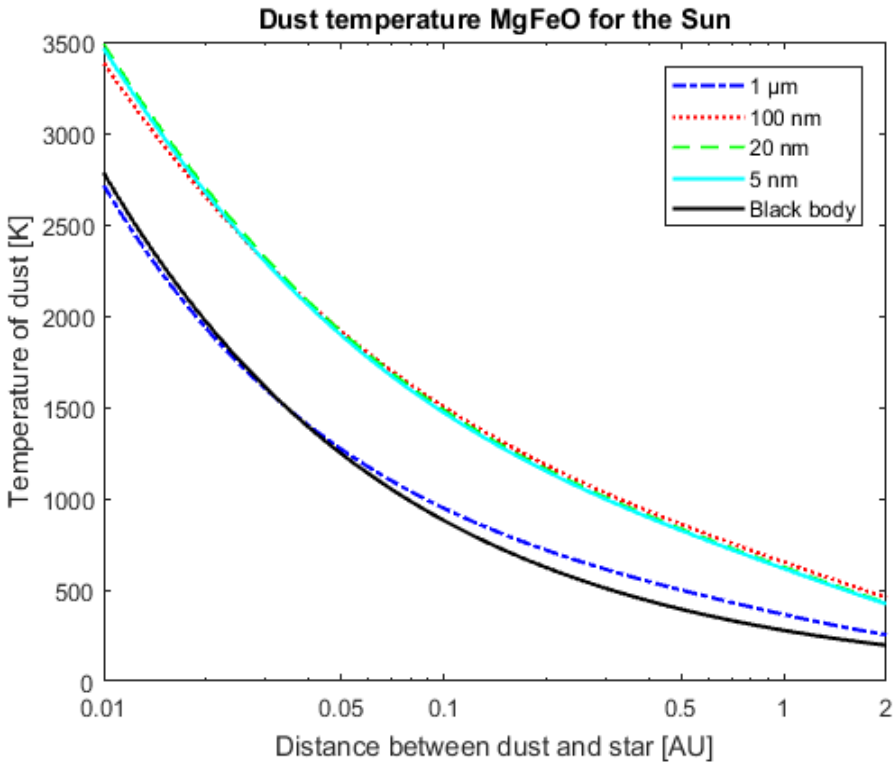

Figure 35: Temperature of dust particles consisting of a mixture of MgO/FeO around the Sun.

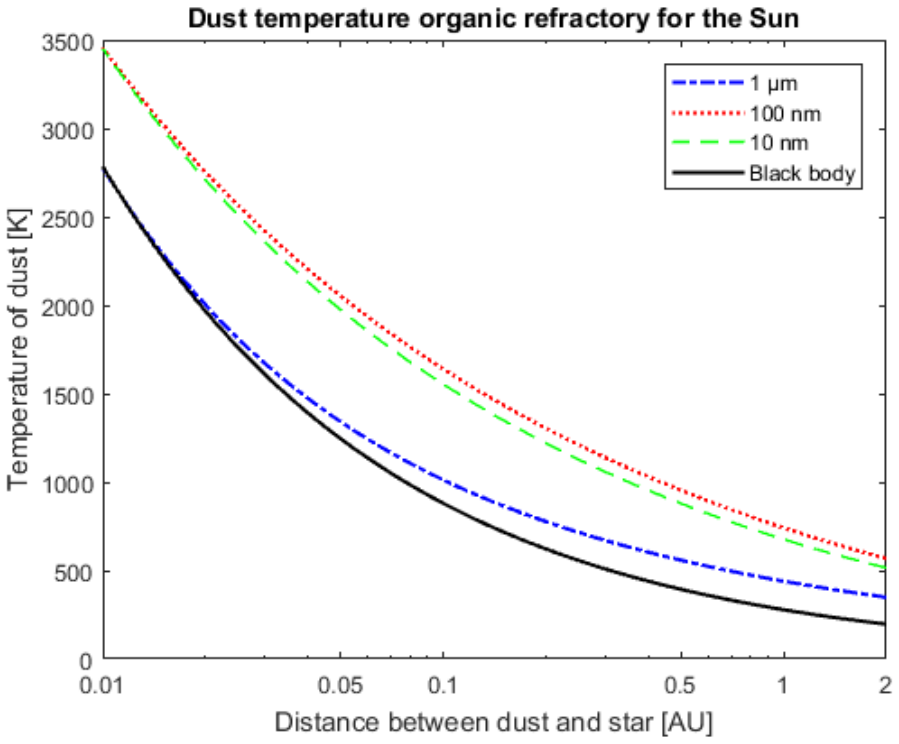

Figure 36: Temperature of dust particles consisting of organic refractory around the Sun.

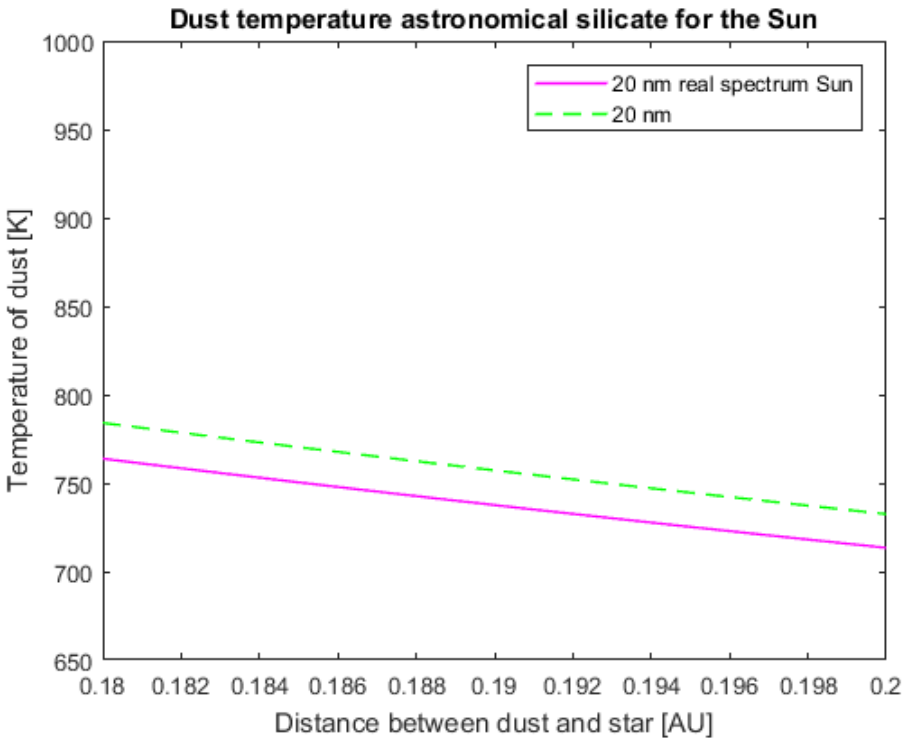

Figure 37: Temperature of dust around the Sun with dust particles consisting of astronomical silicate computed with a real solar spectrum and a black body spectrum. The dust particles have a size of 20 nm.

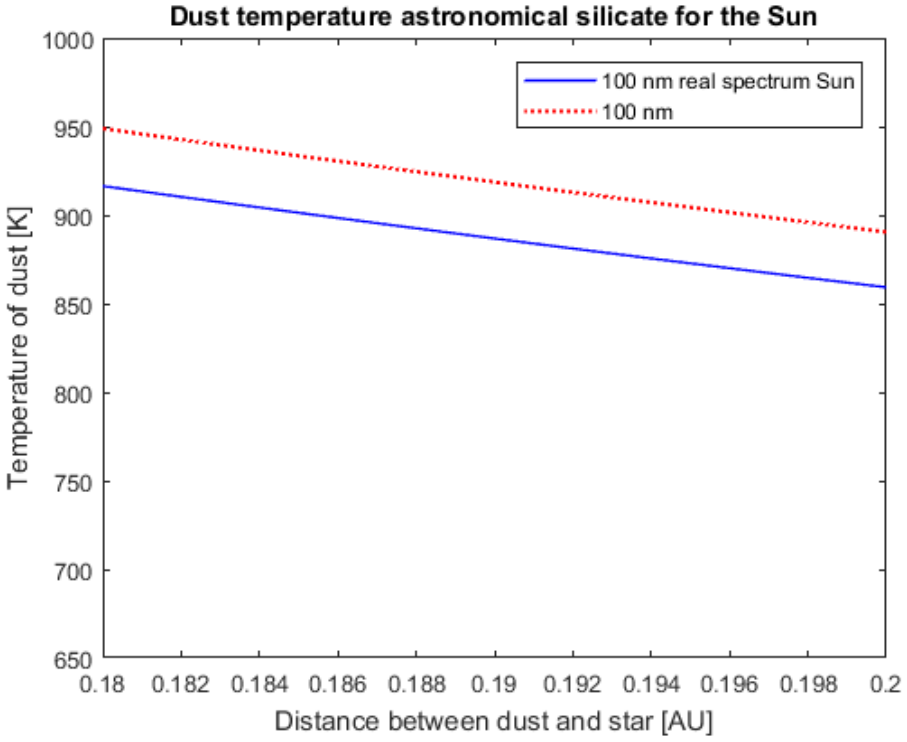

Figure 38: Temperature of dust around the Sun with dust particles consisting of astronomical silicate computed with a real solar spectrum and a black body spectrum. The dust particles have a size of 100 nm.

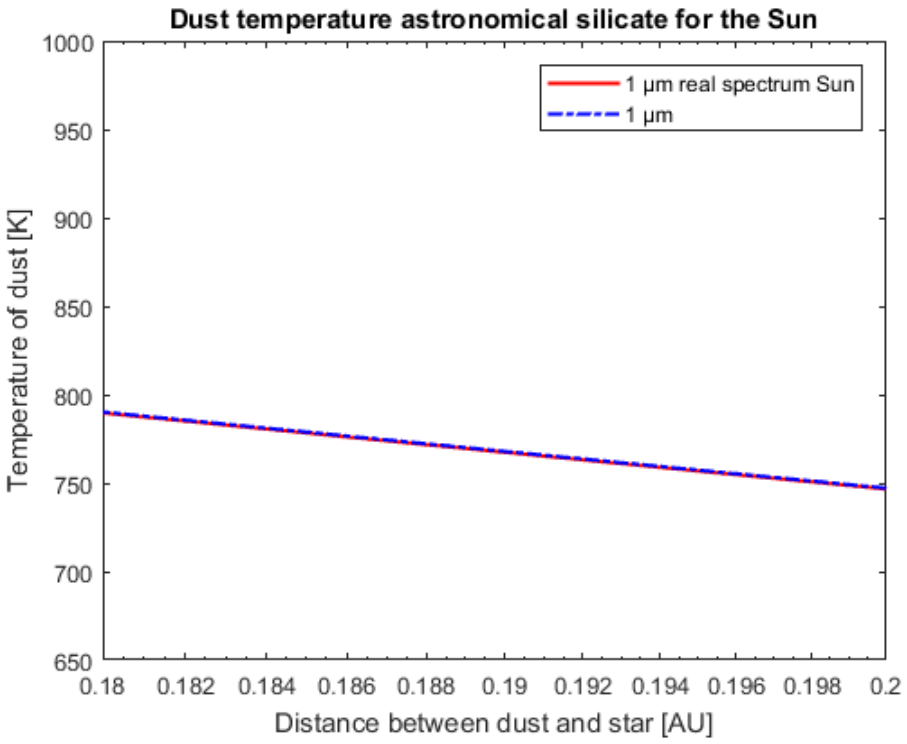

Figure 39: Temperature of dust around the Sun with dust particles consisting of astronomical silicate computed with a real solar spectrum and a black body spectrum. The dust particles have a size of 1 μm.

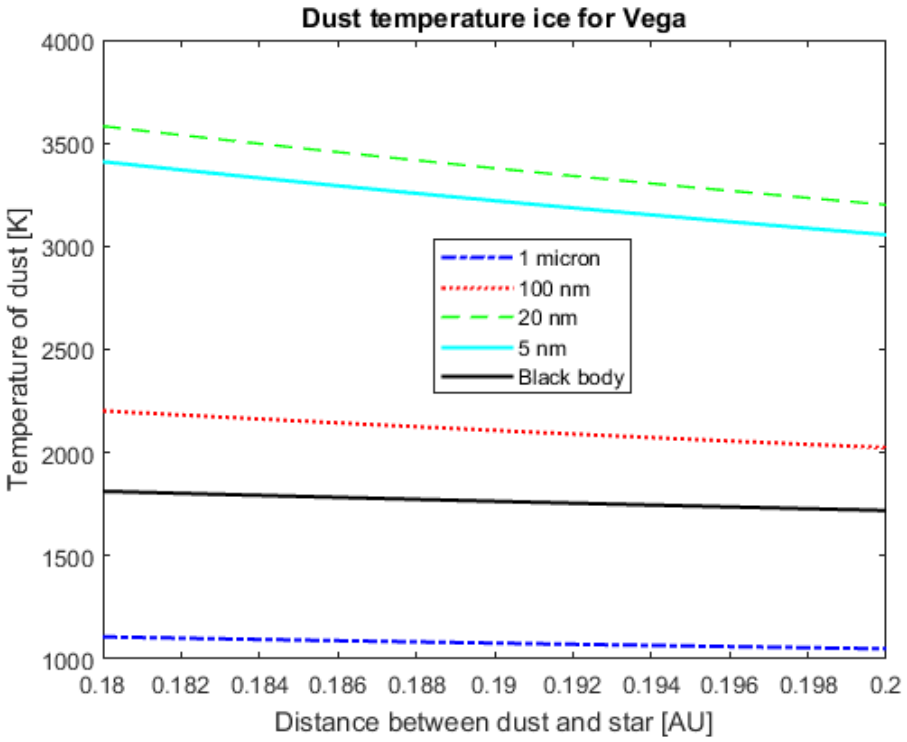

Figure 40: Temperature of dust around Vega with dust particles consisting of ice.

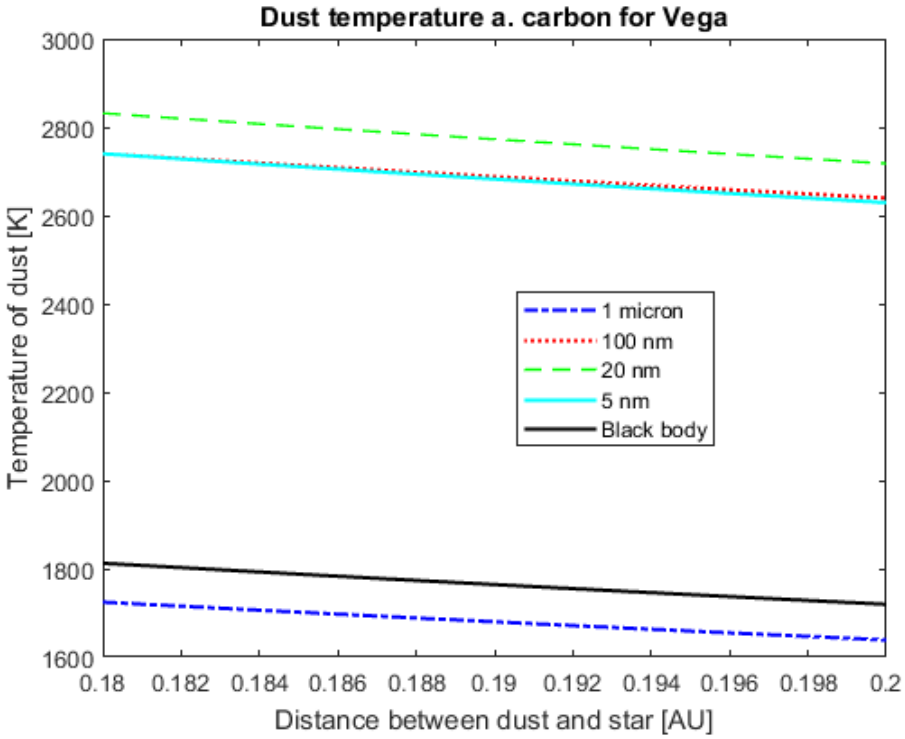

Figure 41: Temperature of dust around Vega with dust particles consisting of amorphous carbon.

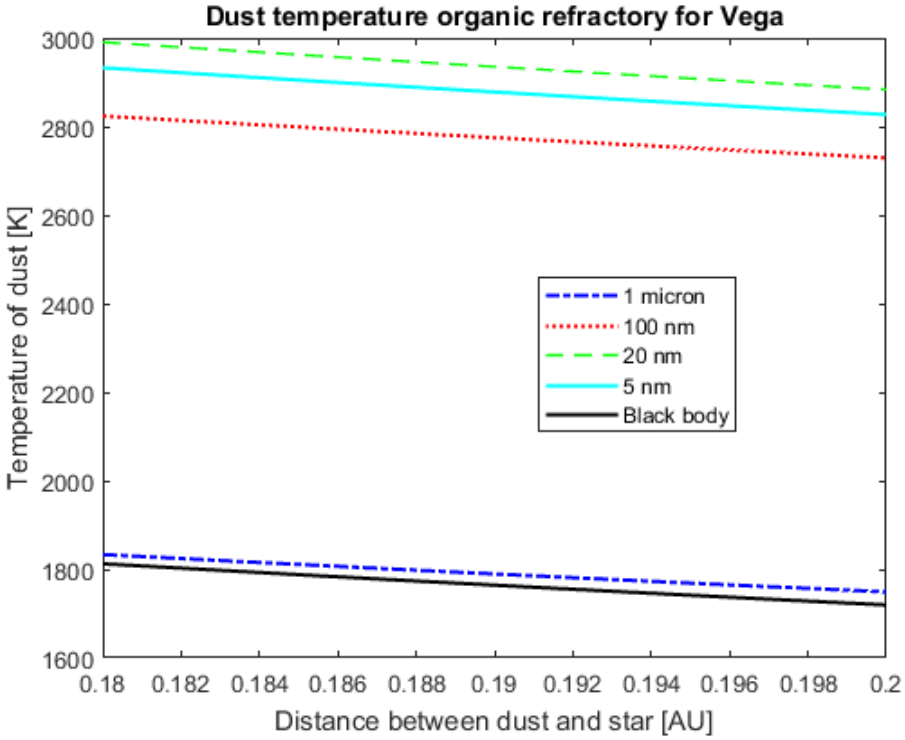

Figure 42: Temperature of dust around Vega with dust particles consisting of organic refractory.

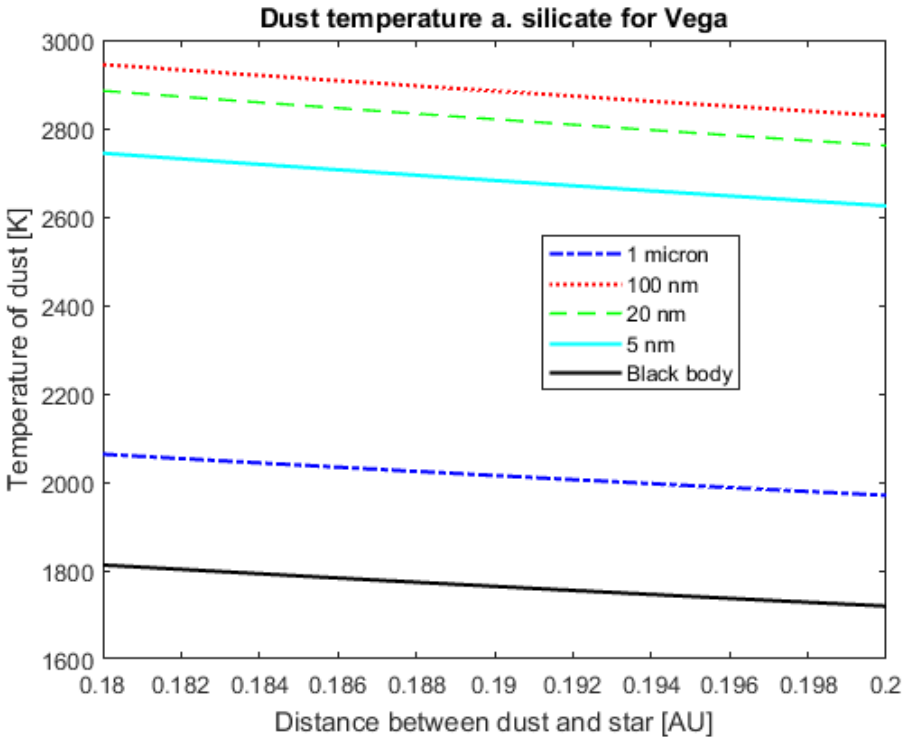

Figure 43: Temperature of dust around Vega with dust particles consisting of astronomical silicate.

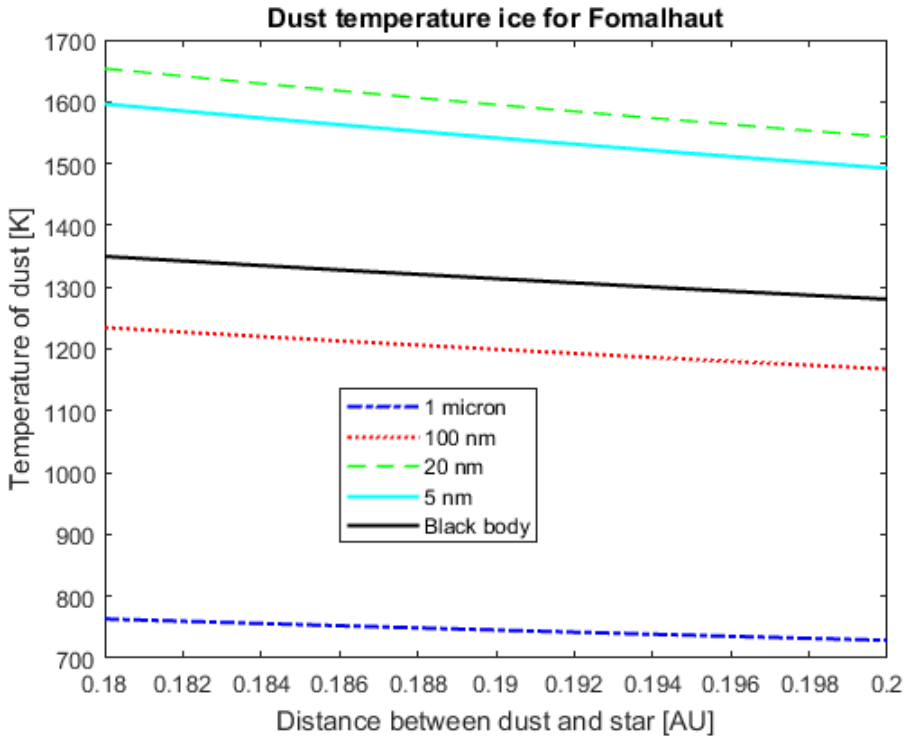

Figure 44: Temperature of dust around Fomalhaut with dust particles consisting of ice.

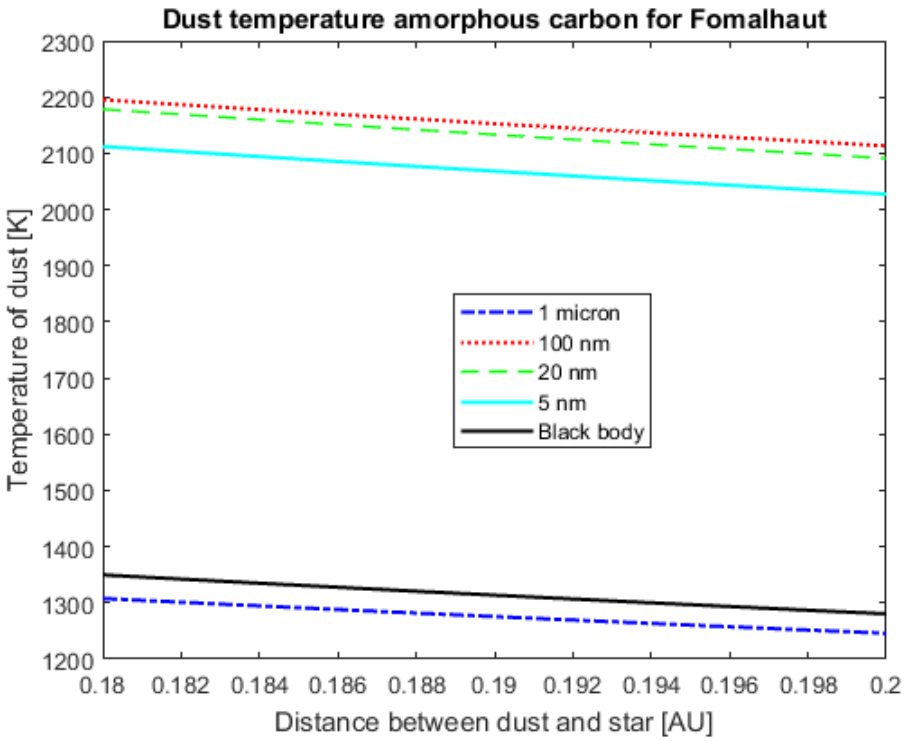

Figure 45. Temperature of dust around Fomalhaut with dust particles consisting of amorphous carbon.

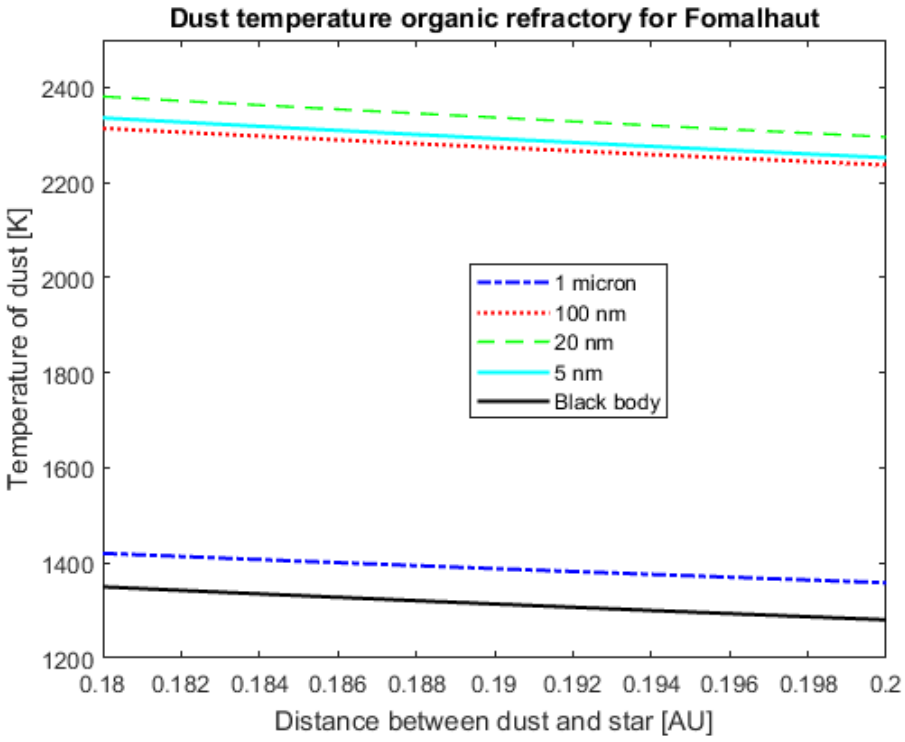

Figure 46: Temperature of dust around Fomalhaut with dust particles consisting of organic refractory.

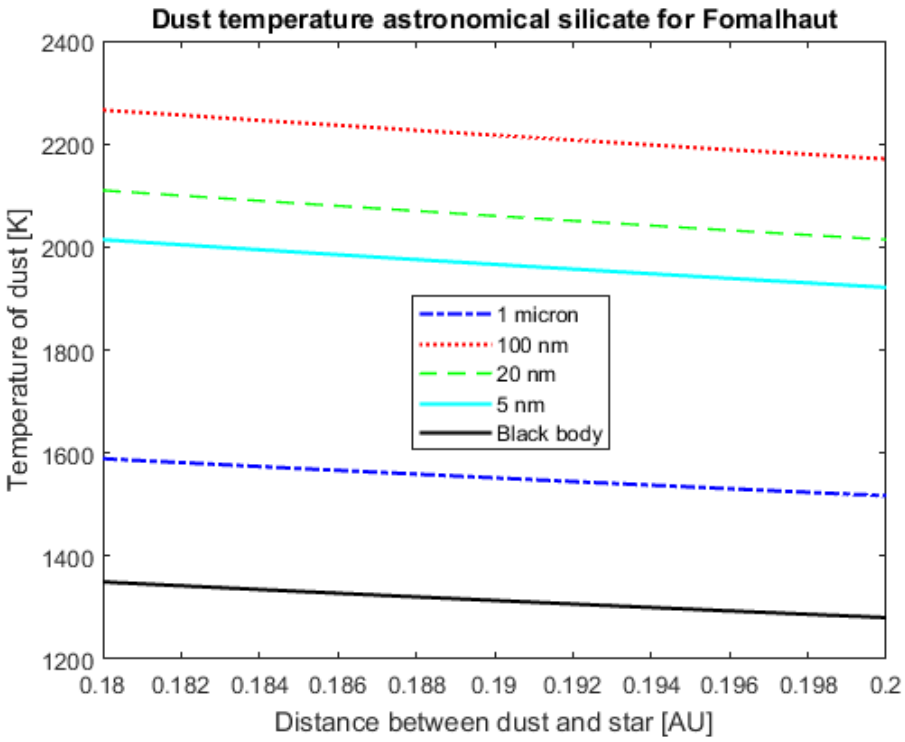

Figure 47: Temperature of dust around Fomalhaut with dust particles consisting of astronomical silicate.

9.2.2 Sublimation lifetimes

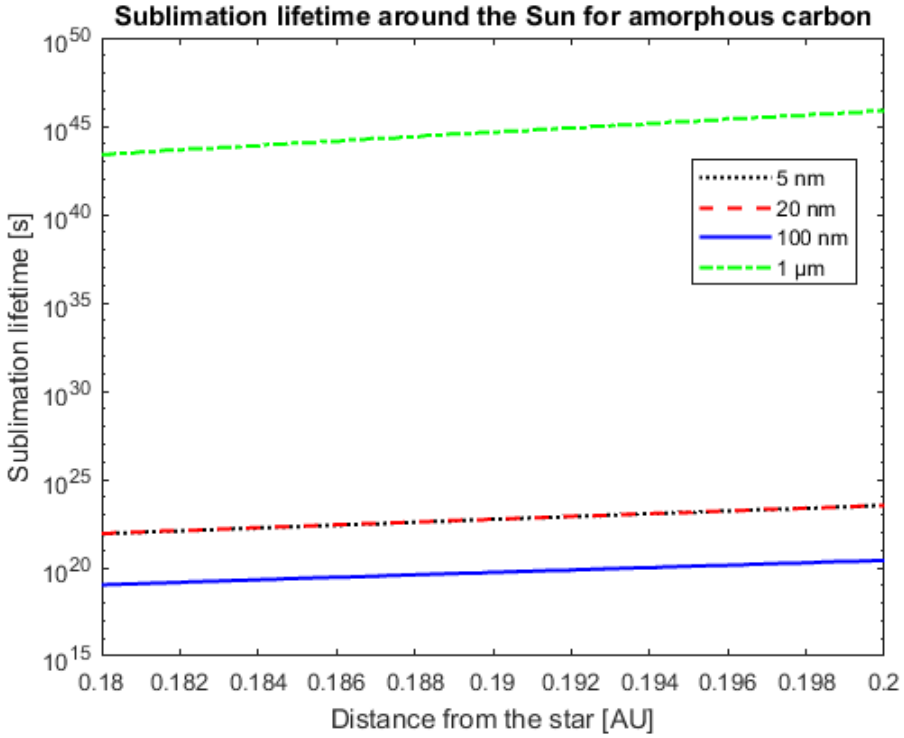

Figure 48: Sublimation lifetime in units of seconds around the Sun for dust particles consisting of amorphous carbon.

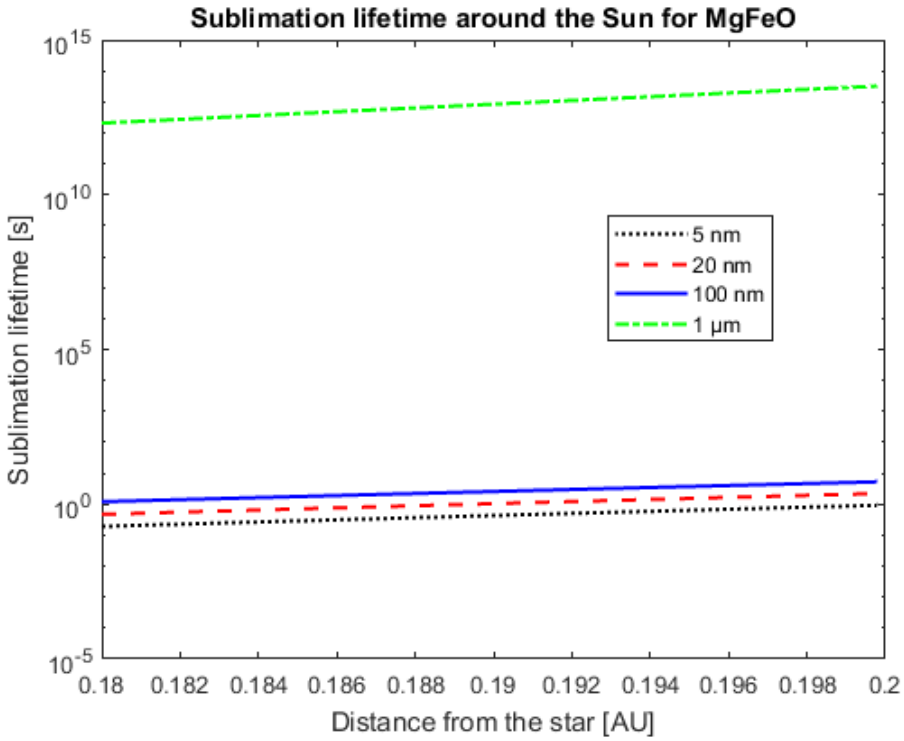

Figure 49: Sublimation lifetime in units of seconds around the Sun for dust particles consisting of a mixture of MgO/FeO.

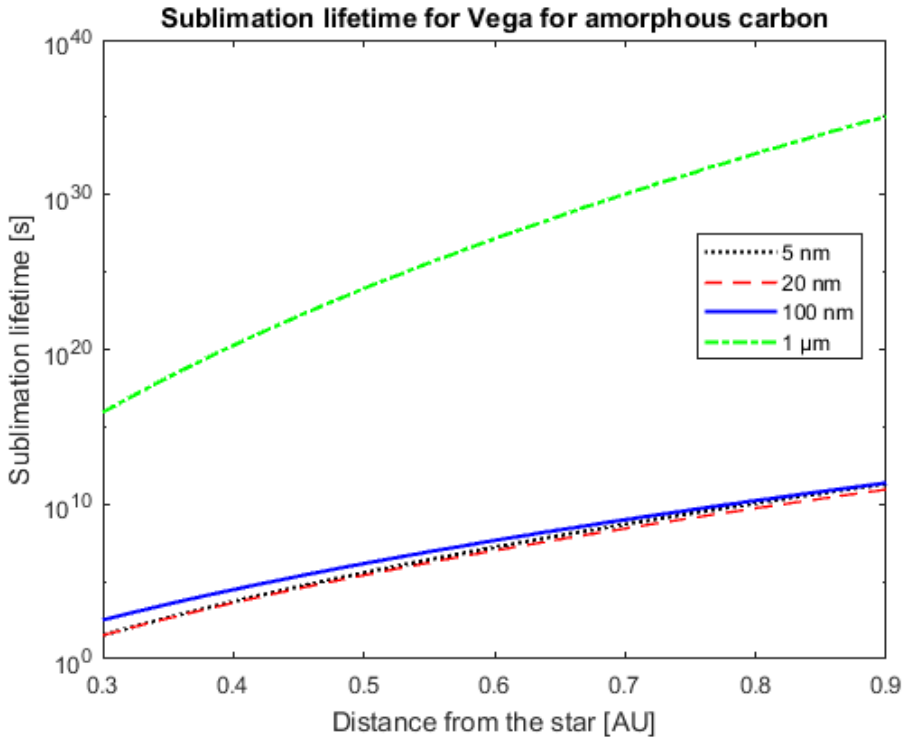

Figure 50: Sublimation lifetime in units of seconds around Vega for dust particles consisting of amorphous carbon.

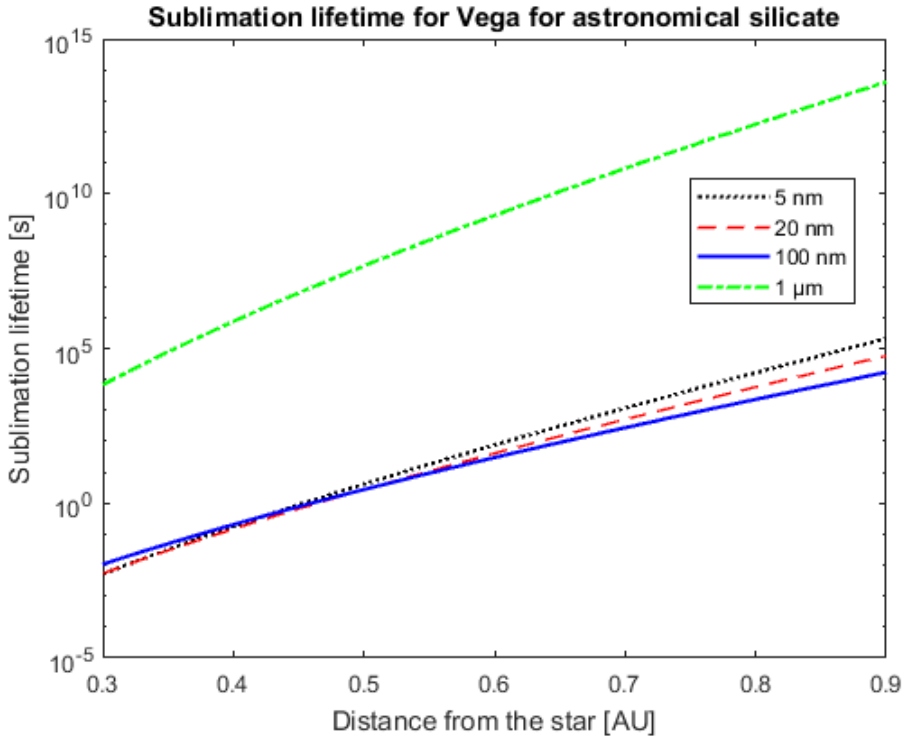

Figure 51: Sublimation lifetime in units of seconds around Vega for dust particles consisting of astronomical silicate.

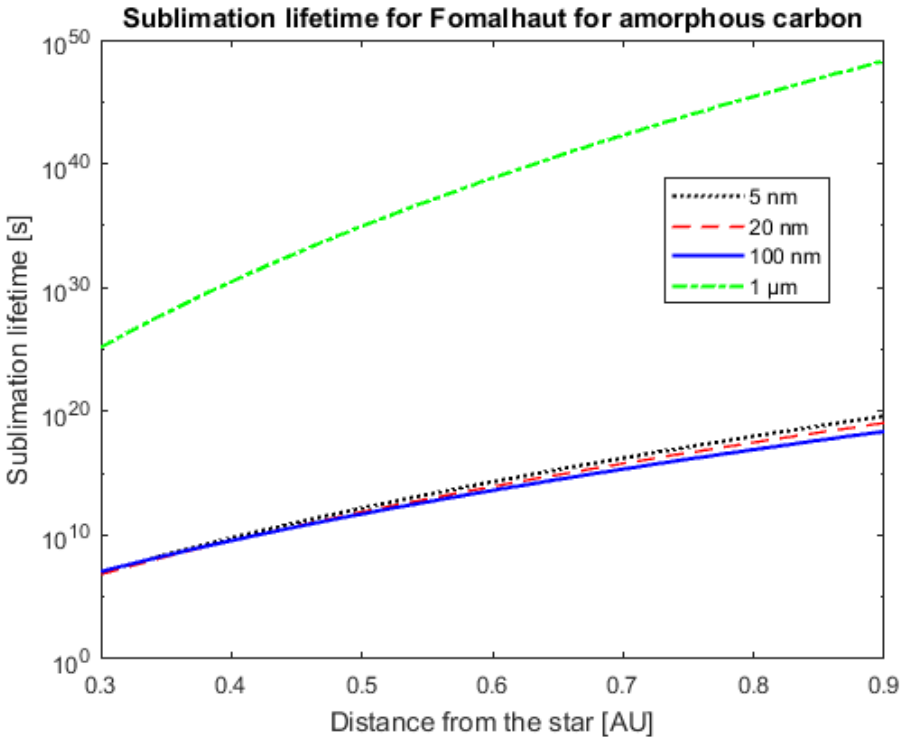

Figure 52: Sublimation lifetime in units of seconds around Fomalhaut for dust particles consisting of amorphous carbon.

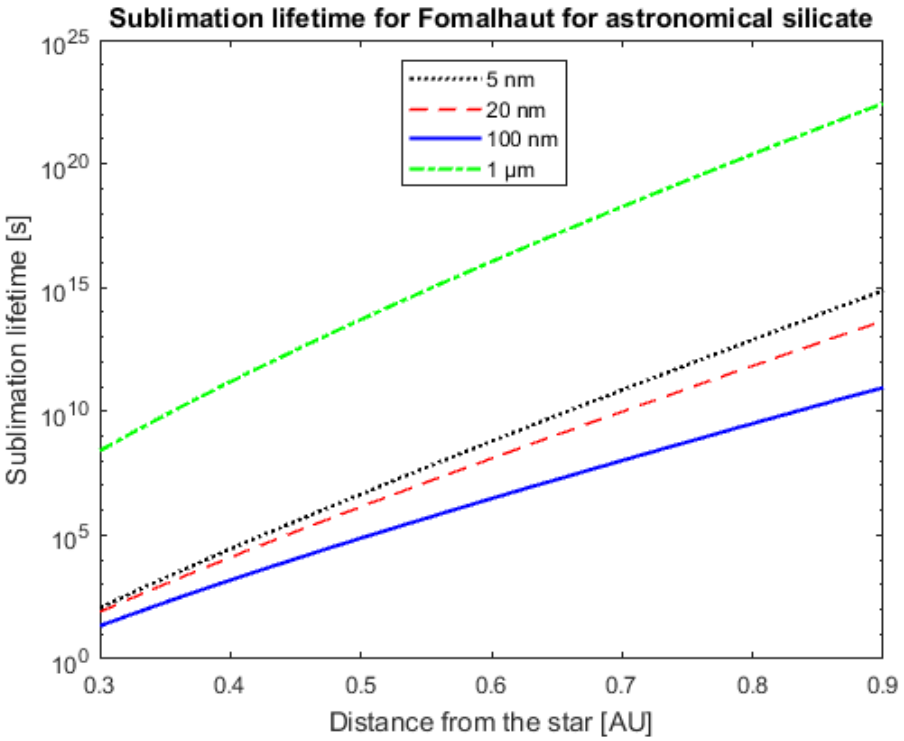

Figure 53: Sublimation lifetime in units of seconds around Fomalhaut for dust particles consisting of astronomical silicate.

9.2.3 Thermal emission brightness

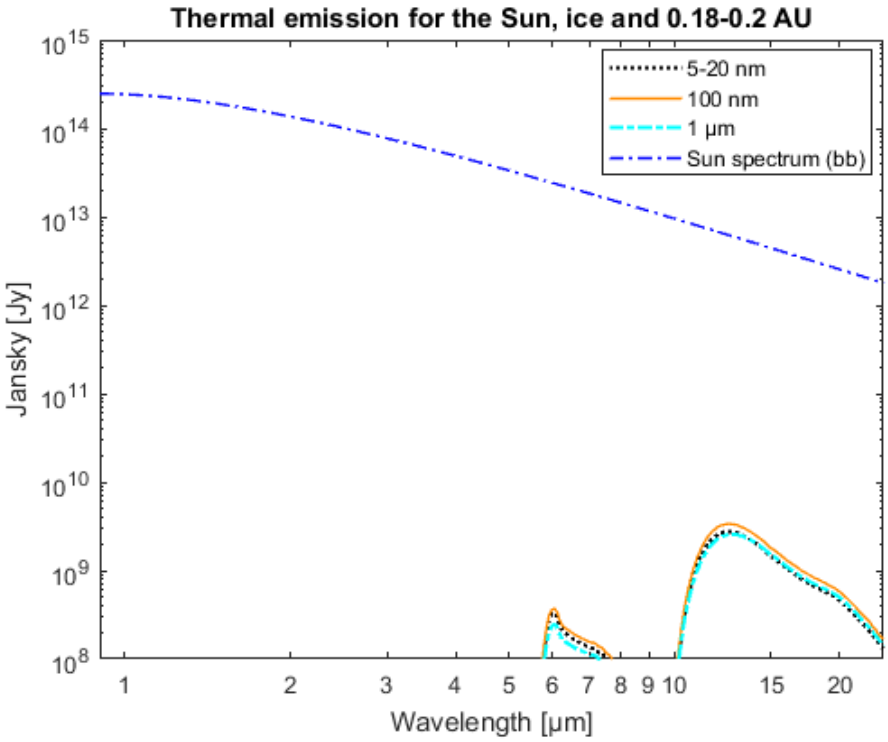

Figure 54: Thermal emission brightness for dust around the Sun with dust particles consisting of ice where the dust is distributed in a narrow ring between 0.18-0.2 AU.

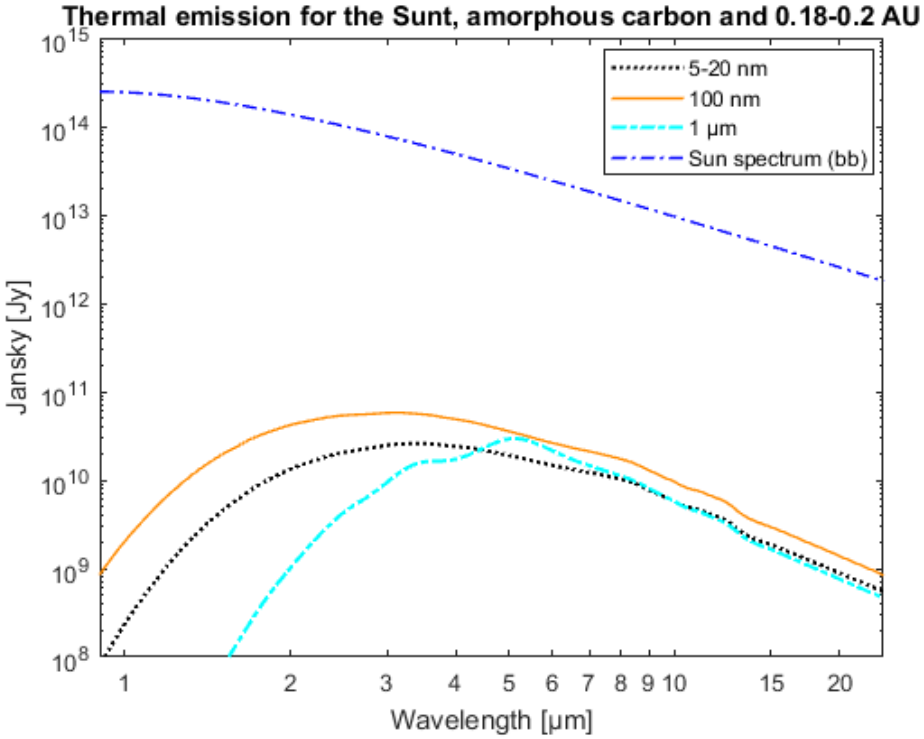

Figure 55: Thermal emission brightness for dust around the Sun with dust particles consisting of amorphous carbon where the dust is distributed in a narrow ring between 0.18-0.2 AU.

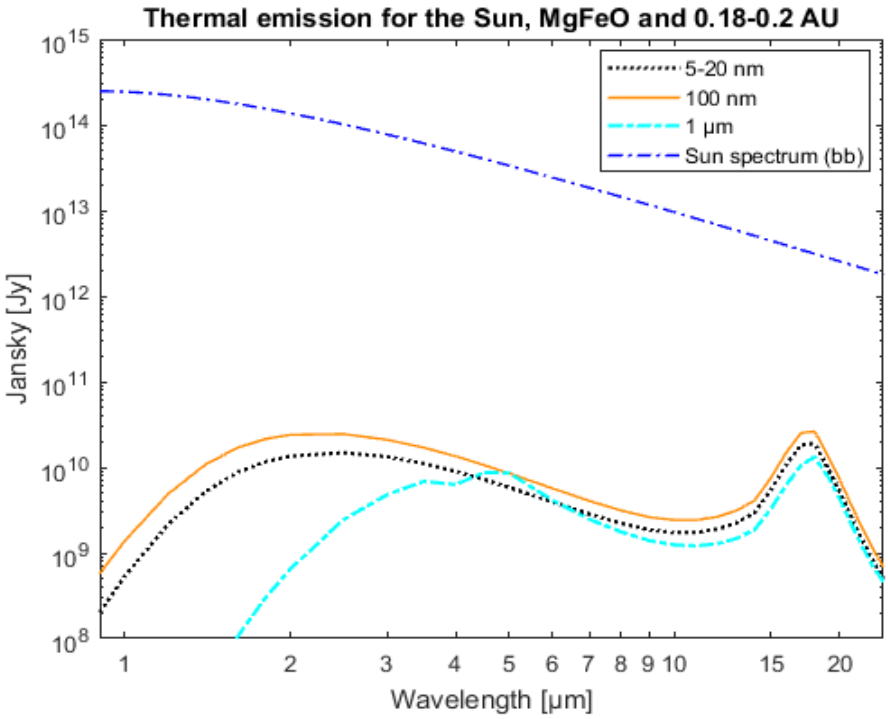

Figure 56: Thermal emission brightness for dust around the Sun with dust particles consisting of a mixture of MgO/FeO where the dust is distributed in a narrow ring between 0.18-0.2 AU.

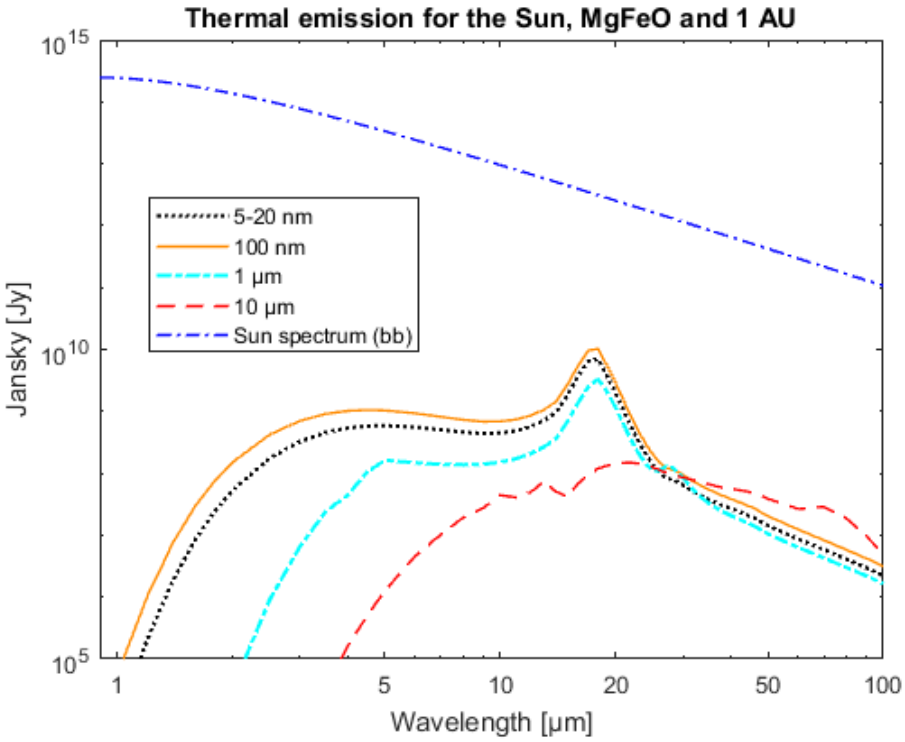

Figure 57: Thermal emission brightness for dust around the Sun with dust particles consisting of MgO/FeO where the dust is at 1 AU.

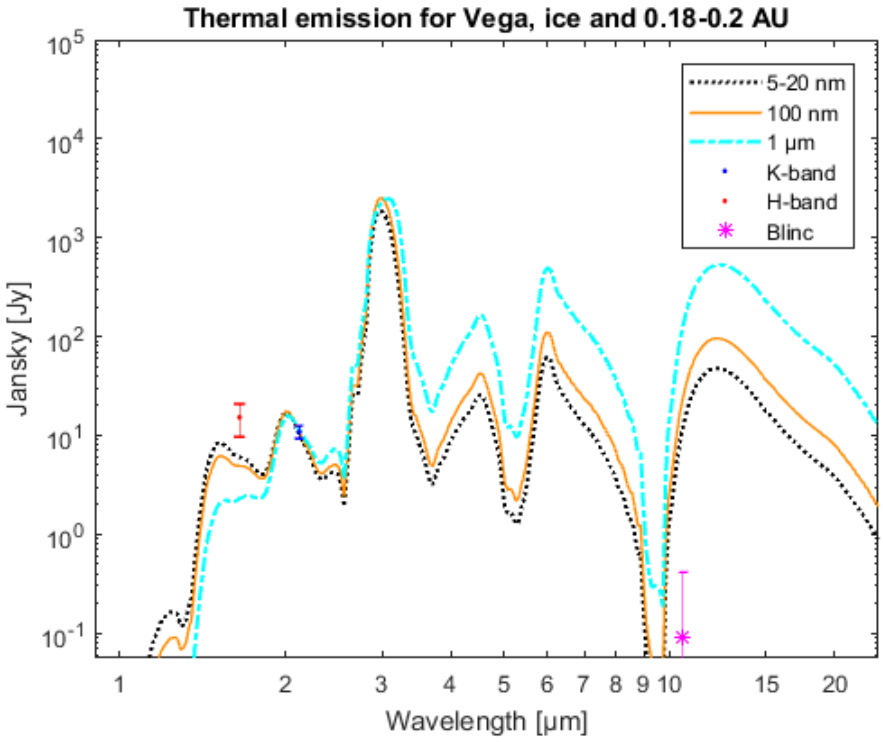

Figure 58: Thermal emission brightness for dust around Vega with dust particles consisting of ice where the dust is distributed in a narrow ring between 0.18-0.2 AU.

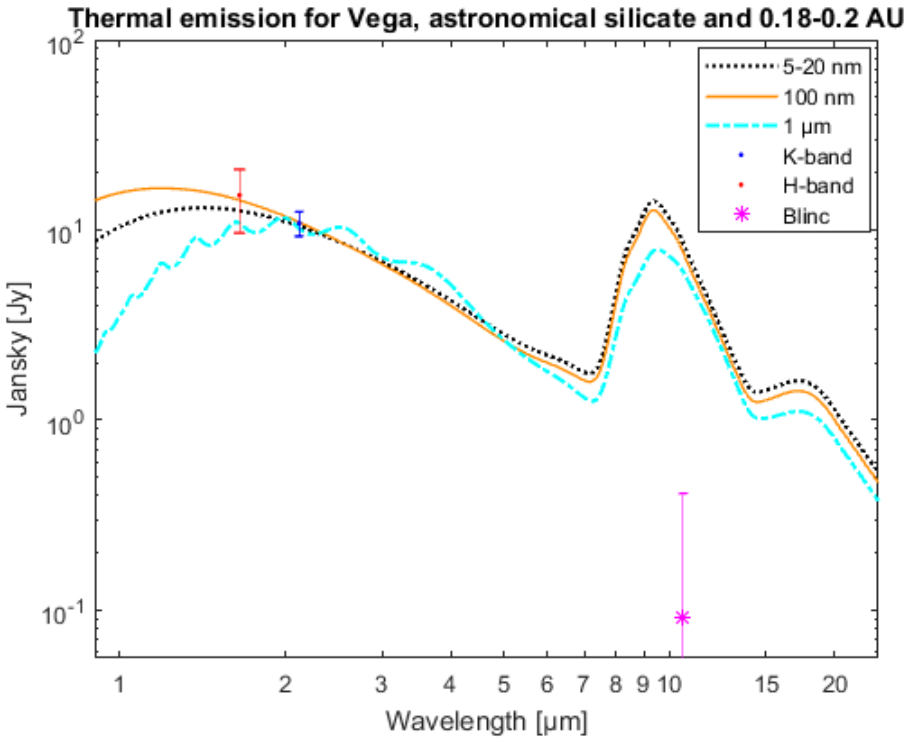

Figure 59: Thermal emission brightness for dust around Vega with dust particles consisting of astronomical silicate where the dust is distributed in a narrow ring between 0.18-0.2 AU.

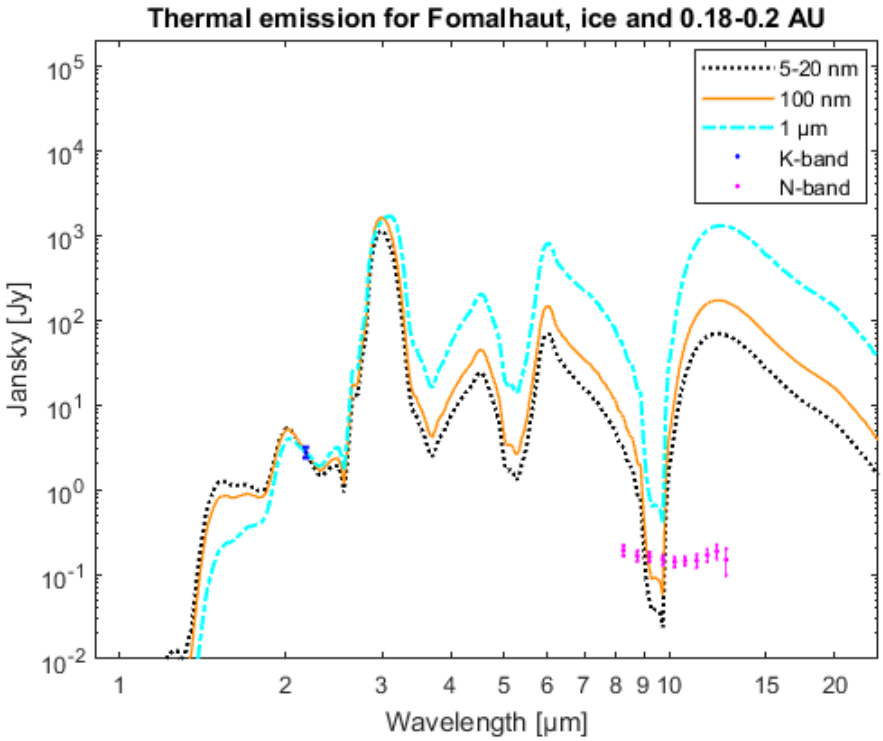

Figure 60: Thermal emission brightness for dust around Fomalhaut with dust particles consisting of ice where the dust is distributed in a narrow ring between 0.18-0.2 AU

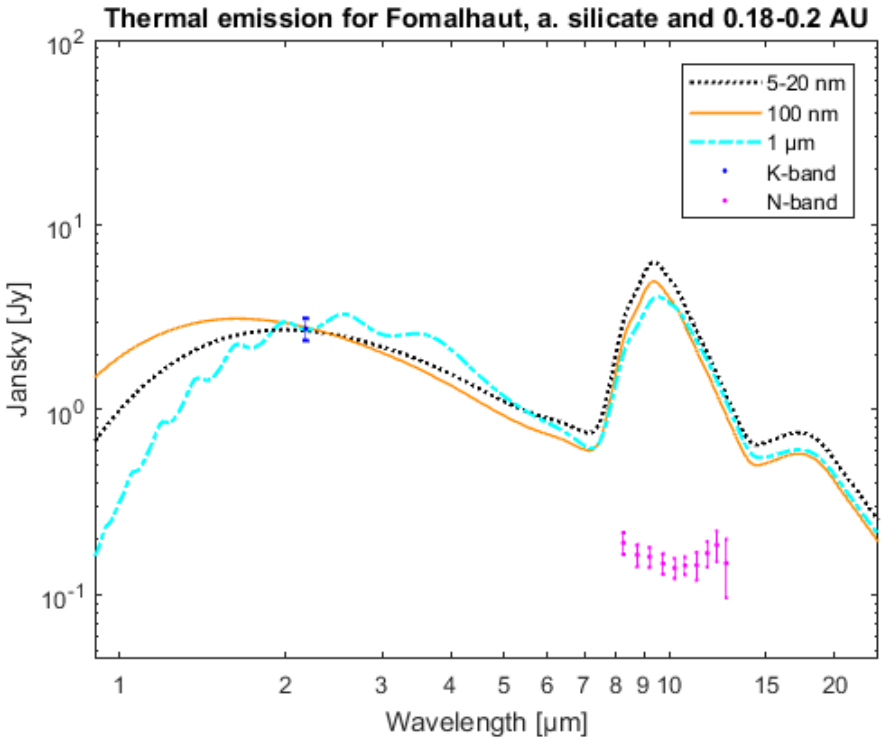

Figure 61: Thermal emission brightness for dust around Fomalhaut with dust particles consisting of astronomical silicate where the dust is distributed in a narrow ring between 0.18-0.2 AU

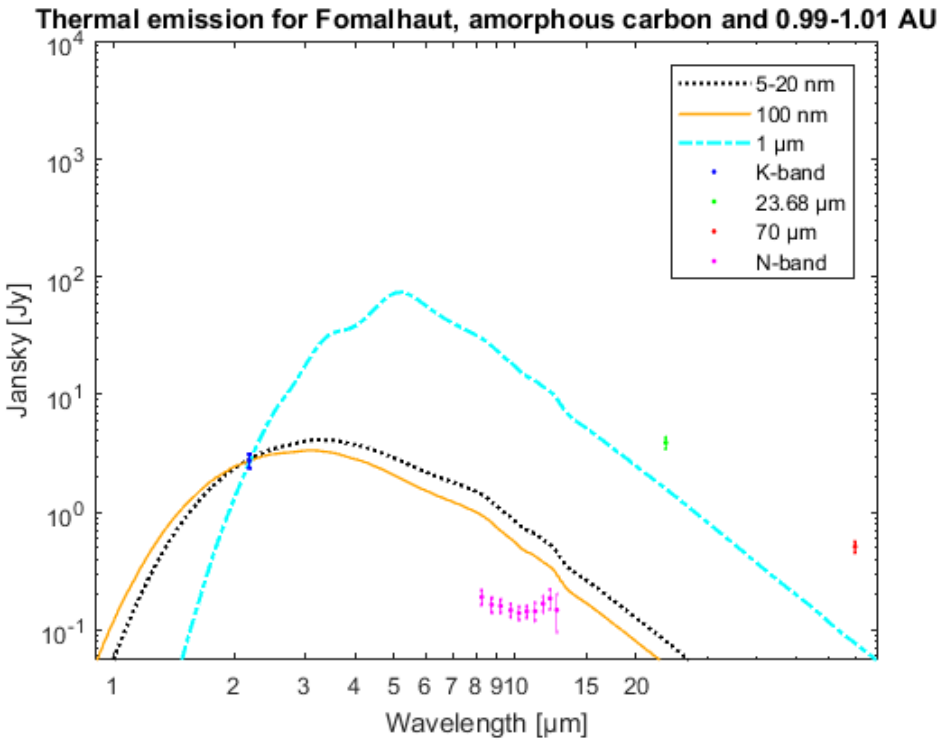

Figure 62: Thermal emission brightness for dust around Fomalhaut with dust particles consisting of amorphous carbon where the dust is distributed in a narrow ring between 0.99-1.01 AU.

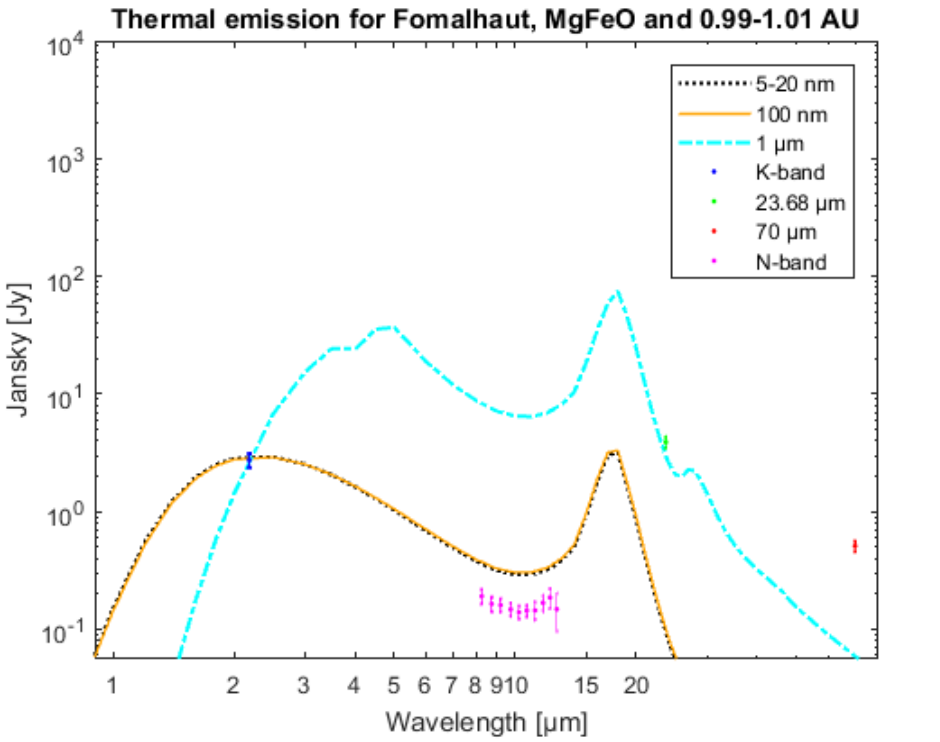

Figure 63: Thermal emission brightness for dust around Fomalhaut with dust particles consisting of a mixture of MgO/FeO where the dust is distributed in a narrow ring between 0.99-1.01 AU.

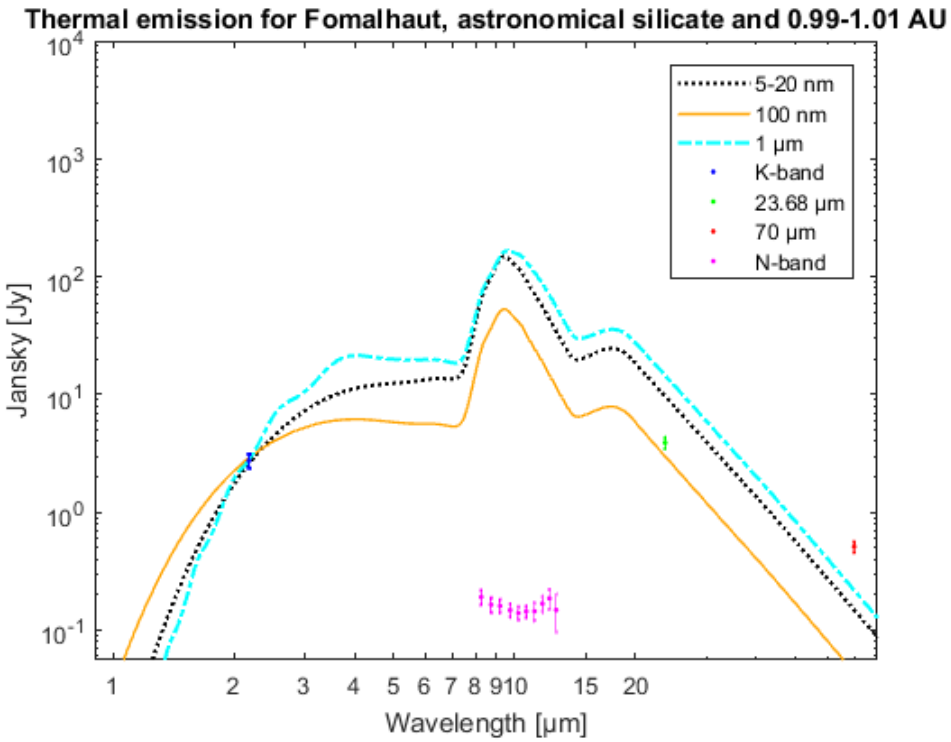

Figure 64: Thermal emission brightness for dust around Fomalhaut with dust particles consisting of astronomical silicate where the dust is distributed in a narrow ring between 0.99-1.01 AU.

9.3 List of acronyms

AU	Astronomical unit
ESA	European Space Agency
NASA	National Aeronautics and Space Administration
PDF	Probability density function
SED	Spectral energy distribution

9.4 List of tables

9.5 List of figures